CHANNEL SPECIFIC CALCIUM DYNAMICS IN PC12 CELLS

A Dissertation Presented

By

KEITH TULLY

Submitted to the Faculty of the

University of Massachusetts Graduate School of Biomedical Sciences, Worcester

In partial fulfillment of the requirements for the degree of

DOCTOR OF PHILOSOPHY

May 21, 2004

Program in Neuroscience

CHANNEL SPECIFIC CALCIUM DYNAMICS IN PC12 CELLS

A Dissertation Presented By

KEITH TULLY

Approved as to style and content by:

Jose Lemos, Chair of Committee

Vincent Dionne, Member of Committee

Harvey Florman, Member of Committee

Hong-Sheng Li, Member of Committee

Charles Sagerstrom, Member of Committee

Steven Treistman, Thesis Advisor

Anthony Carruthers, Ph.D.,

Dean of the Graduate School of Biomedical Sciences

Program in Neuroscience

5/21/04

ACKNOWLEDGEMENTS

I would like to thank my advisor, Dr. Steven Treistmen, for his outstanding personal and scientific mentoring. I am grateful to my committee members: Jose Lemos, Vincent Dionne, Harvey Florman, Hong-Sheng Li, and Charles Sagerstrom. I would like to thank my lab-mates for all of their help, insight, and comradery. Perhaps most importantly, I would like to thank my family for their support and encouragement.

ABSTRACT

Calcium ions (Ca^{2+}) are involved in almost all neuronal functions, providing the link between electrical signals and cellular activity. This work examines the mechanisms by which a neuron can regulate the movement and sequestration of Ca^{2+} through specific channels such that this ubiquitous ion can encode specific functions. My initial focus was using intracellular calcium ($[Ca^{2+}]_i$) imaging techniques to study the influence of the inhibition of specific voltage gated calcium channels (VGCC) by ethanol on a depolarization induced rise in $[Ca^{2+}]_i$ in neurohypophysial nerve terminals. This research took an unexpected turn when I observed an elevation of $[Ca^{2+}]_i$ during perfusion with ethanol containing solutions. Control experiments showed this to be an artifactual result not directly attributable to ethanol. It was necessary to track down the source of this artifact in order to proceed with future ethanol experiments. The source of the artifact turned out to be a contaminant leaching from I.V. drip chambers. Due to potential health implications stemming from the use of these drip chambers in a clinical setting as well as potential artifactual results in the ethanol field where these chambers are commonly used, I choose to investigate this phenomenon more rigorously. The agent responsible for this effect was shown to be di(2-ethylhexyl)phthalate (DEHP), a widely used plasticizer that has been shown to be carcinogenic in rats and mice. The extraction of this contaminant from the I.V. drip chamber, as measured by spectrophotometry, was time-dependent, and was markedly accelerated by the presence of ethanol in the solution. DEHP added to saline solution caused a rise in $[Ca^{2+}]_i$ similar to that elicited by the contaminant containing solution. The rise in calcium required transmembrane flux through membrane

channels. Blood levels of DEHP in clinical settings have been shown to exceed the levels which we found to alter $[Ca^{2+}]_i$. This suggests that acute alterations in intracellular calcium should be considered in addition to long-term effects when determining the safety of phthalate-containing plastics.

As part of a collaboration between Steven Treistman and Robert Messing's laboratory at UCSF, I participated in a study of how ethanol regulates N-type calcium channels which are known to be inhibited acutely, and upregulated in the chronic presence of ethanol. Specific mRNA splice variants encoding N-type channels were investigated using ribonuclease protection assays and real-time PCR. Three pairs of N-type specific α-subunit $Ca_v2.2$ splice variants were examined, with exposure to ethanol observed to increase expression of one alternative splice form in a linker that lacks six bases encoding the amino acids glutamate and threonine (ΔET). Whole cell electrophysiological recordings that I carried out demonstrated a faster rate of channel activation and a shift in the voltage dependence of activation to more negative potentials after chronic alcohol exposure, consistent with increased expression of ΔET variants. These results demonstrate that chronic ethanol exposure not only increases the abundance of N-type calcium channels, but also increases the expression of a $Ca_v2.2$ splice variant with kinetics predicted to support a larger and faster rising intracellular calcium signal. This is the first demonstration that ethanol can up-regulate ion channel function through expression of a specific mRNA splice variant, defining a new mechanism underlying the development of drug addiction.

Depolarizing a neuron opens voltage gated Ca^{2+} channels (VGCC), leading to an influx of Ca^{2+} ions into the cytoplasm, where Ca^{2+} sensitive signaling cascades are stimulated. How does the ubiquitous calcium ion selectively modulate a large array of neuronal functions? Concurrent electrophysiology and ratiometric calcium imaging were used to measure transmembrane Ca^{2+} current and the resulting rise and decay of $[Ca^{2+}]_i$, showing that equal amounts of Ca^{2+} entering through N-type and L-type voltage gated Ca^{2+} channels result in significantly different $[Ca^{2+}]_i$ temporal profiles. When the contribution of N-type channels was reduced, a faster $[Ca^{2+}]_i$ decay was observed. Conversely, when the contribution of L-type channels was reduced, $[Ca^{2+}]_i$ decay was slower. Potentiating L-type current or inactivating N-type channels both resulted in a more rapid decay of $[Ca^{2+}]_i$. Channel-specific differences in $[Ca^{2+}]_i$ decay rates were abolished by depleting intracellular Ca^{2+} stores suggesting the involvement of Ca^{2+}-induced Ca^{2+} release (CICR). I was able to conclude that Ca^{2+} entering through N-type, but not L-type channels, is amplified by ryanodine receptor mediated CICR. Channel-specific activation of CICR generates a unique intracellular Ca^{2+} signal depending on the route of entry, potentially encoding the selective activation of a subset of Ca^{2+}-sensitive processes within the neuron.

TABLE OF CONTENTS

Title Page i

Signature Page ii

Acknowledgements iii

Abstract iv

Table of contents vii

List of figures ix

Introduction 1

Calcium Ion 1

Voltage Gated Calcium Channels 1

Calcium Sequestration 3

Intracellular Calcium Release Channels 5

Spatial Dimensions of neuronal calcium signaling 7

PC12 Cells 9

Methods for investigating Calcium Dynamics. 10

Chapter one 13

Abstract 15

Introduction 16

Materials and Methods 18

Results 22

Discussion 33

Acknowledgements 35
References 36
Chapter two. 39
Abstract 41
Introduction 42
Materials and Methods 44
Results 50
Discussion 62
Acknowledgements 65
References 66
Chapter three 71
Abstract 73
Introduction 74
Materials and Methods 76
Results 79
Discussion 97
Acknowledgements 101
References 102

Discussion 108
Cumulative References 124

LIST OF FIGURES

Introduction

Structure, subunit composition, and evolution of VGCCs 2

Mechanisms of calcium sequestration 3

Direct visualization of CICR in neurons 6

Spatial dimensions of neuronal calcium signaling 7

Importance of calcium localization 8

Spatial relationship between RyR, N-type VGCC, and CAK channels 9

Methods for investigating calcium dynamics 11

Chapter one

Figure 1 $[Ca^{2+}]_i$ in isolated cells exposed to contaminant containing medium . . 23

Figure 2 Contaminant from drippers in DEHP 26

Figure 3 $[Ca^{2+}]_i$ response to DEHP mimics $[Ca^{2+}]_i$ response to contaminant . . . 28

Figure 4 Time-dependent leaching of DEHP from drippers 30

Figure 5 Rise in $[Ca^{2+}]_i$ requires Ca^{2+} influx 32

Chapter two

Figure 1 Schematic diagram of Cav2.2a1 51

Figure 2 Chronic ethanol increases dET and both SFMG spice variants 52

Figure 3 Ethanol increases both variants of exon 18a 55

Figure 4 Rate of activation and voltage dependence of N-type VGCC 56

Figure 5 Ethanol-induced changes in cells expressing domain of PKCE 60

Chapter three

Figure 1 Relationship between Q and $[Ca^{2+}]_i$ 80

Figure 2 Route of entry and $[Ca^{2+}]_i$ profile 83

Figure 3 Channel selection by BayK and voltage 87

Figure 4 CICR underlies the differences in $[Ca^{2+}]_i$ profile 91

Figure 5 Discontinuity in the relationship between Ca^{2+} entry and $[Ca^{2+}]_i$ 96

Discusion

Inhibition of depolarization induced $[Ca^{2+}]_i$ rise 110

$[Ca^{2+}]_i$ decay in cell bodies and neurites 114

Regenerative capacity of intracellular Ca^{2+} release 118

Residual $[Ca^{2+}]_i$ for differing stimulation patterns 120

INTRODUCTION

Calcium Ion

Electrical signals of excitable cells are translated into functional outcomes through the actions of Ca^{2+} fluxes through Ca^{2+} permeable channels (Hagiwara and Byerly, 1981). The influx of Ca^{2+}, a divalent cation, contributes not only to the electrical signal, but also serves as a second messenger capable of activating numerous cell functions by binding with high affinity to numerous regulatory proteins (Tsien et al., 1988). The cytoplasmic free Ca^{2+} level is kept very low (~100 nM) through the actions of ATP-dependent Ca^{2+} pumps and Ca^{2+} exchange systems, resulting in significant alterations in cytoplasmic concentrations during neuronal depolarizations (Bertil Hille, Ion Channels of Excitable Membranes, 3rd edition). Tight control of $[Ca^{2+}]_i$, through the actions of influx channels, pumps, buffers, and intracellular release, is required to allow high fidelity of signaling in neurons.

Voltage gated calcium channels

Voltage gated calcium channels (VGCC) are multisubunit complexes composed of a central channel forming α_1 subunit and auxiliary subunits, including the regulatory β subunit and the disulfide-linked $\alpha_2\delta$ subunit (See figure below from Spafford and Zamponi, 2003). The α_1 subunit has 4 domains, each containing 6 transmembrane α helices and a pore loop thought to form the lining of the ion-conducting pore. VGCCs can be defined in several ways; 1) according to their threshold of activation 2) by the gene

encoding the α_1 subunit 3) by pharmacology.

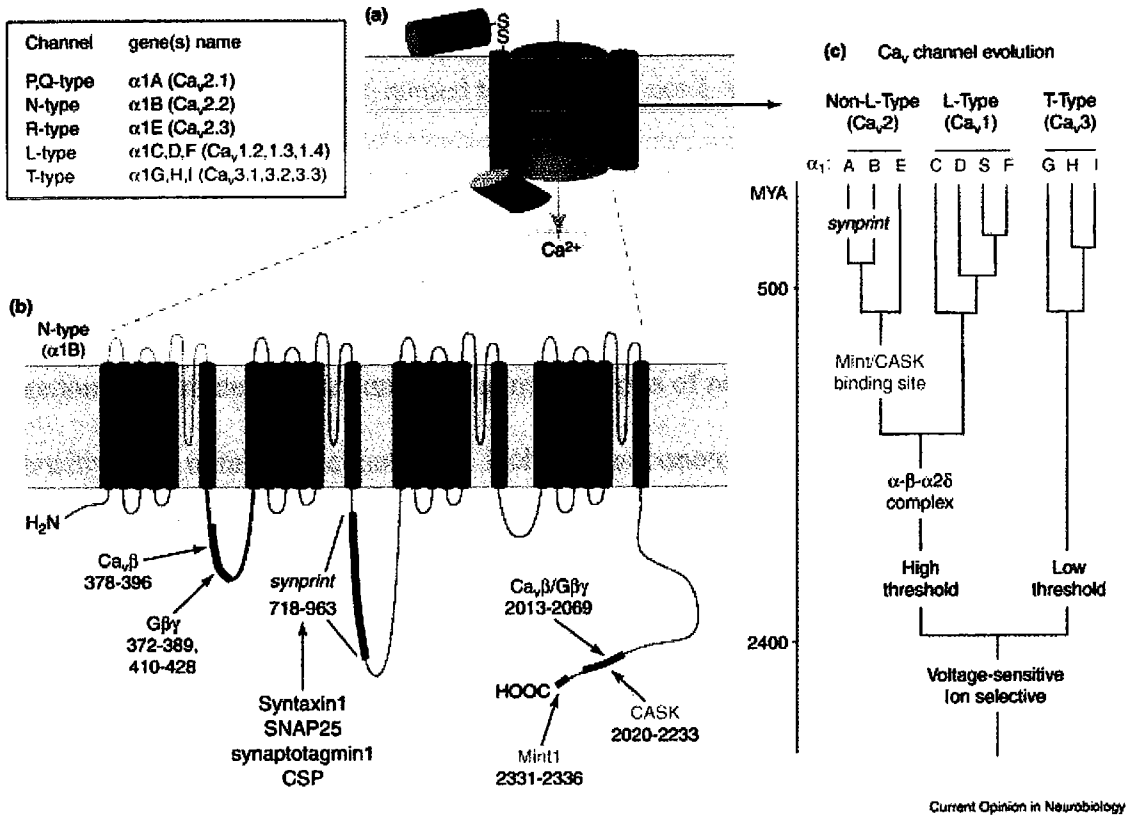

The low-voltage activated channels, encoded by the Ca_v3 family of genes, is referred to as "T type". There are several high voltage activated channels, the Ca_v1 gene family referred to as "L-type", the Ca_v2 family which is further subdivided into $Ca_v2.1$ "P/Q type", $Ca_v2.2$ "N-type", and $Ca_v2.3$ "R-type".

L-type calcium channels, named for their long lasting current which shows limited voltage dependent inactivation during long pulses with barium as the charge carrier, activate from relatively depolarized (greater that –40 mV) holding potentials. These channels are highly permeable to barium and calcium and exhibit a single channel conductance of 25-28 picosiemens (Tsien et al., 1987). Dihydropyridines are highly

selective ligands for L-type channels, can be either agonistic or antagonistic, and can be used to identify them in a heterogenous channel population (Tanabe et al., 1987).

N-type calcium channels, named for neither T nor L and neuronal, have both a slow inactivating and long lasting component of current (Plummer et al., 1989). N-type channels are permeable to barium and calcium, and exhibit a single channel conductance of 11-15 picosiemens (Tsien et al., 1987). N-type channels are believed to be the predominant route of entry underlying many forms of neurotransmitter release, and are sensitive to a number of conotoxins, including ω-conotoxin MVIIA.

Calcium sequestration

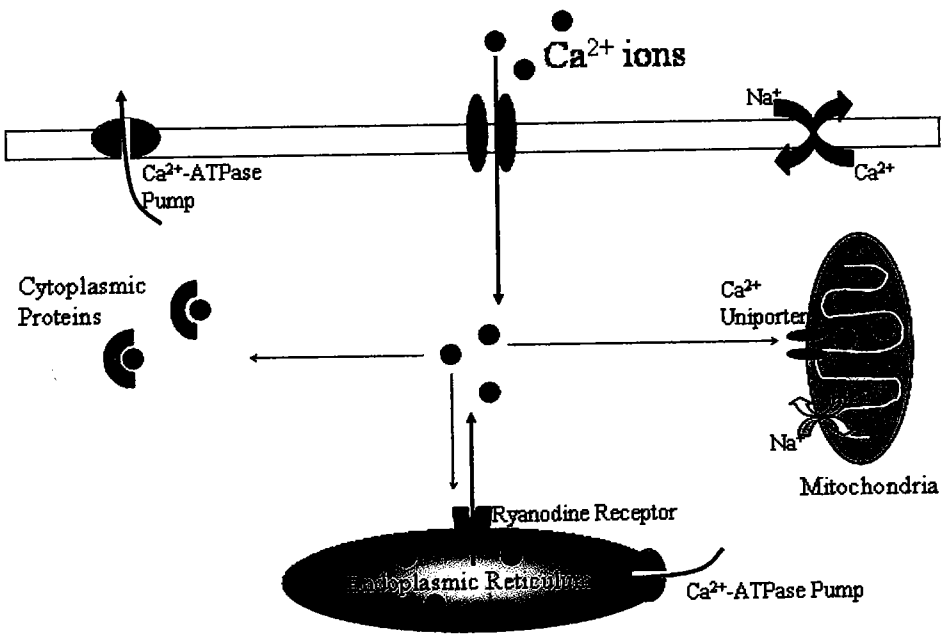

What is the destination of Ca^{2+} ions once they enter a neuron? Ca^{2+} is removed from the cytoplasm by various pumps and exchangers. The plasma membrane Ca^{2+}-ATPase pumps and Na^{+}/ Ca^{2+} exchangers extrude Ca^{2+} to the outside whereas the endoplasmic reticulum ATPase pumps return Ca^{2+} to the internal stores (Berridge, 1998). Much of the Ca^{2+} inside of a cell is sequestered, leaving a free cytosolic concentration in the nM range. There are numerous high affinity calcium binding proteins inside a neuron, many of which serve in calcium sensitive signaling cascades. These proteins are rapidly saturated by influx during trains of action potentials, while mitochondria forms a low affinity, high capacity buffering system for Ca^{2+} (Stuenkel, 1994). Babcock et al. (1997) simultaneously monitored mitochondrial and cytoplasmic free calcium at high temporal resolution, showing fast and high capacity sequestration of Ca^{2+} that limits the rise of cytoplasmic Ca^{2+} from either Ca^{2+} entry or mobilization of reticular stores. They further showed that declining mitochondrial Ca^{2+} prolongs complete recovery. Mitochondria have an electrochemical gradient that is used to drive Ca^{2+} uptake through a uniporter that has a low sensitivity to Ca^{2+}. The mitochondrion has an enormous capacity to accumulate Ca^{2+} and the mitochondrial matrix contains buffers that prevent the concentration from rising too high. Once the cytosolic Ca^{2+} has returned to its resting level , a Na^{+}/ Ca^{2+} exchanger pumps the Ca^{2+} back into the cytoplasm (Blaustein and Ector, 1976). Ca^{2+} can additionally serve as a Ca^{2+} mobilizing signal, stimulating further release from internal stores through the activation of release channels.

Calcium release channels

Calcium ions can be released from intracellular stores such as the endoplasmic reticulum where millimolar concentrations are accumulated due to the actions of ATP-dependent pumps (Blaustein et al., 1978a). The two main families of intracellular Ca^{2+} release channels are the IP_3 receptors and the ryanodine receptors. Both are formed by tetramers of homologous subunits with large N-terminal domains containing regulatory sites that allow for the integration of multiple signaling cascades (Simpson et al., 1995). Their large single channel conductances allow large changes in the local Ca^{2+} concentration.

The ryanodine receptor, identified by its binding of the ryanodine alkaloid, has 3 isoforms in mammals (RyR1, RyR2, RyR3) that are encoded by 3 different genes on different chromosomes (for review see Fill and Copello, 2002). The amino acid sequence reveals consensus ligand binding sites for ATP, Ca^{2+}, caffeine, calmodulin and phosphorylation motifs. Single RyR channel activity is a bell shaped function of cytosolic Ca^{2+}, activating at μM concentrations while inhibited at mM concentrations. Ryanodine receptors have a large conductance, with unitary channels in a bilayer having a slope conductance of around 100 pS, showing little selectivity between different divalent and monovalent cations (Tinker and Williams, 1992).

The entry of Ca^{2+} through Ca^{2+} permeable ion channels can stimulate the opening of ryanodine receptors, resulting in the release of Ca^{2+} from the endoplasmic reticulum in a process termed calcium induced calcium release (CICR). CICR is believed to shape neuronal $[Ca^{2+}]_i$ transients (Friel and Tsien, 1992; Hua et al., 1993; Usachev et al., 1993),

and modulate functions including synaptic transmission (Emptage et al., 2001) and plasticity (Rose and Konnerth, 2001). Solovyova et al. (2002) have directly demonstrated Ca^{2+} release activated by Ca^{2+} entry through plasmalemmal Ca^{2+} channels using real-time simultaneous monitoring of intraluminal free Ca^{2+} dynamics and transmembrane Ca^{2+} currents. The figure below is of a dorsal root ganglia neuron that was challenged with 20mM caffeine and then a depolarization from -70 to 0 mV, showing an increase of cytoplasmic Ca^{2+} and a decrease in luminal Ca^{2+} in both instances. It is important to note that the release of luminal Ca^{2+} takes place over several seconds, dynamicly shaping the cytoplasmic Ca^{2+} transient.

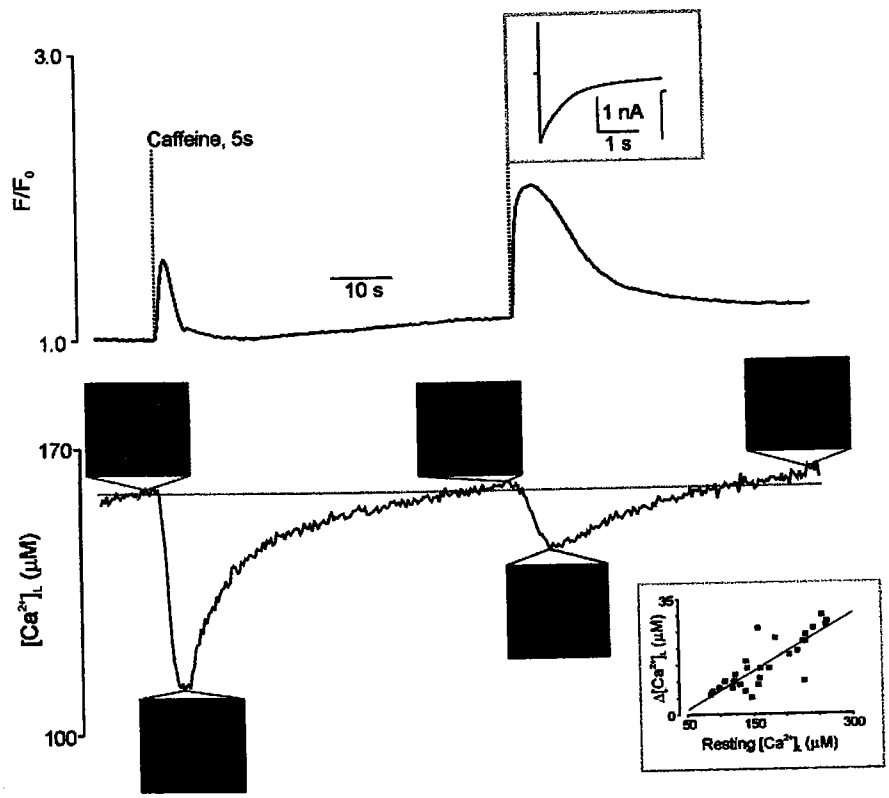

While the CICR process should be self-regenerating because the Ca^{2+} released by ryanodine receptors should feedback and further activate the channel and its neighbors,

the amplitude and duration of a triggering Ca^{2+} stimulus finely grades the CICR process, suggesting a negative feedback mechanism such as the Ca^{2+} dependent inactivation of ryanodine receptors (Fabiato, 1985).

Spatial Dimensions of Neuronal Ca^{2+} Signaling

Calcium ions enter a neuron by passive diffusions through channels and subsequently diffuse away from the point of entry, with diffusion limited by cytoplasmic buffers, some of which serve to activate physiological processes (Augustine and Neher, 1992). The geometric relationship between channels and Ca^{2+} sensors determines the nature of the physiological response. As shown below in the figure from Augustine et al. (2003), different types of geometries can be distinguished according to the distance between channels and between channels and the Ca^{2+} sensors.

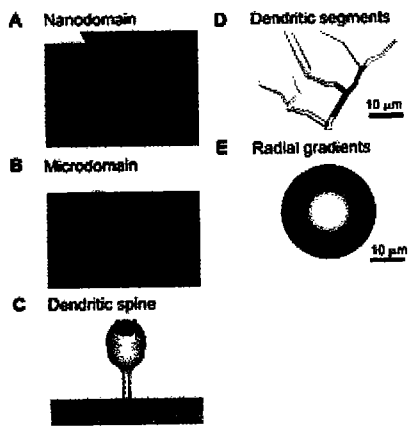

A nanodomain is caused by the influx through a single channel, requiring a sensor to be within 50 nm. Clusters of channels can produce microdomains which arise from the summation of Ca^{2+} entering from multiple channels and require sensors to be within a fraction of a μm. Dendritic spines and segments can further create restricted

compartments. The distance between Ca^{2+} channels and sensors is critical, with the speed and magnitude of the Ca^{2+} signal inversely related to distance. The figure below by Erwin Neher (1998), describes the importance of localization by contrasting a mean distance for randomly mixed channels and release sites with a distance characteristic of a channel that is colocalized with release machinery.

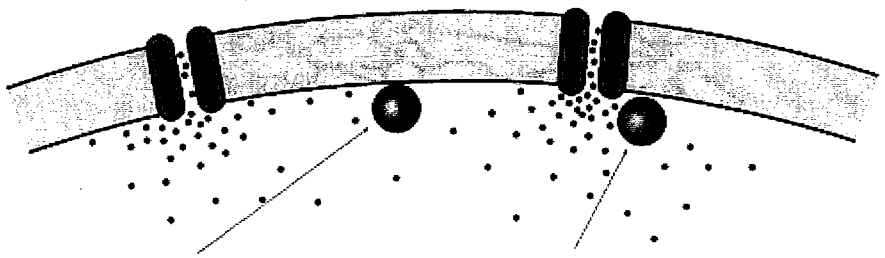

At 200 nm distance:

1.) $[Ca^{++}] \approx 5\text{-}10\ \mu M$
2.) Rises and falls in = 10 msec
3.) Is at equilibrium with mobile buffers
4.) Strongly dependent on buffers; EGTA as effective as BAPTA
5.) $[Ca^{++}]$ determined by mean activity of several neighbouring channels

At 20 nm distance:

1.) $[Ca^{++}] = 100\ \mu M$
2.) Rises and falls within µsec
3.) Is not at equilibrium with mobile buffers
4.) Almost independent of Ca-buffers; EGTA totally ineffective
5.) $[Ca^{++}]$ predominantly determined by the local channel

The existence of these calcium domains requires Ca^{2+} sensors with binding properties that are appropriate for the local Ca^{2+} signal that are to be detected. Akita and Kuba (2000), used calcium activated potassium channels, with known Ca^{2+} sensitivities, to probe the nature of these spatial relationships in bullfrog sympathetic neurons, showing that ryanodine receptors form a functional triad with N-type Ca^{2+} channels and BK channels, and a loose coupling with SK channels. The figure below illustrates this spatial relationship, with $[Ca^{2+}]_D$ representing the microdomain generated by ryanodine receptors and N-type channels, and numbers in percents indicating the fraction of the

contribution of CICR to the activation of BK or SK channels following either a single or high frequency action potentials.

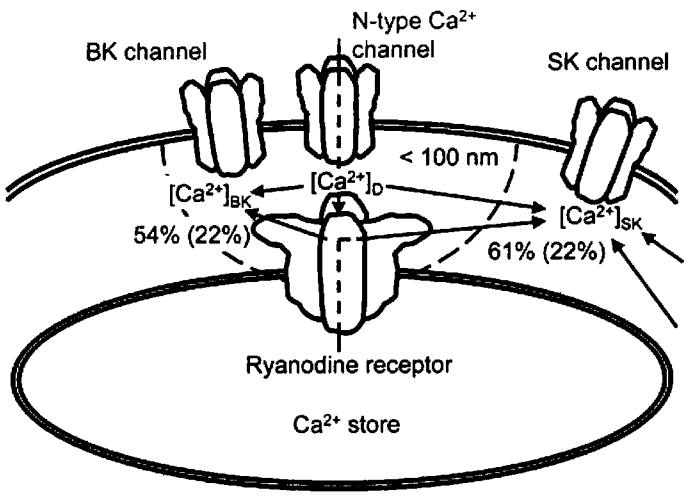

PC12 Cells

Pheochromocytoma (PC12) cells, derived from a spontaneous rat adrenal medullary tumor, were established as a cell line by Greene and Tischler (1976). Undifferentiated PC12 cells multiply logarithmically, and resemble cells of late embryonic rat adrenal medulla in their ability to synthesize, store, and secrete dopamine and acetylcholine in response to calcium influx during depolarization (for review, see Shafer and Atchison, 1991). PC12 cells also release catecholamines in a Ca^{2+} dependent fashion in response to nicotinic (Greene and Rein, 1977) and muscarinic cholinergic agonists (Rabe et al., 1987). PC12 cells contain several voltage gated calcium channels. The mRNA encoding 3 pore forming α_1 subunits (C,B,A for L-, N-, P/Q-type, respectively and 3 auxiliary β subunits (1,2,3) have been detected in PC12 cells (Liu et al., 1996). Culturing PC12 cells

with nerve growth factor (NGF) causes them to become differentiated and display a neuronal like phenotype with altered surface and metabolic properties similar to sympathetic neurons (for review see Meakin and Shooter, 1992). L-type channels represent the predominant influx pathway for calcium in undifferentiated PC12 cells, with N-type channels strongly upregulated in a time dependent fashion with NGF treatment (Plummer et al., 1989; Usowicz et al., 1990), allowing experimental control of the ratio of the two channel types. Johenning et al. (2002), using immunocytochemistry, Western blotting, and calcium imaging in differentiated PC12 cells, showed that IP3R type III is exclusively expressed in the soma, and that IP3R type I, and ryanodine receptors type 2 and 3 are expressed throughout the cell. Differentiated PC12 cells are a neuronal cell line previously used to study the specificity of Ca^{2+} signaling. Examples include the differential induction of gene transcription, regulated by the route of Ca^{2+} entry into the cell (West et al., 2001), and the presence of fast and slow Ca^{2+}-dependent exocytosis, triggered by synaptotagmins with differing Ca^{2+} affinities (Sugita et al., 2002). L- and N-type channels have been found to contribute equally to the excitation secretion coupling process in various chromaffin cells with release determined by the total amount of Ca^{2+} entering (Lukyanetz and Neher, 1999; Kim et al., 1995).

Methods for Investigating Calcium Dynamics

Fluorescent probes that show a spectral response upon binding Ca^{2+} enable the measurement of intracellular free Ca^{2+} concentrations using ratiometric fluorescent

microscopy. Ratio-imaging involves alternating excitation wavelengths (340, 380 nm) while monitoring emission at a third wavelength (510 nm).

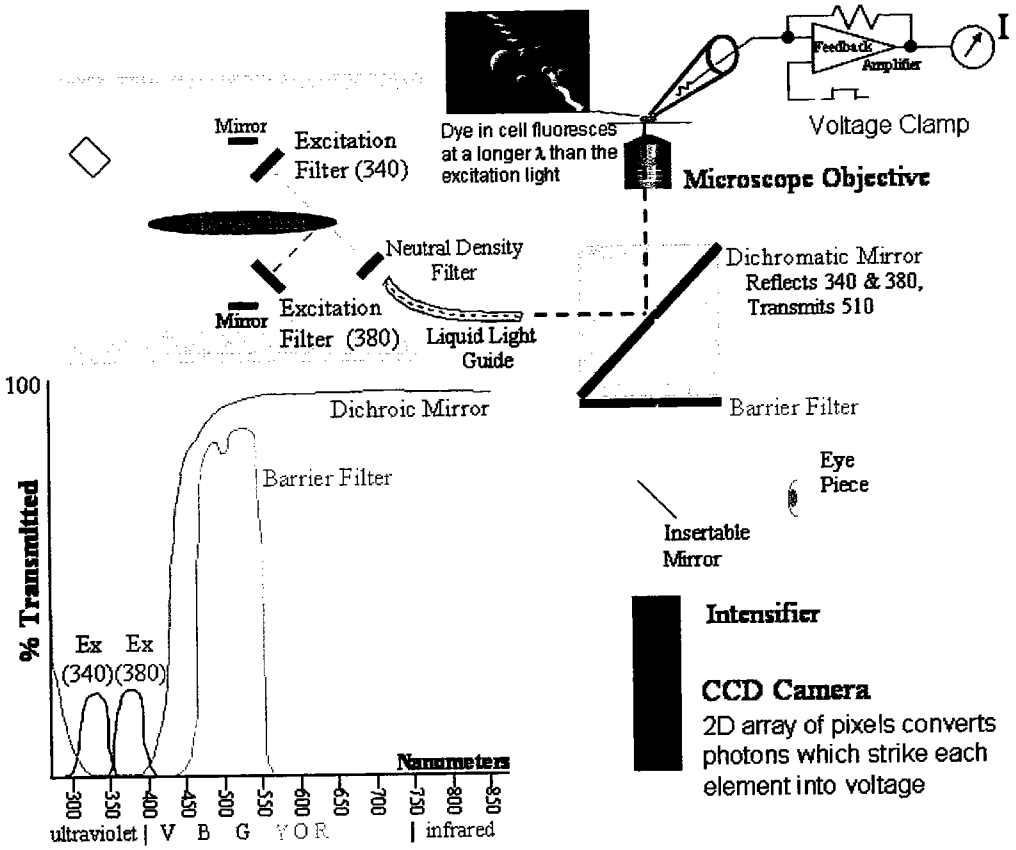

These measurements are independent of dye concentration, cell thickness, it is compatible with the Ca^{2+} concentration range of interest (Grynkiewicz et al., 1985). The acetoxymethyl (AM) ester form of Fura-2 allows for non-invasive loading of the dye, which passively diffuses across the cell membrane where it is subsequently cleaved by esterases (Yuste and Katz 1991).

Voltage clamp techniques involve the application of a voltage across a membrane while measuring the resulting ionic currents. Using a non-invasive perforated patch method, a pipette containing a pore-forming antibiotic is sealed to a cell, with the pores

formed in the on-cell patch allowing electrical access to the whole cell. Maintenance of the structural integrity of a neuron is critical when investigating $[Ca^{2+}]_i$ since breaking of the membrane using a whole cell patch clamp configuration leads to the rundown of Ca^{2+} currents and disruption of the intracellular buffering, sequestration, and release processes.

CHAPTER ONE

A Plasticizer Released from IV Drip Chambers Elevates Calcium Levels in Neurosecretory Terminals

As published in the journal of

Toxicology and Applied Pharmacology 168, 183-188 (2000)

ABSTRACT

We report that intracellular calcium levels rise in mammalian neurosecretory terminals and in cultured pheochromocytoma cells during acute exposure to physiological medium incubated in IV drip chambers. The agent responsible for this effect is shown to be di(2-ethylhexyl)pthalate (DEHP). DEHP (800nM) added to saline solution caused a rise in $[Ca^{2+}]_i$ similar to that elicited by the contaminant-containing solution. The extraction of this contaminant from the I.V. drip chamber, as measured by spectrophotometry, was time-dependent and was markedly accelerated by the presence of 50 mM ethanol in the solution. Larger $[Ca^{2+}]_i$ increases were observed in terminals exposed to solutions incubated in I.V. drip chambers for greater durations. The rise in $[Ca^{2+}]_i$ requires transmembrane calcium flux through membrane channels, as the response is blocked by either 100 μM cadmium or by lowering the extracellular free Ca^{2+} concentration to 10 μM. Our results suggest that acute alterations in intracellular calcium should be considered in addition to long-term effects when determining the safety of phthalate-containing plastics and that laboratory researchers using plastic perfusion materials consider this potential source of artifactual results

INTRODUCTION

Di(2-ethylhexyl)pthalate (DEHP) is a plasticizer widely used during manufacturing to impart flexibility to polyvinyl chloride (PVC) products. The final content of DEHP is up to half of the weight of resulting products, and DEHP can leach out of products since it is not covalently bound to the plastic matrix (Ganning *et al.*, 1990). Long-term exposure to DEHP has been demonstrated to cause deleterious effects in rats and mice, including liver tumors (Kluwe *et al.* 1982, Rao et. al. 1990, Cattley et al. 1987), seminiferous tubular degeneration (Kluwe et al. 1982), and hypertrophy of cells in the anterior pituitary (Kluwe et al. 1982). In a purified protein kinase C preparation from rat brain, acute exposure to DEHP has been shown to inhibit the phoshporylation of histone (Shukla et al., 1989). Acute exposure to mono-ethylhexyl phthalate (MEHP), the predominant metabolite of DEHP, activates Kupffer cell production of oxidants via mechanisms involving protein Kinase C (Rose et al., 1999) and causes increases in cyclooxygenase-2 (COX-2) mRNA in immortalized mouse liver cells (Ledwith et al., 1997), providing a possible link between acute exposure and long-term carcinogenic effects of DEHP. Acute changes in intracellular calcium ($[Ca^{2+}]_i$) may underlie some long-term consequences of DEHP. For example, treatment by thapsigargin, and the calcium ionophore A23187, both of which alter $[Ca^{2+}]_i$, increase COX-2 expression similar to MEHP (Ledwith et al., 1997). A particular concern regarding DEHP is its use in blood storage bags and IV drippers, where appreciable amounts can leach into blood (Huber et al., 1996.

During experiments probing the actions of ethanol on $[Ca^{2+}]_i$ dynamics in cultured pheocromocytoma cells (PC12), we noted a rise in intracellular calcium in ethanol-containing medium. However, in constructing an ethanol concentration-response curve, it was apparent that the effect was present even when ethanol concentrations were decreased, and still present (although diminished, see below) when only physiological medium (i.e., without ethanol) which had passed through the perfusion system was present. Subsequent experiments were performed in neurohypophysial nerve terminals (which release the peptide hormones arginine-vasopressin (AVP) and oxytocin (OT)) to extend the finding to a system for which a significant literature exist regarding the role of intracellular calcium and the actions of ethanol on peptide hormone release (Treistman et al., 1999, Giovannucci and Stuenkel, 1997). The observed rise in $[Ca^{2+}]_i$ will be shown to be attributable to DEHP leached from an IV drip chamber of a type commonly used for clinical and research applications. In this paper, we present data obtained both in the presence and absence of ethanol, since chemical identification of the contaminant and studies using exogenous DEHP require ethanol for solubilization of the compound.

MATERIALS AND METHODS

Microscope and Perfusion System

Glass coverslips (22x22mm No.1) coated with poly-ornithine and laminin were secured to a chamber with a bath volume of approximately 50 µl (Warner Instrument Corp., Hamden, CT) using vacuum grease. The chamber was then mounted on an inverted Olympus IX70 microscope with an oil immersion 100x objective lens. Multiple solutions were gravity fed from syringes through an automated snap valve system (Automate Scientific, Oakland, CA) into a micro-manifold with a single output into the chamber. The bath was constantly perfused at a rate of 1 ml/min providing a rapid exchange of the bath solution. The I.V. drip chamber used was a component of the "Primary IV Set" (Abbott Laboratories, North Chicago, IL, Product No. 1820, Lot No. 28 101 NS).

Neurohypophysial nerve terminals

Male Sprague-Dawley rats (Taconic Farms, Germantown, NY) were housed in central animal quarters where routine care was provided. All aspects of the animals' care was in accordance with the recommendations in the NIH Guide for the Care and Use of Laboratory Animals (NIH, 1985). Preparation of isolated terminals was as previously described (Dopico et al., 1996). Briefly, the posterior lobe of the pituitary was removed following decapitation and the nerve terminals were dissociated by homogenizing the posterior lobe in 200 µl of (mM) 270 sucrose, 0.01 EGTA, and 10 HEPES, pH 7.0. Lockes medium containing (mM) 135 NaCl, 5 $KHCO_3$, 2.2 $CaCl_2$, 2 $MgCl_2$, 10 HEPES,

12 Glucose, pH 7.4, was then continuously perfused over the terminals at a rate of 1 ml/min at room temperature (20°C), following dye loading with perfussed Locke's medium containing 3 μM Fura2AM (Molecular Probes, Eugene, OR) for 16 min at 35 °C. Terminals that had resting baseline $[Ca^{2+}]_i$ values of either greater than 200 nM (assumed to have been damaged during preparation) or less than 10 nM (reflecting poorly loaded terminals) were excluded from analysis.

PC12 Cells

PC12 Cells obtained from Dr. E. Shooter (Stanford University) were grown in Dulbecco's modified Eagles medium (Sigma, St. Louis, MO) supplemented with 25 mM glucose, 2 μM glutamin, 5% fetal calf serum (Sigma), 10% horse serum (J.H.R. Biosciences, Lenexa, KS), 50 units/ml penicillin G (Sigma), and 50 mg/ml streptomycin (Sigma). Krebs medium containing (mM) 125 NaCl, 5 KCl, 1.2 KH_2PO_4, 1.2 $MgSO_4$, 2 $CaCl_2$ 25 HEPES, 6 glucose, pH 7.4, was constantly perfused over PC12 cells at a rate of 1 ml/min at room temperature (20°C), following dye loading with Kreb's medium containing 2.5 μM Fura2AM for 30 min at 37°C.

$[Ca^{2+}]_i$ measurement

The concentration of calcium to be calculated from the ratio of the fluorescence at two different wavelengths using the equation $[Ca^{2+}]_i = Kd \times (R-R_{min})/(R_{max}-R) \times \beta$ where Kd is the dissociation constant for fura-2; R_{min} and R_{max} are the 340/380 nm (background subtracted) ratio for fura2 free acid in zero Ca^{2+} and 1 mM Ca^{2+}, respectively; and β is the ratio (background subtracted) between fura2 free acid in zero Ca^{2+} and 1 mM Ca^{2+} at 380 nm excitation (Grynkiewicz et. al. 1985). Fluorescence images with excitation at 340

and 380 nm were recorded with an intensified CCD camera (Ion Optix, Milton, MA). DEHP added to fura-2-free acid (pentapotassium salt) solutions did not affect fluorescence over a range of Ca^{2+} levels (0-1mM Ca^{2+}). An increase in the ratio was interpreted as a rise in calcium concentration only if there was both an increased fluorescence at 340 nm and a decreased fluorescence at 380 nm.

Statistics

Following subtraction of baseline values, we computed the integral (i.e., area under the curve, AUC) of the $[Ca^{2+}]_i$ for each terminal during the 600 s of exposure. AUC values plotted represent the mean ± SEM of n terminals. The Kolmogorov-Smirnov test was used to evaluate the normality of the data describing the response. A natural log transformation of the data was used to achieve a normal distribution and homogeneity of variances. Since the log-transformed data did not adequately meet the assumption of normality, the untransformed data was analyzed using nonparametric methods. Kruskal Wallis analysis of variance by rank showed that the $[Ca^{2+}]_i$ effect in neurohypophysial terminals differed significantly as a function of time of incubation. Bonferroni adjusted Mann-Whitney U-tests were used for between group comparisons of the effects of incubation times, with the $[Ca^{2+}]_i$ increase becoming significantly different from the zero incubation time at 24 h. In addition, a regression between the natural log response in neurohypophysial terminals to solutions incubated in I.V. drip chambers and time of incubation was performed.

Spectrophotometry

A Beckman DU-70 spectrophotometer was used for all spectral scans. Both UV and visible spectra were examined (190 to 700 nm), with peaks digitally selected. Samples were prepared in either absolute ethanol or 50 mM ethanol medium with the respective solvents serving as blanks. A standard curve of DEHP dissolved in medium (optical density vs. concentration of DEHP) was generated to determine the concentration of the DEHP in the perfusate.

Thin Layer Chromatography

Following incubation of absolute ethanol in IV drip chambers, the ethanol phase was evaporated at room temperature under a stream of nitrogen gas. The residue dissolved in fresh ethanol was spotted in an adjacent lane to an ethanolic solution of DEHP. TLC was performed on normal phase thin-layer silica gel plates containing a preadsorbent strip and a fluorescent indicator (LK6DF 60A, 250 μm, Whatman Inc., Clifton, NJ). The chromatogram was developed in 7:1 (v:v) chloroform / methanol and visualized and photographed under short wavelength (254 nm) UV light.

RESULTS

We measured fluorescence from isolated rat neurohypophysial terminals (Fig.1A,B) and PC12 cells (Fig. 1C,D) loaded with the calcium indicator dye fura-2, during perfusion with medium that had been exposed to an I.V drip chamber. For comparison, exposure to an elevated potassium medium (50 mM KCl) subsequent to the contaminant-containing medium is also shown (Fig. 1A,B). High K^+ medium depolarizes the membrane, activating voltage-gated calcium channels, leading to a large influx of Ca^{2+}. In addition to the fact that the high K^+ response is significantly larger, there are two differences in the response, compared to the response with the contaminant. First, the lag time to the $[Ca^{2+}]_i$ rise is significantly longer for the contaminant-mediated rise (2-6 min in response to the contaminant vs. less than 5 sec for high K^+), and second, the $[Ca^{2+}]_i$ rise is maintained for longer than 1 hr after return to control medium for cells exposed to the contaminant, whereas $[Ca^{2+}]_i$ levels returned to pre-exposure values much more quickly after removal of high K^+ solution (Fig. 1A,B). The differences in lag time and duration were independent of the size of the evoked Ca^{2+} rise. The lag time and sustained response may reflect the involvement of active metabolites, or the mediation of second messengers, among other possibilities (a portion of the sustained response may also reflect the continued presence of the contaminant resistant to washout; see below). Medium incubated in either the hard PVC syringe which served as the bath reservoir, or the perfusion tubing (Dow Corning; Silastic brand tubing) leading from the drip chamber to the dish produced neither a change in intracellular calcium levels, nor detection of the contaminant by spectrophotometry (see below).

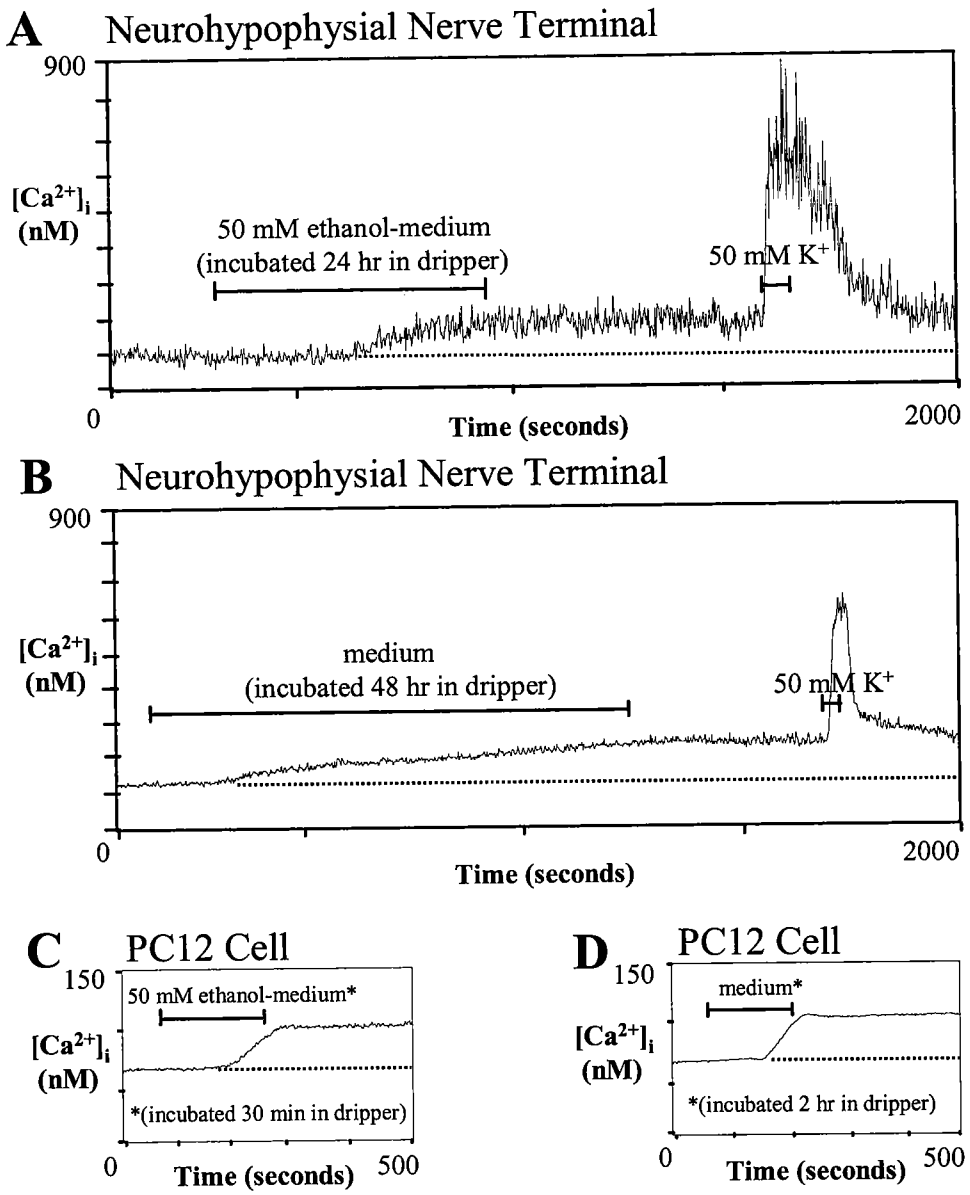

FIG. 1. Representative records of $[Ca^{2+}]_i$ derived from the 340/380 nm fluorescence ratio in isolated cells loaded with fura-2. Dotted line indicates baseline $[Ca^{2+}]_i$ level. Eight different drippers were used for these measurements, and medium incubated in each of

them produced elevated $[Ca^{2+}]_i$. **(A)** Rat neurohypophysial nerve terminal exposed to medium (containing 50 mM ethanol) incubated in dripper for 24 hrs and then to 50 mM KCl (representative of 14/18 terminals). The use of 50 mM ethanol allows comparison with spectrophotometric studies, in which some ethanol was necessary to assure dissolution of pure DEHP. **(B)** Rat neurohypophysial nerve terminal exposed to medium (no ethanol present) incubated in dripper for 48 hrs and then to 50 mM KCl (representative of 17/19 terminals). The apparent potentiation of the response to 50 mM K^+ by ethanol in the selected traces does not reflect a consistent difference between the two groups. **(C)** Undifferentiated PC12 cell exposed to 50 mM ethanol-medium incubated in dripper for 30 min (representative of 65/68 cells). **(D)** Undifferentiated PC12 cell exposed to medium (no ethanol) incubated in dripper for 2 hrs (representative of 16/16 cells). Ethanol (50mM) added to unincubated medium did not affect $[Ca^{2+}]_i$.

Spectrophotometric analysis (UV and visible spectra) demonstrated that DEHP was, indeed, present in the medium exposed to the I.V. drip chambers. Absolute ethanol was incubated in the chambers to allow collection of sufficient material for correct identification of all potential contaminants. The spectral scan of the contaminant was identical to that of DEHP (Aldrich Chemical, Milwaukee, WI) dissolved in ethanol (Fig. 2A), with peaks at 274 and 226 nm and a shoulder at 210 nm for both the contaminant and DEHP. To match the conditions in the imaging experiments described above, 50 mM ethanol-medium was incubated in a drip chamber. The spectral characteristics of this incubated medium was identical to that observed when DEHP was added to 50 mM ethanol-medium, with matching peaks at 232 nm and a broad shoulder between 270-280 nm (Fig. 2B). The concentration of DEHP in 50 mM ethanol-medium was determined to be approximately 800 nM, based upon comparison with absorbance values of known concentrations of DEHP added to this medium. Spectroscopic analysis of the perfusate collected during our Ca^{2+} imaging experiments suggests that levels of DEHP had dropped to 23% of peak values within 0-5 min of the initiation of washout of the contaminant-containing solution and that 12% of the peak value remained present over the following 50 minutes. The residual DEHP presumably reflects phthalate compound released from the drip chamber which then remained associated with plastics in the recording chamber and associated tubing. Thus, the residual contaminant may contribute to the sustained Ca^{2+} response observed.

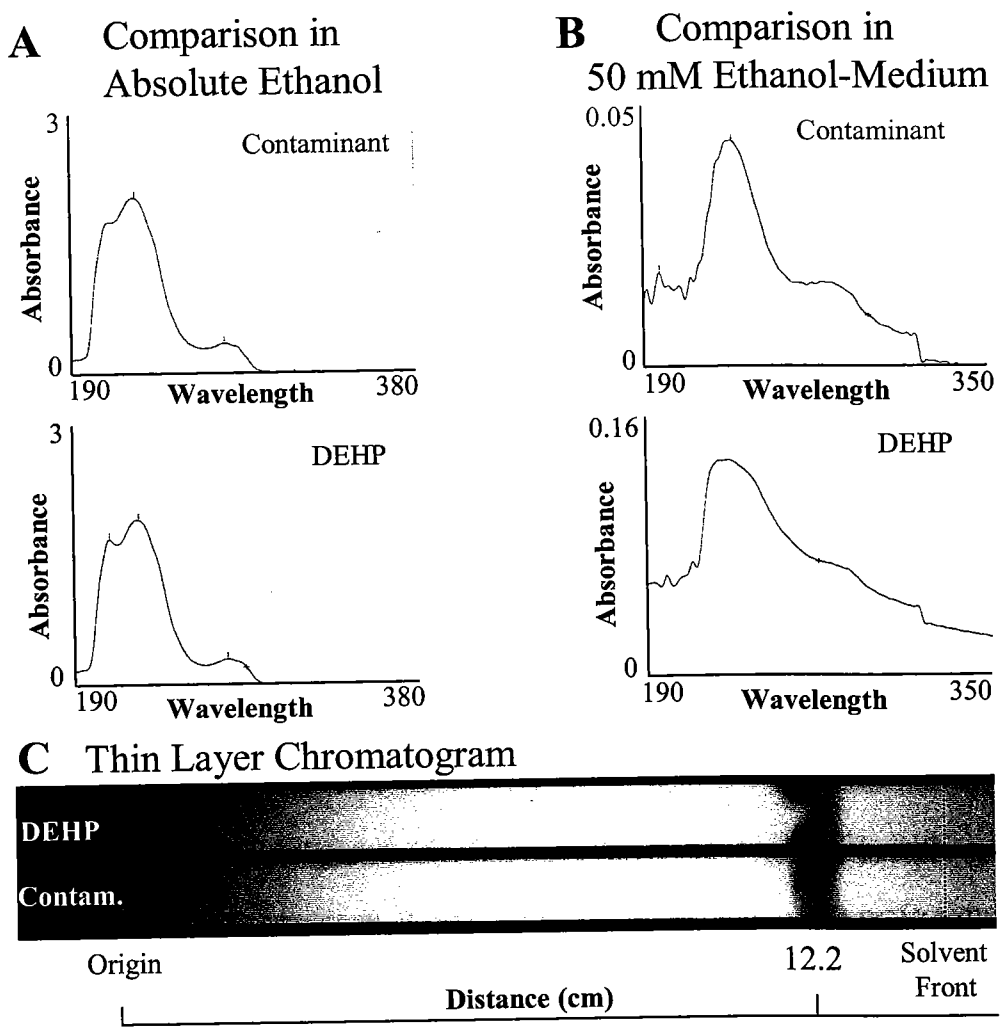

FIG. 2. Contaminant from drippers is DEHP. **(A)** Spectrophotometric comparison of contaminant (incubated 12 hrs in drip chamber) and DEHP (250μM) in absolute ethanol. Absolute ethanol served as a blank. **(B)** Spectrophotometric comparison of contaminant (incubated 12 hrs in drip chamber) and DEHP (640nM) in 50 mM ethanol-medium. The blank was 50 mM ethanol-medium. **(C)** Thin layer chromatogram of DEHP and contaminant.

To obtain further evidence that the contaminant was DEHP, and to rule out the presence of additional contaminants, thin layer chromatography was performed. The contaminant(s) was extracted with absolute ethanol from the I.V. drip chambers. Both the contaminant and DEHP lanes exhibited a single UV absorbing band 12.2 cm from the origin, yielding identical R_f values of 0.83 (Fig. 2C). The figure also shows that no other bands were present. In addition, iodine vapor staining of the chromatogram failed to show additional bands (not shown).

Further evidence that the contaminant is, indeed, DEHP was provided by determining that this compound mimicked the effect of the contaminant. As with the contaminant-containing medium, DEHP produced an elevated level of $[Ca^{2+}]_i$ (Fig. 3A,B). In addition, the lag time to the onset of this effect was long (2-6 min), comparable to that seen for the contaminant effect. The $[Ca^{2+}]_i$ signal observed with DEHP, while qualitatively similar to that produced by the contaminant, differed in two respects. First, it was less stable than the contaminant-produced signal, exhibiting rapid fluctuations in $[Ca^{2+}]_i$, with neurohypophysial terminals oscillating at 0.8 ± 0.3 spikes per min and PC12 cells at 2.0 ± 0.2 spikes per min. Second, it returned to baseline following washout of the contaminant. Difficulty in dissolving pure DEHP in aqueous medium, even in the presence of ethanol, makes it possible that some DEHP was in suspension rather than in solution when applied exogenously, leading to a response slightly different than that observed with DEHP leached from the drip chamber. In spite of these slight differences, the characteristic

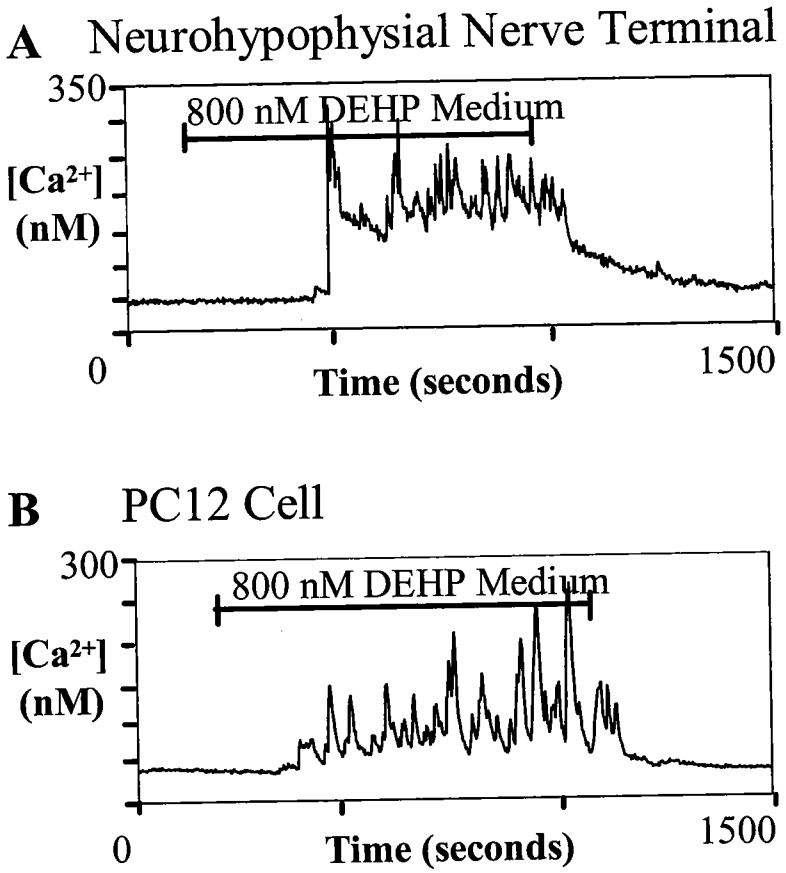

FIG. 3. $[Ca^{2+}]_i$ response to DEHP mimics $[Ca^{2+}]_i$ response to contaminant. Representative recordings of $[Ca^{2+}]_i$ derived from the 340/380 fluorescence ratio in isolated cells loaded with fura-2. **(A)** Rat neurohypophysial nerve terminal exposed to medium containing 800 nM DEHP (representative of 6/9 terminals). **(B)** Undifferentiated PC12 cell exposed to medium containing 800 nM DEHP (representative of 15/16 cells).

feature of elevating $[Ca^{2+}]_i$ was shared by the exogenous DEHP and the contaminant-containing medium.

Next, we tested whether the accumulation of contaminant and the $[Ca^{2+}]_i$ effect of contaminant-containing medium increase with time of incubation in the I.V. drip chamber. Figure 4A shows the absorbance of the UV peak (at 230 nm) for medium incubated for various duration's in the I.V. drippers, revealing a time-dependent accumulation of DEHP. The accumulation was accelerated by the presence of 50 mM ethanol in the medium. The Ca^{2+} response in neurohypophysial terminals (Fig. 4B) also increased as a function of incubation time. ANOVA and regression analysis (see Methods) indicated that the $[Ca^{2+}]_i$ rise in neurohypophysial nerve terminals varied with exposure time ($p=.001$), exhibiting a positive linear relationship between incubation time and $[Ca^{2+}]_i$ with a slope of 0.12 x log $[Ca^{2+}]_i$ ($p<.0002$).

The rise in $[Ca^{2+}]_i$ could result from altered buffering and release from intracellular stores, from influx from extracellular Ca^{2+}, or from a combination of these two possibilities. To test this, PC12 cells were perfused with medium incubated in an I.V. drip chamber, while influx of extracellular Ca^{2+} through plasma membrane ion channels was prevented by addition of 100 μM Cd^{2+} to the medium (Fig. 5A), or by lowering the Ca^{2+} concentration of the medium to 10 μM (Fig. 5B). In both cases, the rise in $[Ca^{2+}]_i$ was no longer observed during perfusion with incubated medium, suggesting that an influx of extracellular Ca^{2+} through gated membrane channels is a necessary element in the response.

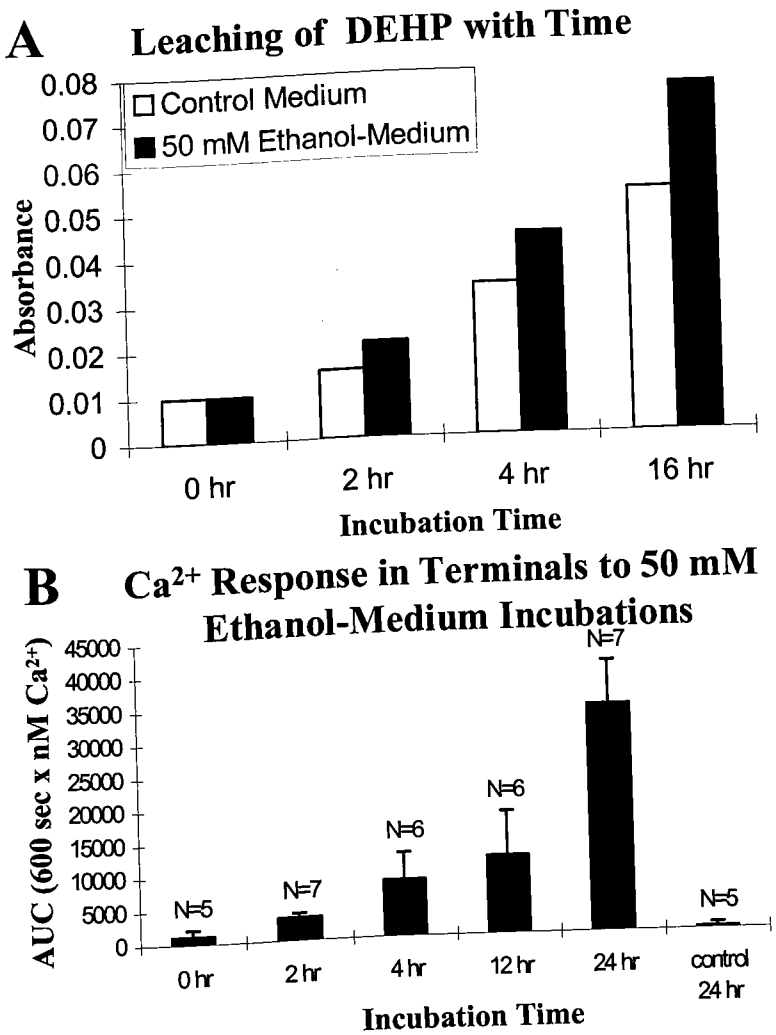

FIG. 4. Time-dependent leaching of DEHP from drippers. **(A)** Accumulation of contaminant in medium without ethanol (open bars), or with 50 mM ethanol added (closed bars), measured at λ=230 nm. DEHP (1μM) in medium had an absorbance of 0.044. Solutions were combined from the same two drippers for each incubation. To avoid artifact due to repetitive incubation, the order of incubation was as follows: 0 hr

medium, 0 hr 50 mM ethanol-medium, 2 hr 50 mM ethanol-medium, 2 hr medium, 16 hr medium, 16 hr 50 mM ethanol-medium, 4 hr medium, 4 hr 50 mM ethanol-medium **(B)** $[Ca^{2+}]_i$ measured by fura-2 in rat neurohypophysial terminals exposed to 50 mM ethanol-medium incubated for varying times in drippers, or in glass vial (control). For the zero incubation time the solution was passed through the drippers without incubation, leading to a trace amount of contaminant.

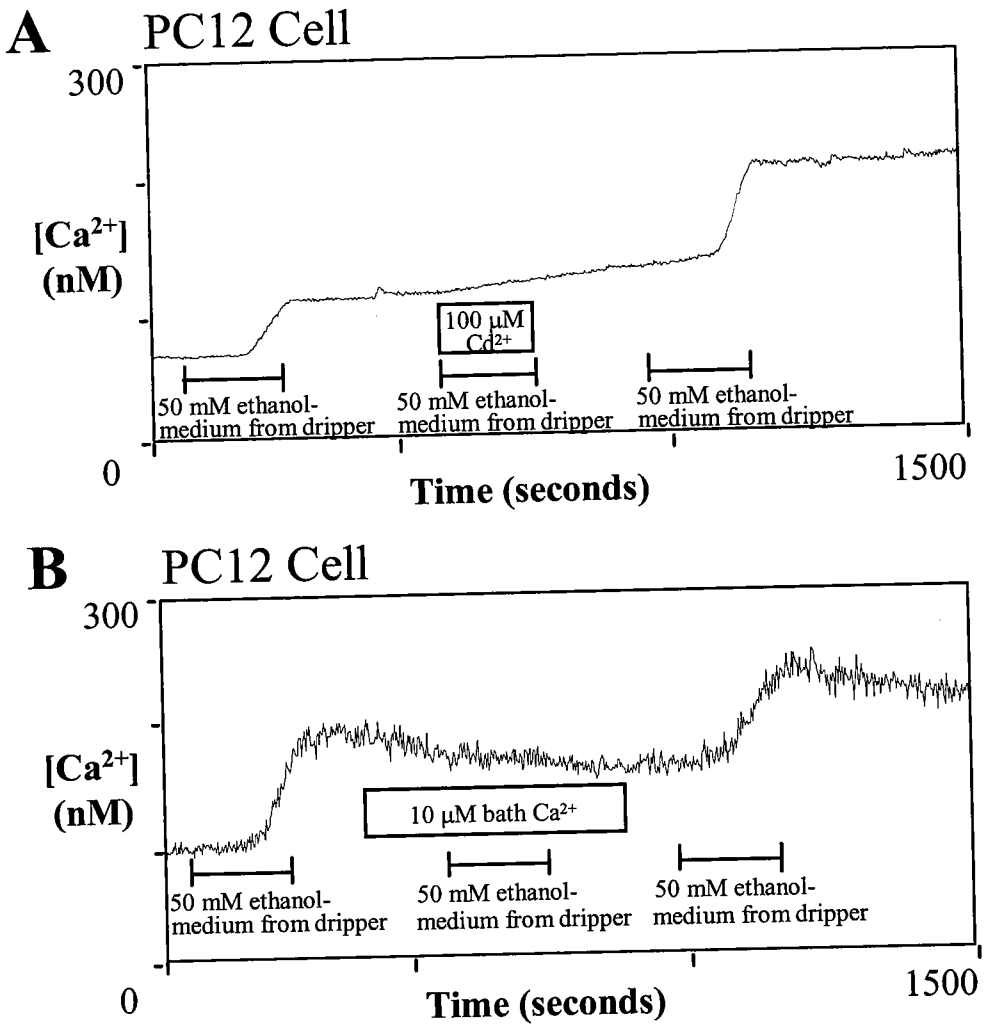

FIG. 5. Rise in $[Ca^{2+}]_i$ requires Ca^{2+} influx. Representative records obtained from undifferentiated PC12 cells loaded with fura-2. **(A)** Exposure to 50 mM ethanol-medium; (30 min incubation in dripper) before, during, and after inclusion of 100 µM cadmium (representative of 6/6 cells). **(B)** Exposure to 50 mM ethanol-medium; (30 min incubation in dripper) before, during, and after the extracellular calcium concentration was reduced to 10 µM (representative of 6/6 cells).

DISCUSSION

We have described the presence of a contaminant leached from IV drip chambers, which produce elevated levels of intracellular Ca^{2+} in PC12 cells and neurohypophysial terminals. A number of pieces of evidence support the identity of this contaminant as DEHP: (1) DEHP is detected in the medium which has been exposed to the plastic chamber; (2) application of exogenous DEHP results in a rise in Ca^{2+}, after a lag time similar to that characterizing the actions of the contaminant; (3) both the amount of DEHP detected in the perfusate and the potency of the perfusate in elevating intracellular Ca^{2+} rise in tandem, as a function of incubation time in the plastic chamber. To our knowledge this is the first report of an acute effect of DEHP on Ca^{2+} dynamics in nervous tissue. Intracellular Ca^{2+} plays important roles in nerve cells, including modulation of excitability, neurotransmitter release, and gene expression (Berridge, 1998). In neurohypophysial terminals, depolarization-evoked increases in capacitance, associated with hormone release, have been correlated with increases of $[Ca^{2+}]_i$ of approximately 75 nM from baseline (Giovannucci and Stuenkel 1997). The increases of $[Ca^{2+}]_i$ reported here (up to160 nM above baseline) are, therefore, potential modulators of release. The mechanisms controlling intracellular Ca^{2+} levels in both neurohypophysial terminals and PC12 cells include dynamic intracellular storage sites and gated transmembrane pores through which extracellular Ca^{2+} can enter. These sources may be coupled, since release from intracellular stores can be triggered by Ca^{2+} entering from the extracellular compartment (Berridge, 1998). Oscillations may reflect bursts of action potentials (unpublished observations). Our results strongly suggest that the initiation of

the rise in $[Ca^{2+}]_i$ requires transmembrane Ca^{2+} flux. It is unclear whether the maintained response produced by the contaminant reflects a continued transmembrane flux, or modulation of intracellular storage sites. Furthermore, the basis of transmembrane entry may involve the direct gating of channels or may reflect a depolarization-mediated activation of voltage-gated Ca^{2+} channels. Interestingly, similar results have been reported for the action of polychlorinated biphenyls (PCBs) in uterine tissue. Exposure to PCBs led to a rise in intracellular Ca^{2+} levels, requiring transmembrane Ca^{2+} flux and exhibiting a lag time on the order of minutes and a duration of many minutes after the removal of the toxicant from the bathing medium (Bae et al., 1998).

The finding that DEHP, a widely used plasticizer and environmental contaminant, has acute effects on mammalian nervous tissue must be considered when evaluating the safety of its use. A review by Huber et. al. (1996) concludes that the levels of DEHP observed during various clinical procedures (2.3-250 μM blood concentrations) are considerably below the levels which have been found to be carcinogenic in rats and mice, and, therefore do not present a significant danger. However, our findings suggest that values as low as 800 nM could elicit the observed acute $[Ca^{2+}]_i$ response. The effect of DEHP described in this paper occurs in the nanomolar concentration range, within minutes of exposure, suggesting the potential for biological, potentially deleterious effects in situations where prolonged contact with the perfusion tubing occurs. In addition, the use of phthalate-releasing perfusion materials in laboratory research studies presents the potential for artificial results.

ACKNOWLEDGMENTS

We thank Shangara Dehal and Andrew Wilson for expert assistance, and Stephen Baker for help with statistics. This work was supported by National Institutes of Health Grants AA08003 to S.N.T. and ES00834 to D.K.

REFERENCES

Bae J, Stuenkel EL and Loch-Caruso R. Stimulation of oscillatory uterine contraction by the PCB mixture Aroclor 1242 may involve increased [Ca2+]i through voltage-operated calcium channels. *Toxicol Appl Pharmacol* 155: 261-272, 1999.

Berridge MJ. Neuronal calcium signaling. *Neuron* 21: 13-26, 1998.

Cattley RC, Conway JG and Popp JA. Association of persistent peroxisome proliferation and oxidative injury with hepatocarcinogenicity in female F-344 rats fed di(2-ethylhexyl)phthalate for 2 years. *Cancer Lett* 38: 15-22, 1987.

Dopico AM, Lemos JR and Treistman SN. Ethanol increases the activity of large conductance, Ca(2+)-activated K+ channels in isolated neurohypophysial terminals. *Mol Pharmacol* 49: 40-48, 1996.

Ganning AE, Olsson MJ, Brunk U and Dallner G. Effects of prolonged treatment with phthalate ester on rat liver. *Pharmacol Toxicol* 67: 392-401, 1990.

Giovannucci DR and Stuenkel EL. Regulation of secretory granule recruitment and exocytosis at rat neurohypophysial nerve endings. *J Physiol* 498 (Pt 3): 735-751, 1997.

Grynkiewicz G, Poenie M and Tsien RY. A new generation of Ca2+ indicators with greatly improved fluorescence properties. *J Biol Chem* 260: 3440-3450, 1985.

Huber WW, Grasl-Kraupp B and Schulte-Hermann R. Hepatocarcinogenic potential of di(2-ethylhexyl)phthalate in rodents and its implications on human risk. *Crit Rev Toxicol* 26: 365-481, 1996.

Kluwe WM, Haseman JK, Douglas JF and Huff JE. The carcinogenicity of dietary di(2-ethylhexyl) phthalate (DEHP) in Fischer 344 rats and B6C3F1 mice. *J Toxicol Environ Health* 10: 797-815, 1982.

Ledwith BJ, Pauley CJ, Wagner LK, Rokos CL, Alberts DW and Manam S. Induction of cyclooxygenase-2 expression by peroxisome proliferators and non-tetradecanoylphorbol 12,13-myristate-type tumor promoters in immortalized mouse liver cells. *J Biol Chem* 272: 3707-3714, 1997.

National Institutes of Health (NIH). (1985). Publication No. 85-23, National Institutes of Health, Bethesda, MD. [Revised]

Rao MS, Yeldandi AV and Subbarao V. Quantitative analysis of hepatocellular lesions induced by di(2-ethylhexyl)phthalate in F-344 rats. *J Toxicol Environ Health* 30: 85-89, 1990.

Rose ML, Rivera CA, Bradford BU, Graves LM, Cattley RC, Schoonhoven R, Swenberg JA and Thurman RG. Kupffer cell oxidant production is central to the mechanism of peroxisome proliferators. *Carcinogenesis* 20: 27-33, 1999.

Shukla RR, Albro PW, Corbett JT and Schroeder JL. In vitro studies of the inhibition of protein kinase C from rat brain by di-(2-ethylhexyl)phthalate. *Chem Biol Interact* 69: 73-85, 1989.

Treistman, S.N., Chu, B., and Dopico, A. M. (1999). Molecular targets underlying ethanol-mediated reduction of hormone release from neurohypophysial nerve terminals. In *The "Drunken" Synapse* (Liu, Y., and Hunt, W., Eds.), pp. 27-38. Kluwer Academia/Plenum Publishers, New York.

CHAPTER TWO

Chronic Ethanol Exposure Induces an N channel Splice Variant with Altered Channel Kinetics

As submitted for publication in the journal of Molecular Pharmacology.

This is the work of Dr. Robert O. Messing, with the experiments involving riboprobe generation, ribonuclease protection assay, and real-time-PCR completed in his laboratory by Philip Newton, Helen Walter, Thomas McMahon, Jackie Connolly, and Jahan Dadgar. Dr. Messing requested the collaboration of Dr. Steve Treistman to asses a change in channel function predicted by the altered mRNA expression. I then contributed the electrophysiological experiments shown in Figure 4 under the supervision of Dr. Treistman.

ABSTRACT

Chronic ethanol exposure increases the number of functional N-type channels in PC12 cells through a mechanism that requires protein kinase C ε (PKCε). We investigated whether this involves ethanol-induced increases in mRNA for the N-type specific α-subunit $\alpha_1$2.2 by examining 3 pairs of $\alpha_1$2.2 alternative splice variants. Exposure to 150 mM ethanol for 1-6 days increased expression of one alternative splice form in which the IVS3-S4 linker lacks six bases encoding the amino acids glutamate and threonine (ΔET). Ethanol exposure also increased the abundance of both pairs of splice variants in the IIIS3-S4 linker and in the intracellular loop between repeats II and III. Whole cell recordings demonstrated a faster rate of channel activation and a shift in the voltage dependence of activation to more negative potentials after chronic alcohol exposure. These results demonstrate that chronic ethanol exposure not only increases the abundance of N-type calcium channels, but also increases the expression of channels with kinetics predicted to support a larger and faster rising intracellular calcium signal. This may be due in part to increased expression of a specific $\alpha_1$2.2 splice variant. Ethanol-induced alterations in the abundance of channel splice variants may be an important mechanism for increased neuronal excitability following chronic ethanol exposure.

INTRODUCTION

Neuronal voltage-gated calcium channels permit calcium entry into cells in response to changes in membrane potential, thereby regulating several calcium-dependent processes such as neurotransmitter release, gene expression, differentiation, and ion channel function (Dunlap et al., 1995; Ghosh and Greenberg, 1995). Calcium channels are multimeric complexes of at least three subunits (α_1, $\alpha_2\delta$, and β) and diversity within α_1 subunits is responsible for the major features that distinguish different channel classes. Ten α_1 genes identified in mammals comprise three subgroups: $\alpha_1$1.1-1.4 (dihydropyridine (DHP) sensitive L-type), $\alpha_1$2.1-2.3 (DHP insensitive, peptide toxin sensitive, P/Q-, N- and R-types), and $\alpha_1$3.1-3.3 (DHP and toxin insensitive T-type) (Ertel et al., 2000). Alternative splicing of precursor mRNA transcripts further extends this diversity (Lipscombe et al., 2002).

Chronic ethanol exposure increases the density and function of L-type channels (Brennan et al., 1990; Grant et al., 1993; Knott et al., 2002; Little, 1991; Messing et al., 1986), which in the neural crest-derived PC12 cell line requires protein kinase C (PKC) δ (Gerstin et al., 1998). This appears to contribute to hyperexcitability during alcohol withdrawal since L-type channel inhibitors decrease alcohol withdrawal seizures in rodents made dependent on ethanol (Little et al., 1986). In PC12 cells, increases in L-type channels are associated with increased abundance of mRNA for a specific $\alpha_1$1.2 splice variant (Walter et al., 2000). This does not require PKCδ, suggesting that PKCδ regulates $\alpha_1$1.2 translation, post-translational processing, or transport to the cell surface rather than $\alpha_1$1.2 mRNA transcription or splicing.

Chronic exposure to ethanol also increases the abundance of P-type currents in the rat inferior colliculus (N'Gouemo and Morad, 2003) and N-type channels in PC12 cells and in mouse frontal cortex and hippocampus (McMahon et al., 2000). In PC12 cells, increases in N-type channels require PKCε. It is not known whether this also involves increases in mRNA for the N-type channel subunit $\alpha_1$2.2. Recently, three $\alpha_1$2.2 splice variants have been described that are generated by exon skipping and modify channel function in the central nervous system (Lipscombe et al., 2002). Like other α_1 subunits, $\alpha_1$2.2 contains four homologous repeats (I-IV) each consisting of six transmembrane segments (S1-S6). There is a 21 amino acid sequence within the intracellular loop between repeats II and III that is encoded by exon 18a, and when present, shifts the voltage-dependence of inactivation towards more depolarized potentials (Pan and Lipscombe, 2000). The tetrapeptide SFMG in IVS3-4 is encoded by exon 24a, and when present shifts the voltage dependence of activation by about 2 mV to more positive potentials (Lin et al., 1999). The dipeptide Glu-Thr (ET) in IVS3-4 linker is encoded by exon 31a, and when present slows the rate of channel opening and shifts the voltage dependence of channel activation to more depolarized voltages (Lin et al., 1997; Lin et al., 1999).

Here we investigated whether ethanol alters levels of mRNA for $\alpha_1$2.2. Using PC12 cells, we found that ethanol selectively increases mRNA abundance for variants lacking ET in IVS3-4 linker. This is associated with altered channel kinetics that resembles kinetics ascribed to $\alpha_1$2.2 subunits lacking ET. Our results suggest a new mode

of ion channel regulation by ethanol that could contribute to neuronal hyperexcitability following chronic ethanol exposure.

MATERIALS AND METHODS

Materials. Radioisotopes and nucleotides were purchased from Amersham Pharmacia Biotech (Piscataway, NJ). Restriction endonucleases and modifying enzymes were purchased from Promega (Madison, WI). JM109 (Promega) and XL-1 Blue (Stratagene, La Jolla, CA) bacteria were used. All other reagents were analytical grade and were from Sigma Chemical (St. Louis, MO) or Gibco-BRL (Rockville, MD).

Cell culture. PC12 cells (J.Wagner, Cornell University) were cultured at 37°C in Dulbecco's modified Eagle's medium supplemented with 5% fetal calf serum, 10% horse serum, 50 units/ml penicillin, 50 μg/ml streptomycin and 2 mM glutamine in a humidified atmosphere of 90% air and 10% CO_2. Cells were cultured with 120-150 mM ethanol in tightly capped flasks and the medium was changed daily as in prior work (Gerstin et al., 1998). Control samples were cultured in parallel without ethanol.

Riboprobe generation. Full-length rat $\alpha_{1B\text{-}a}$ and $\alpha_{1B\text{-}c}$ cDNAs (gifts from D. Lipscombe, Brown University) were used as templates to generate probes for ET and SFMG splice variants. To generate a probe for ET, two oligonucleotide primers were constructed from rat $\alpha_{1B\text{-}a}$ (GenBank accession number AF055477) to flank the sequence GAAACG encoding ET in the IV S3-4 linker: HW32 (5'-CCGGAATTCCGGAGTATAAGACATG-3'), upstream with a *EcoRI* site incorporated

into sequence, and HW33 (3'-CGCGGATCCGCGATGAAGAACAGC-5') downstream with a *Bam HI* site incorporated into the sequence. To generate a probe for SFMG, two oligonucleotide primers were constructed from rat $\alpha_{1B\text{-}c}$ (GenBank accession number M92905) to flank the sequence GAGCTTCATGGA encoding SFMG in the III S3-4 linker: HW30 (5'-CCGGAATTCCGGGATTCTTGTGGTC-3'), upstream with a *EcoRI* site incorporated into sequence, and HW36 (3'-CGGGGYACCCCGACATTCTTCAGAG-5') downstream with a *Kpn1* site incorporated into the sequence.

The reaction mixture contained 1X Polymerase Chain Reaction (PCR) buffer (Perkin Elmer, Foster City, CA), 0.5 mM dNTP mix, 2.5 units Amplitaq (Perkin Elmer), and 100 pmol of each primer pair. The reaction mixture was heated to 94°C for 4 min, 55°C for 45 sec and 72°C for 2 min. This was followed by 30 amplification cycles, each consisting of 94°C for 1 min, 55°C for 45 sec and 72°C for 2 min. Finally, the mixture was incubated at 55°C for 45 seconds, 72°C for 10 minutes, and then placed on ice. PCR products were digested with the appropriate restriction enzymes and separated on a 1.2% agarose gel. The resultant fragments were excised and gel purified using a QIAEX II Gel Extraction kit (Qiagen, Chatsworth, CA). Purified fragments were subcloned into pGEM3Zf(+) (Promega) and positive colonies were sequenced. A *Hind III*-linearized plasmid was used as a template with T3 RNA polymerase to generate [α-^{32}P]CTP-labeled 582 bp cRNA probes.

Ribonuclease protection assay. Total RNA was extracted from PC12 cells using the RNA STAT-60 method (Tel-Test, Friendswood, TX) and quantified by optical

density at 260 nm. Ribonuclease protection assays (RPAs) were performed as described previously (Walter et al., 1999). Briefly, total RNA (20 μg) was dissolved in 30 μl of hybridization solution containing 60,000 cpm of a ^{32}P-labeled calcium channel subunit cRNA probe and 10,000 cpm of a ^{32}P-labeled GAPDH cRNA probe. The cRNA probes were allowed to anneal to the endogenous RNA at 45°C overnight. The next day, digestion was performed at 37°C for 30 minutes using an RNase solution containing a final concentration of 30 μg/ml RNase A (Ambion, Austin, TX) and 800 units RNase T1. The RNA:RNA hybrids were separated on a 5% polyacrylamide/8 M urea sequencing gel. The gel was dried and mRNA fragments were visualized, and densities calculated using a Storm 860 Phosphoimager and ImageQuant software (Amersham Biosciences, Piscataway, NJ). Century Template RNA markers (Ambion) were used to determine molecular weights.

Real-Time RT-PCR of Exon 18a containing splice variants. RNA, extracted from PC12 cells was reverse transcribed using the Ambion Retroscript kit. Taqman® (Applied Biosystems, Foster City, CA) fluorescent real-time RT-PCR was used to quantify transcripts containing (+21) or lacking (Δ21) exon 18a, with data normalized to β-actin. Primer and probe sequences were: +21 forward primer: CTG TAT CTC GCA GCT CAT CTG TCT, +21 reverse primer: AGC GCG CCT TGG CC, +21 Taqman probe: AGC GTA AAC TCA CCC AGG CAG CAG AAC. Δ21 forward primer: GAG TTC TGC TGC CTG GCA, Δ21 reverse primer: GCC AAA GAA GTA GCT GAA GTC A, Δ21 Taqman probe: AAT GGA GAT GTT GGC AGC AGA CAT GG, β-actin forward primer: CGT GAA AAG ATG ACC CAG ATC A, β-actin reverse primer: CAC AGC

CTG GAT GGC TAC GT, rat β-actin Taqman probe: TTT GAG ACC TTC AAC ACC CCA GCC A. Exon 18a probes were labeled at the 5' end with the reporter dye FAM. The β-actin probe was labeled at the 5' end with the reporter dye VIC. All probes were labeled at the 3' end with the quencher TAMRA. All primers and probes were synthesized by Applied Biosystems (Foster City, CA). Real-time PCR conditions were for +21: 95°C for 10min, followed by 40 cycles of (50°C for 60s, 95°C for 15s). Conditions for Δ21 and β-actin were identical except that the 50°C steps were at 53°C (Δ21) or 58°C (β-actin). All Taqman PCR reactions were carried out using the Taqman Universal Master Mix (Applied Biosystems). BLAST searches were performed to ensure all primer and probe sequences would not recognize targets other than those intended.

In order to ensure that performance of the +21 primer and probe would not be impaired by the presence of Δ21 sequence (and vice versa), positive control fragments were generated by PCR using the following primers: Forward CATTGCTGTGGACAACCTTGC (=JD 2825), reverse CCATGTGTGTCTTCATGTCTGGC (=JD 2826). Positive control fragments were generated using full length $\alpha_{1B\text{-}a}$ (+21) or $\alpha_{1B\text{-}a\text{-}+21}$ ((Δ21; Genbank accession number AF222337; from D. Lipscombe, Brown University) under the following conditions: 94°C for 1 minute, 25 cycles of (58°C for 45s, 72°C for 120s, 94°C for 60s), followed by a final 58°C for 45s and 72°C for 10 minutes. This generated positive control fragments for +21 (324bp) and Δ21 (261bp) respectively, which were gel-purified using the QiaQuick Gel Extraction Kit. To demonstrate specificity, increasing concentrations (0.4-8 pg) of

one control fragment were added to a reaction mixture containing 8 pg of the other control fragment and each +21 or Δ21 primer and probe set. Neither reaction was inhibited by the control fragment corresponding to the alternate splice variant. Primers for +21 amplified only the +21 control fragment. Primers for Δ21 weakly amplified the +21 control fragment (C_T = 15.32 for Δ21 fragment and C_T = 29.82 for +21 fragment).

All experiments were carried out according to the ABI 7700 Sequence Detection System User Bulletin #2 (Applied Biosystems). Standard curves for +21, Δ21 and β-actin were generated using a dilution series from a randomly selected PC12 cDNA sample. The same sample was used to construct the standard curve for all experiments. This standard curve was then used to calculate the amount, in arbitrary units, of each mRNA species in each cDNA sample. The amount of +/Δ21 was then divided by the amount of β-actin to give the relative expression level. Data for each treatment day was expressed relative to Day 0. Three sets of RNA were analyzed for each time point.

Electrophysiology. Patch clamp studies were performed using the nystatin perforated patch technique with a Dagan 8900 patch clamp amplifier. Current signals were filtered at 3 kHz. Experimental protocols were controlled using pClamp software (Axon Instruments, Union City, CA). Electrodes were coated with Sylgard to reduce pipette capacitance and fire polished just before recording to a resistance of 4 to 6 MΩ. The patch pipette solution consisted of (in mM) 135 CsCl, 10 $CaCl_2$, 1.2 $MgCl_2$, 25 HEPES, and 10 glucose in the tip. The electrode was backfilled with the same solution, to which 200 μg/ml nystatin was added. After formation of a gigaseal, the series resistance was monitored to evaluate when perforation was complete and stable. For the recording

of Ba^{2+} currents, the cells were perfused with a solution containing (in mM): 75 TEA-Cl, 20 NaCl, 20 $BaCl_2$, 5 KCl, 0.5 $CaCl_2$, 1.2 $MgCl_2$, 25 HEPES, 10 glucose, 0.001 tetrodotoxin citrate (Research Biochemicals International, Natick, MA), and 0.005 nifedipine (Sigma, St. Louis, MO). ω-conotoxinMVIIA (Sigma) was prepared as a 100-μM stock in H_2O containing 0.01% acetic acid. An inverted Olympus IX70 microscope equipped with an oil immersion 40x objective lens was used to observe cells loaded on glass coverslips (22 × 22mm No.1) coated with poly-ornithine and laminin attached to a chamber with a bath volume of approximately 50 μl (Warner Instrument Corp., Hamden, CT). Solutions were gravity fed from syringes through an automated snap valve system (Automate Scientific, Oakland, CA) into a micro-manifold with a single output into the chamber. The bath was constantly perfused at a rate of 1 ml/min, providing rapid exchange of the bath solution.

RESULTS

Chronic ethanol exposure increases the abundance of specific splice variants of $\alpha_1$2.2 in PC12 cells.

We previously found that ethanol-induced increases in L-type channels are associated with increased abundance of mRNA encoding a specific splice variant of $\alpha_1$1.2 (Walter et al., 2000). We therefore investigated whether ethanol-induced increases in N-type channels are associated with increased abundance of splice variants of the N-type channel specific subunit $\alpha_1$2.2. We examined three sets of alternative splice variants previously shown to modify N channel function (Lin et al., 1997; Lin et al., 1999; Pan and Lipscombe, 2000). All three are generated by exon inclusion/skipping, each resulting in two variants, one containing and the other lacking the exon.

We used a ribonuclease protection assay to study two variant pairs, one involving the dipeptide ET in the IVS3-4 linker and the other the tetrapeptide SFMG in the IIIS3-4 linker (Fig. 1). Signals corresponding to the predicted sizes for the fully protected probes were identified for ET (454 bp) and SFMG (394 bp). For each deleted variant, two bands were detected corresponding to predicted sizes for cleaved probes of 287 and 161 bp for ΔET, and 246 and 134 bp for ΔSFMG. These signals were normalized to those obtained for GAPDH. Exposure to 150 mM ethanol for 1-6 days increased the abundance of the variant lacking ET (ΔET) without altering the abundance of the ET variant (Fig. 2*A* and *B*). In contrast ethanol exposure increased the abundance of both SFMG splice variants (Fig. 2*A* and *C*). Increases in ΔET were associated with a 2-fold increase in the relative proportion of ΔET to ET forms (Fig. 2*D*). In

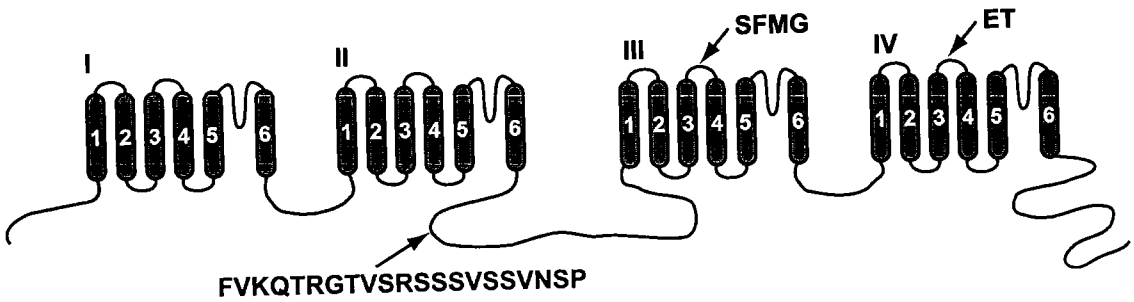

Fig. 1. Schematic diagram of the putative transmembrane topology of $\alpha_1$2.2. Shown are the approximate position of alternatively expressed exons 18a, 24a, and 31a. 18a encodes a 21 amino acid sequence, 24a encodes the tetrapeptide SFMG, and 31a encodes the dipeptide ET.

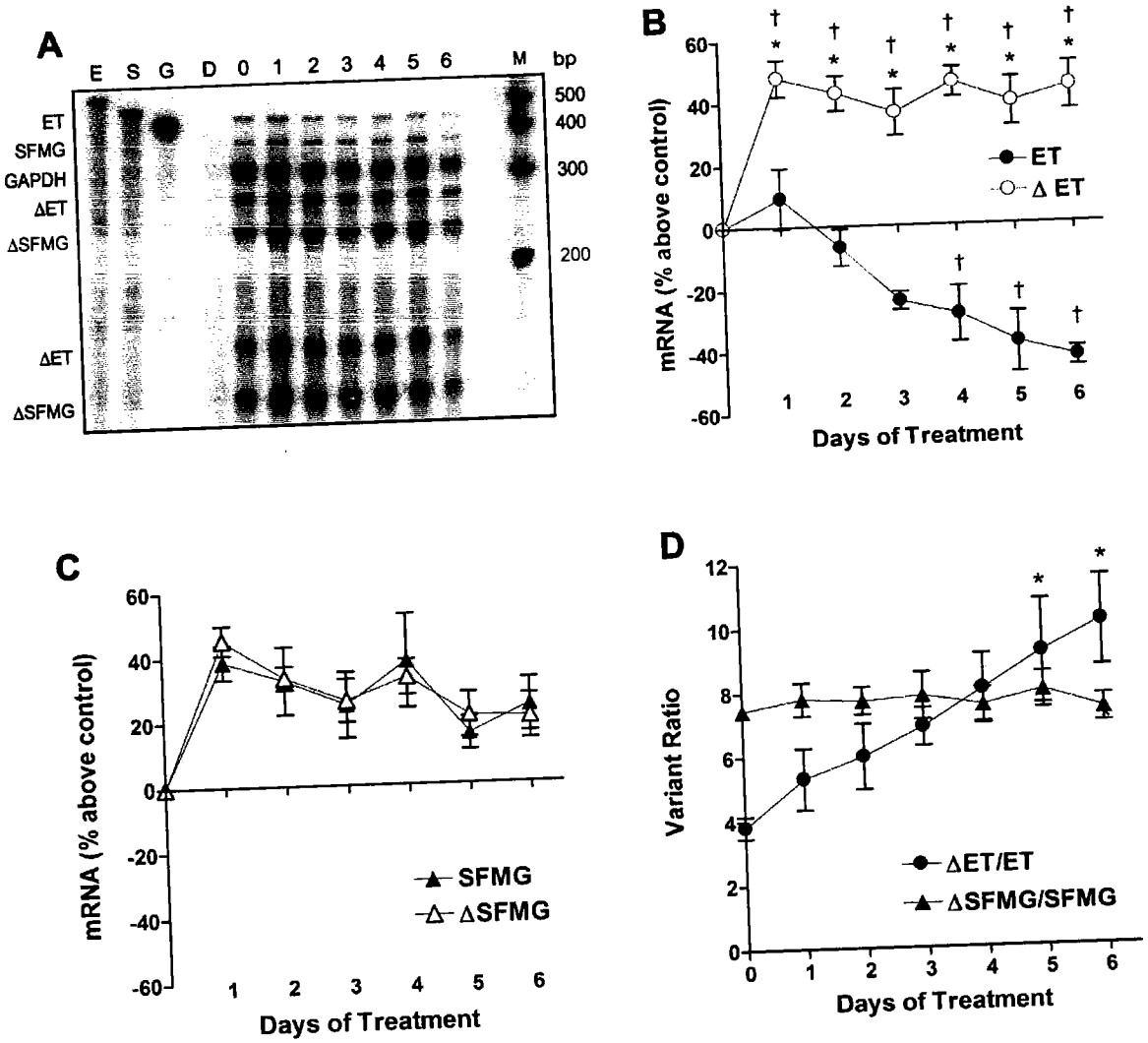

Fig. 2. Chronic ethanol exposure increases levels of ΔET and both SMFG $\alpha_1$2.2 splice variants. *A*, representative ribonuclease protection assay of samples from PC12 cells treated 0-6 days with 150 mM ethanol. Signals corresponding to the fully protected probes for ET, SFMG, and GAPDH appear at the top of the gel whereas two shorter bands corresponding to each of the cleaved probes for RNA species lacking ET (ΔET) or SFMG (ΔSFMG) appear in the lower portions of the gel. *B*, abundance of ET and ΔET is shown relative to levels in controls cells treated without ethanol. Two factor ANOVA

revealed a significant effect of splice variant type ($F = 255.8$, $p < 0.0001$) and day of treatment ($F = 5.55$, $p = 0.0007$) without an interaction between these two factors. $^{*}p < 0.05$ compared with ET and $^{\dagger}p < 0.05$ compared with day 0 (Bonferroni tests). *C*, abundance of SFMG and ΔSFMG variants is shown relative to control cells treated without ethanol. There was a significant effect of treatment day ($F=7.19$, $p < 0.0001$) without an effect of variant type ($F = 0.04$, $p =$ N.S.) or a significant interaction between these factors ($F = 0.18$, $p =$ N.S.). *D*, relative abundance of splice variants expressed as a ratio revealing a decline in the relative abundance of ΔET compared with the ET variant (one factor ANOVA: $F=4.21$, $p = 0.0125$), without a change in the relative abundance of the two SFMG variants (one factor ANOVA, $F = 0.19$, $p =$ N.S.). $^{*}p < 0.05$ compared with day 0 (Dunnett's test).

contrast chronic ethanol exposure did not alter the relative proportion of ΔSFMG to SFMG containing variants (Fig. 2*D*).

We used real-time RT-PCR to quantify the relative abundance of the third variant pair involving a 21-amino acid peptide in the II-III intracellular loop (Fig. 1). These data were normalized to β-actin mRNA, which is unaffected by chronic ethanol exposure in neuronal tissues (Hirouchi et al., 1993; Nakahara et al., 2002; Sohma et al., 1999). We found that after one day of ethanol exposure there was a modest increase in both +21 and Δ21 variants (Fig. 3). The level of +21 mRNA returned to baseline by the second day of ethanol exposure whereas Δ21 mRNA remained elevated until day 5.

Chronic ethanol exposure alters N-type channel activation kinetics and threshold.

Since chronic exposure to ethanol selectively increased the expression of the ΔET variant, we examined whether this was associated with a change in channel function. Based on previous work (Lin et al., 1999) we predicted that the increased abundance of ΔET containing channels would shift the voltage dependence of channel activation to more negative potentials and increase the rate of channel opening. Nifedipine (5 uM) was introduced in these studies to block L-type channels, resulting in a predominance of current flowing through N-type channels. We chose to focus on the first 20 ms of the voltage step, where the kinetics could be well fit by a first order exponential. The currents in cells treated with 150 mM ethanol for 6 days activated faster than in control cells, as seen in the averaged macroscopic current (Fig. 4*A*). In these experiments, there remained the possibility that although L-type currents were blocked, a small contribution from

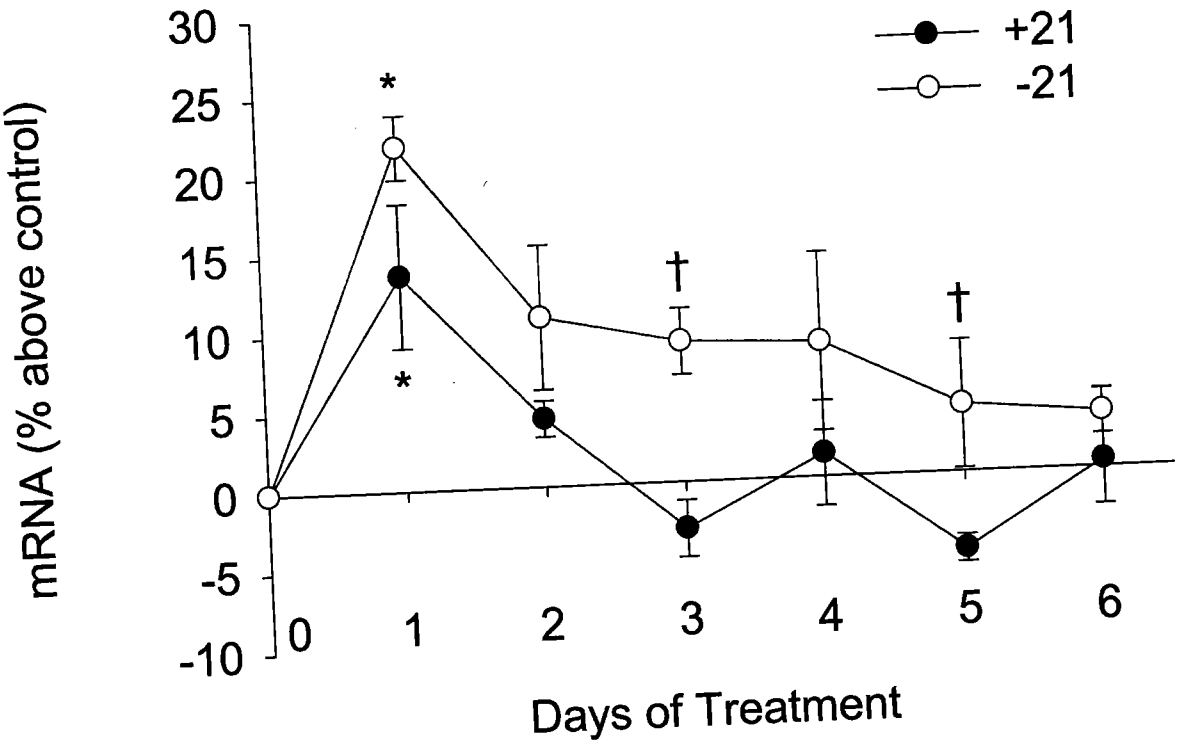

Fig. 3. Ethanol increases both variants of exon 18a in the II-III intracellular loop of $\alpha_1$2.2. Shown is the relative abundance of mRNA encoding variants containing (+21) or excluding (Δ21) exon 18a after exposure to 150 mM ethanol. Data are expressed relative to untreated control. Two way ANOVA revealed main effects of splice variant type [$F(1, 28) = 16.713$, $p < 0.001$] and day [$F(6, 28) = 8.74$, ;$p < 0.001$], without a significant interaction between these two factors. $^{*}p < 0.05$ compared with day 0 within each variant and $^{\dagger}p < 0.05$ compared with +21 on the same day (Tukey test).

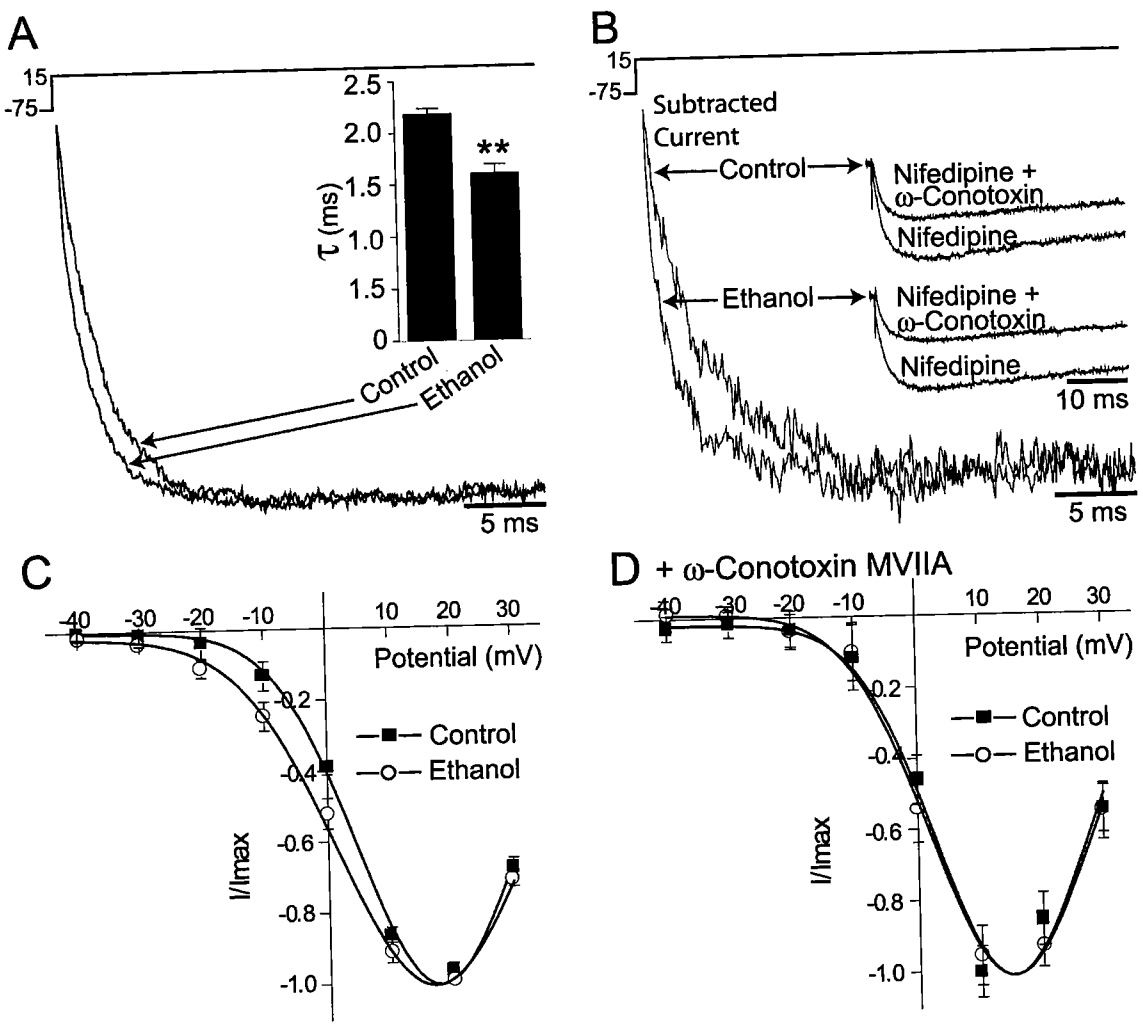

Fig. 4. Rate of activation and voltage dependence of N-type voltage gated Ca^{2+} channels. *A*. Ba^{2+} currents in the presence of 5μM nifedipine during a 50 msec depolarizing step from –75 mV to +15 mV in either control cells (n = 9) or cells treated with 150 mM ethanol for 6 days (n = 11). The time constant (first order exponential fit for the first 20 msec of depolarizing pulse) for ethanol treated cells (1.59 ±0.09 ms) was significantly less (p = 0.007) than for control cells (2.17 ± 0.06 ms). *B*. N-type current isolated by subtraction technique (see text) from a representative control and ethanol

treated cell. Inset shows traces used to compute the "subtracted" currents. 800 nM ω-conotoxin MVIIA inhibited 44 ± 3% (no ethanol treatment, n=6) and 52 ± 4% (ethanol-treated, n=6), of the Ba^{++} current remaining in the presence of 5 μM nifedipine. *C.* Averaged current-voltage plot, normalized using the minimum of the Gaussian fit, showing a difference in the voltage-dependence of channel activation between control (n=9) and ethanol treated (n=11) cells (V_h = -75 mV). *D.* Averaged current-voltage plot, normalized using the minimum of the Gaussian fit, shows no difference in the voltage-dependence of channel activation between control (n=6) and ethanol treated (n=6) cells when N-type channels are blocked by 800 nM ω-conotoxin MVIIA (V_h = -75 mV).

other voltage-gated calcium channel types contributed to the shift in kinetic properties, leading to an incorrect attribution of a change in N-type splice variant. To address this, we performed additional experiments in which the current in nifedipine + ω-conotoxin MVIIA (800 nM) was subtracted from currents obtained in the presence of nifedipine alone (Fig. 4*B* inset), yielding an uncontaminated N-type current (Fig. 4*B*), before and after chronic ethanol exposure. Our results using this technique confirm that it is, indeed, a modification of the N-type current that leads to the accelerated activation kinetics. Currents also activated at more negative test potentials following ethanol treatment (Fig. 4*C*), consistent with the expression of the ΔET variant. This shift in the current-voltage relationship was absent when N-type current was eliminated by ω-conotoxin MVIIA treatment (Fig. 4*D*).

Ethanol-induced increase in ΔET $\alpha_1$2.2 mRNA is not dependent on PKCε.

In PC12 cells, ethanol-induced increases in N-type channel function and ω-conotoxin GVIA binding require PKCε since these effects are not present in cell lines that express the C2-like domain of PKCε which acts a dominant-negative inhibitor of PKCε (McMahon et al., 2000). We used these same cell lines to examine whether ethanol-induced increases in the abundance of $\alpha_1$2.2 splice variants are also PKCε-dependent. Similar to what was observed in the parent PC12 cell line (Fig. 2), exposure to 150 mM ethanol for 1-6 days increased the abundance of ΔET and both SFMG forms in ε1V1

PC12 cells that express the PKCε inhibitor (Fig. 5). Similar results were obtained using a second PC12 cell line, ε2V1 (data not shown).

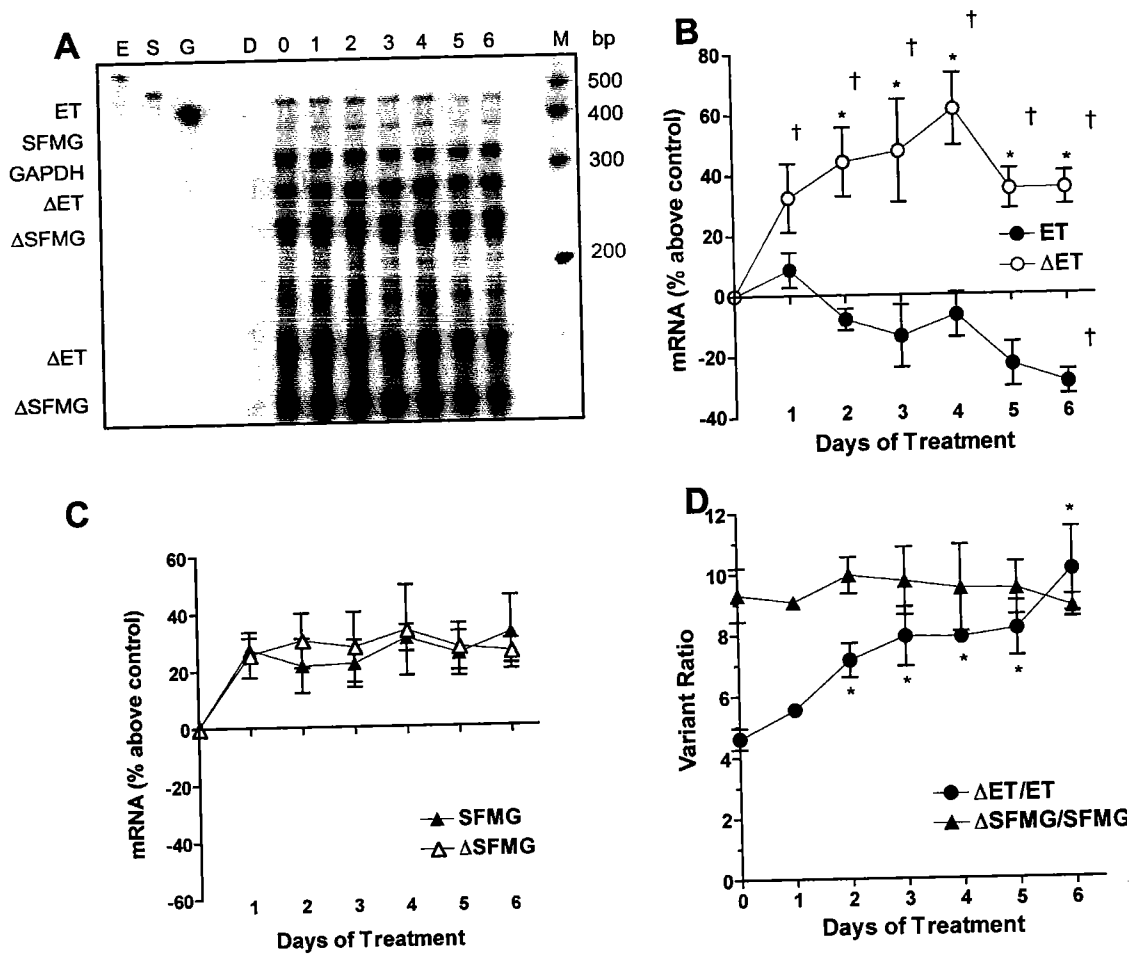

Fig. 5. Ethanol-induced changes in ET and SMFG $\alpha_1$2.2 splice variants in cells expressing the C2-like domain of PKCε. *A*, representative ribonuclease protection assay of samples from V1ε2 cells treated 0-6 days with 150 mM ethanol. *B*, abundance of ET and ΔET is shown relative to levels in control cells treated without ethanol. Two factor ANOVA revealed a significant effect of splice variant type ($F = 102.9$, $p < 0.0001$) and day of treatment ($F = 2.81$, $p = 0.029$) with a significant interaction between these two factors ($F = 4.29$, $p = 0.0035$). $^*p < 0.05$ compared with ET on the same day and $^\dagger P<0.05$ compared with day 0 (Bonferroni *post hoc* tests). *C*, abundance of SFMG and

ΔSFMG variants is shown relative to control cells treated without ethanol. Two-way ANOVA showed a significant main effect of treatment day ($F = 3.05$, $p = 0.02$) but no effect of variant type ($F = 0.12$, p = N. S.), and there was no significant interaction between these factors ($F = 0.17$, p = N.S.). *D*, relative abundance of splice variants expressed as a ratio revealing a decline in the relative abundance of ΔET compared with the ET variant (one factor ANOVA; $F=5.43$, $p = 0.04$), without a change in the relative abundance of the two SFMG variants ($F=0.18$, p = N.S.). $^*p < 0.05$ compared with day 0 (Dunnett's *post hoc* test).

DISCUSSION

In this study we found that chronic exposure to ethanol increases the abundance of mRNA for specific splice variants of $\alpha_1$2.2. These include mRNAs that contain or lack the tetrapeptide SFMG encoded by exon 24a, contain or lack the 21 amino acid peptide encoded by exon 18a, and lack the dipeptide ET encoded by exon 31a. Although the ET-containing variant is expressed in PC12 cells, its abundance was not increased by chronic ethanol exposure. Rather ethanol selectively increased the level of ΔET, suggesting that ethanol can modulate alternative splicing. This was associated with a shift in the voltage dependence of channel activation to more negative potentials and an increase in the rate of channel opening, which are properties associated with ΔET variants of $\alpha_1$2.2 (Lin et al., 1997; Lin et al., 1999). This suggests that increased abundance of ΔET variants contributes to these ethanol-induced changes in channel kinetics. Such changes in channel function are predicted to generate a more active population of N-type channels (Lin et al., 1999) and thus could contribute to neuronal hyperexcitability associated with alcohol withdrawal.

This change in N-type channel function occurred even though the absolute increase in the relative abundance of ΔET mRNA was not very large. In control cells ΔET forms accounted for approximately 80% of the total $\alpha_1$2.2 mRNA pool and following alcohol exposure for 6 days, this increased to 90%. In contrast, the change in N-type channel function was clearly discerned and similar in magnitude to that observed in oocytes expressing ΔET subunits of $\alpha_1$2.2 compared with oocytes expressing ET-containing subunits. This suggests that the change in ΔET mRNA we observed in PC12

cells underestimated the increase in abundance in subunit proteins lacking the ET sequence. Alternatively other ethanol-induced changes in channel subunits or in coupling to G proteins and kinases may have contributed to these kinetics. For example, we previously found that similar exposure of PC12 cells to ethanol increases the abundance of β_{1b} subunits of calcium channels (Walter et al., 2000). Expression of β_{1b} with $\alpha_1$2.2, results in P/Q-type channels that activate at more negative potentials compared with channels containing β_{2a} or β_3 subunits (De Waard and Campbell, 1995). Since β_{1b} subunits associate with $\alpha_1$2.2 (Scott et al., 1996), it is possible that ethanol-induced increases in β_{1b} also contributed to the kinetic changes we observed with N-type currents.

Chronic exposure of neuronal cells in culture to ethanol has been associated with increased abundance of mRNA for several genes including the heat shock protein HSC70 (Miles et al., 1991), the glucose regulated proteins GRP78 and GRP94 (Miles et al., 1994), dopamine β-hydroxylase (Fletcher and Shain, 1993; Thibault et al., 2000), glial fibrallary acidic protein (Fletcher and Shain, 1993), the α_2 adrenergic receptor (Hu et al., 1993), the delta opioid receptor (Charness et al., 1993), and the NR2B subunit of the NMDA receptor (Kumari, 2001). In none of these studies were changes in splice variants examined. Although chronic ethanol treatment does not increase the abundance of total mRNA for the NR1 subunit of the NMDA receptor, it decreases mRNA and protein levels of exon-5 containing splice variants (Kumari, 2001). It is not known if this alters receptor function. We recently demonstrated that chronic exposure of PC12 cells to ethanol increases the abundance of a specific splice variant of the L-type channel subunit $\alpha_1$1.2 (Walter et al., 2000). However, no particular functional change could be ascribed

to this variant. In contrast, in the present study, we found that the increase in ΔET variants of $\alpha_1$2.2 in ethanol-treated cells is potentially functionally significant. Our findings suggest that ethanol can alter protein function by selectively regulating the abundance of specific splice variants of genes. This indicates a new mechanism by which ethanol can regulate gene expression and function. Further work will be necessary to determine whether ethanol regulates splicesome function or modulates the stability and transport of specific mRNA species.

Our previous work with L-type channels demonstrated that ethanol-induced increases in the abundance of L-type channels are dependent on PKCδ (Gerstin et al., 1998). However, ethanol-induced changes in $\alpha_1$1.2 splice variants are not PKCδ dependent (Walter et al., 2000). Likewise, in the present study we found that although ethanol-induced increases in N-type channels require PKCε (McMahon et al., 2000), the increase in the ΔET splice variant or both SFMG variants of $\alpha_1$2.2 is not PKCε-dependent. This suggests that both PKCδ and PKCε regulate calcium channel expression downstream of transcription and RNA processing. It is not yet known whether these PKC isozymes regulate translation, trafficking, or assembly of calcium channel subunit protein complexes. One possibility is that these PKC isozymes are important for the cellular localization of N-type and L-type calcium channels in neuronal cells. For example, PKCε is abundant at growth cones and in neurites of differentiated PC12 cells (Hundle et al., 1997) and in nerve fibers in brain (Saito et al., 1993). Studies in primary neurons and in brain have demonstrated predominant localization of N-type channels to axon terminals and distal dendrites (Mills et al., 1994; Westenbroek et al., 1992). In

addition, recent work has established that PKCε exists in a complex with $\alpha_1$2.2 and is coupled to this N channel subunit through a linker protein, ENH (Maeno-Hikichi et al., 2003). This interaction may not only facilitate selective regulation of N-type calcium channels by PKCε (Maeno-Hikichi et al., 2003) but it might also direct the subcellular localization of N-type calcium channels in neuronal cells.

ACKNOWLEDGEMENTS

We thank Helen Walter for expert technical assistance and Diane Lipscombe for supplying $\alpha_1$2.2 plasmids. This work was supported by NIAAA grants AA08003 to S.T. and AA08117 and AA013588 to R.O.M.., and by funds provided by the State of California for medical research on alcohol and substance abuse through the University of California at San Francisco.

REFERENCES

Brennan CH, Crabbe J and Littleton JM (1990) Genetic regulation of dihydropyridine-sensitive calcium channels in brain may determine susceptibility to physical dependence on alcohol. *Neuropharmacology* **29**:429-432.

Charness ME, Hu G, Edwards RH and Quermit LA (1993) Ethanol increases δ-opioid receptor gene expression in neuronal cell lines. *Mol Pharmacol* **44**:1119-1127.

De Waard M and Campbell KP (1995) Subunit regulation of the neuronal α_{1A} Ca^{2+} channel expressed in Xenopus oocytes. *J Physiol* **485**:619-634.

Dunlap K, Luebke JI and Turner TJ (1995) Exocytotic Ca^{2+} channels in mammalian central neurons. *Trends Neurosci* **18**:89-98.

Ertel EA, Campbell KP, Harpold MM, Hofmann F, Mori Y, Perez-Reyes E, Schwartz A, Snutch TP, Tanabe T, Birnbaumer L, Tsien RW and Catterall WA (2000) Nomenclature of voltage-gated calcium channels [letter]. *Neuron* **25**:533-535.

Fletcher TL and Shain W (1993) Ethanol-induced changes in astrocyte gene expression during rat central nervous system development. *Alcohol Clin Exp Res* **17**:993-1001.

Gerstin E, McMahon T, Hundle B, Dadgar J and Messing RO (1998) Protein kinase C δ mediates ethanol-induced up-regulation of L–type calcium channels. *J Biol Chem* **273**:16409-16414.

Ghosh A and Greenberg ME (1995) Calcium signaling in neurons: Molecular mechanisms and cellular consequences. *Science* **268**:239-247.

Grant AJ, Koski G and Treistman SN (1993) Effect of chronic ethanol on calcium currents and calcium uptake in undifferentiated PC12 cells. *Brain Res* **600**:280-284.

Hirouchi M, Hashimoto T and Kuriyama K (1993) Alteration of GABAA receptor alpha 1-subunit mRNA in mouse brain following continuous ethanol inhalation. *Eur J Pharmacol* **247**:127-130.

Hu G, Querimit LA, Downing LA and Charness ME (1993) Ethanol differentially increases alpha 2-adrenergic and muscarinic acetylcholine receptor gene expression in NG108-15 cells. *J Biol Chem* **268**:23441-23447.

Hundle B, McMahon T, Dadgar J, Chen C-H, Mochly-Rosen D and Messing RO (1997) An inhibitory fragment derived from protein kinase C ε prevents enhancement of nerve growth factor responses by ethanol and phorbol esters. *J Biol Chem* **272**:15028-15035.

Knott TK, Dopico AM, Dayanithi G, Lemos J and Treistman SN (2002) Integrated channel plasticity contributes to alcohol tolerance in neurohypophysial terminals. *Mol Pharmacol* **62**:135-142.

Kumari M (2001) Differential effects of chronic ethanol treatment on N-methyl-D-aspartate R1 splice variants in fetal cortical neurons. *J Biol Chem* **276**:29764-29771.

Lin Z, Haus S, Edgerton J and Lipscombe D (1997) Identification of functionally distinct isoforms of the N-type Ca2+ channel in rat sympathetic ganglia and brain. *Neuron* **18**:153-166.

Lin Z, Lin Y, Schorge S, Pan JQ, Beierlein M and Lipscombe D (1999) Alternative splicing of a short cassette exon in alpha1B generates functionally distinct N-type calcium channels in central and peripheral neurons. *J Neurosci* **19**:5322-5331.

Lipscombe D, Pan JQ and Gray AC (2002) Functional diversity in neuronal voltage-gated calcium channels by alternative splicing of Ca(v)alpha1. *Mol Neurobiol* **26**:21-44.

Little HJ (1991) Mechanisms that may underlie the behavioural effects of ethanol. *Prog Neurobiol* **36**:171-194.

Little HJ, Dolin SJ and Halsey MJ (1986) Calcium channel antagonists decrease the ethanol withdrawal syndrome. *Life Sci* **39**:2059-2065.

Maeno-Hikichi Y, Chang S, Matsumura K, Lai M, Lin H, Nakagawa N, Kuroda S and Zhang JF (2003) A PKC epsilon-ENH-channel complex specifically modulates N-type Ca2+ channels. *Nat Neurosci* **6**:468-475.

McMahon T, Andersen R, Metten P, Crabbe JC and Messing RO (2000) Protein kinase C epsilon mediates up-regulation of N-type calcium channels by ethanol. *Mol Pharmacol* **57**:53-58.

Messing RO, Carpenter CL and Greenberg DA (1986) Ethanol regulates calcium channels in clonal neural cells. *Proc Natl Acad Sci USA* **83**:6213-6215.

Miles MF, Diaz JE and DeGuzman VS (1991) Mechanisms of neuronal adaptation to ethanol: Ethanol induces Hsc70 gene transcription in NG108-15 neuroblastoma x glioma cells. *J Biol Chem* **266**:2409-2414.

Miles MF, Wilke N, Elliot M, Tanner W and Shah S (1994) Ethanol-responsive genes in neural cells include the 78-kilodalton glucose-regulated protein (GRP78) and 94-kilodalton glucose-regulated protein (GRP94) molecular chaperones. *Mol Pharmacol* **46**:873-879.

Mills LR, Niesen CE, So AP, Carlen PL, Spigelman I and Jones OT (1994) N-type Ca^{2+} channels are located on somata, dendrites, and a subpopulation of dendritic spines on live hippocampal pyramidal neurons. *J Neurosci* **14**:6815-6824.

N'Gouemo P and Morad M (2003) Ethanol withdrawal seizure susceptibility is associated with upregulation of L- and P-type Ca2+ channel currents in rat inferior colliculus neurons. *Neuropharmacology* **45**:429-437.

Nakahara T, Hirano M, Uchimura H, Shirali S, Martin CR, Bonner AB and Preedy VR (2002) Chronic alcohol feeding and its influence on c-Fos and heat shock protein-70 gene expression in different brain regions of male and female rats. *Metabolism* **51**:1562-1568.

Pan JQ and Lipscombe D (2000) Alternative splicing in the cytoplasmic II-III loop of the N-type Ca channel alpha1B subunit: Functional differences are beta subunit-specific. *J Neurosci* **20**:4769-4775.

Saito N, Itouji A, Totani Y, Osawa I, Koide H, Fujisawa N, Ogita K and Tanaka C (1993) Cellular and intracellular localization of ε-subspecies of protein kinase C in the rat brain; presynaptic localization of the ε-subspecies. *Brain Res* **607**:241-8.

Scott VES, De Waard M, Liu H, Gurnett CA, Venzke DP, Lennon VA and Campbell KP (1996) β Subunit heterogeneity in N-type Ca2+ channels. *J Biol Chem* **271**:3207-3212.

Sohma H, Hashimoto E, Shirasaka T, Tsunematsu R, Ozawa H, Boissl KW, Boning J, Riederer P and Saito T (1999) Quantitative reduction of type I adenylyl cyclase in human alcoholics. *Biochim Biophys Acta* **1454**:11-18.

Thibault C, Lai C, Wilke N, Duong B, Olive MF, Rahman S, Dong H, Hodge CW, Lockhart DJ and Miles MF (2000) Expression profiling of neural cells reveals specific patterns of ethanol-responsive gene expression. *Mol Pharmacol* **58**:1593-600.

Walter HJ, Berry M, Hill DJ, Cwyfan-Hughes JM, Holly JMP and Logan A (1999) Distinct sites of insulin-like growth factor (IGF)-II expression and localization in lesioned rat brain: Possible roles of IGF binding proteins (IGFBPs) in the mediation of IGF-II activity. *Endocrinol* **140**:520-532.

Walter HJ, McMahon T, Dadgar J, Wang D and Messing RO (2000) Ethanol regulates calcium channel subunits by protein kinase C delta -dependent and -independent mechanisms. *J Biol Chem* **275**:25717-25722.

Westenbroek RE, Hell JW, Warner C, Dubel SJ, Snutch TP and Catterall WA (1992) Biochemical properties and subcellular distribution of an N-type calcium channel α1 subunit. *Neuron* **9**:1099-1115.

CHAPTER THREE

Distinct Intracellular Calcium Profiles

Following Influx Through N vs. L Type Calcium Channels:

Role of Ca^{2+}-induced Ca^{2+} release

As published in the Journal of Neurophysiology (2004)

ABSTRACT

Selective activation of neuronal functions by Ca^{2+} is determined by the kinetic profile of the intracellular calcium ($[Ca^{2+}]_i$) signal, in addition to its amplitude. Concurrent electrophysiology and ratiometric calcium imaging were used to measure transmembrane Ca^{2+} current and the resulting rise and decay of $[Ca^{2+}]_i$ in differentiated pheochromocytoma (PC12) cells. We show that equal amounts of Ca^{2+} entering through N-type and L-type voltage gated Ca^{2+} channels result in significantly different $[Ca^{2+}]_i$ temporal profiles. When the contribution of N-type channels was reduced by ω-conotoxin MVIIA treatment, a faster $[Ca^{2+}]_i$ decay was observed. Conversely, when the contribution of L-type channels was reduced by nifedipine treatment, $[Ca^{2+}]_i$ decay was slower. Potentiating L-type current with BayK8644, or inactivating N-type channels by shifting the holding potential to -40 mV, both resulted in a more rapid decay of $[Ca^{2+}]_i$. Channel-specific differences in $[Ca^{2+}]_i$ decay rates were abolished by depleting intracellular Ca^{2+} stores with thapsigargin or by blocking ryanodine receptors with ryanodine, suggesting the involvement of Ca^{2+}-induced Ca^{2+} release (CICR). Further support for involvement of CICR is provided by the demonstration that caffeine slowed $[Ca^{2+}]_i$ decay while ryanodine at high concentrations increased the rate of $[Ca^{2+}]_i$ decay. We conclude that Ca^{2+} entering through N-type channels is amplified by ryanodine receptor mediated CICR. Channel-specific activation of CICR provides a mechanism whereby the kinetics of intracellular Ca^{2+} leaves a fingerprint of the route of entry, potentially encoding the selective activation of a subset of Ca^{2+}-sensitive processes within the neuron.

INTRODUCTION

Depolarizing a neuron opens voltage gated Ca^{2+} channels (VGCC), leading to an influx of Ca^{2+} ions into the cytoplasm, where Ca^{2+} sensitive signaling cascades are stimulated. Many neuronal functions, including neurotransmitter release, membrane excitability, gene expression, enzyme activity, cell growth, and apoptosis are sensitive to calcium (Berridge, 1998). The kinetic profile of intracellular calcium concentration ($[Ca^{2+}]_i$), in conjuction with the colocalization of Ca^{2+}-sensitive signaling proteins with particular ion channels (Sheng and Sala, 2001;Marrion and Tavalin, 1998) may help to explain how the ubiquitous calcium ion can selectively modulate this large array of neuronal functions (Dolmetsch et al., 1997;Chawla and Bading, 2001). The $[Ca^{2+}]_i$ profile following a depolarization is the sum of Ca^{2+} influx, Ca^{2+}- induced Ca^{2+} release (CICR), buffering, and extrusion from the neuron.

In addition to the absolute levels of $[Ca^{2+}]_i$, the temporal characteristics of $[Ca^{2+}]_i$ signals are critical in the integration of coincident signals underlying forms of synaptic plasticity such as long term potentiation (LTP) and long term depression (LTD). Mechanisms that render a neuron sensitive to the duration of a $[Ca^{2+}]_i$ signal include the activation of CaMKII, which can become Ca^{2+} independent due to autophosphorylation when neighboring subunits are coincidentally complexed with Ca^{2+} bound calmodulin (Miller and Kennedy, 1986). The temporal regulation of $[Ca^{2+}]_i$ signals is also important in the activation of Ca^{2+}-activated potassium channels which regulate the shape and frequency of action potentials, and in the activity-dependent changes in gene transcription controlled by CREB phosphorylation. While the relationship between the $[Ca^{2+}]_i$ transient

and many neuronal functions has been established, it is not well understood how a neuron shapes the $[Ca^{2+}]_i$ transient subsequent to depolarization.

This study utilizes concurrent electrophysiology and ratiometric calcium imaging to measure transmembrane Ca^{2+} current and the resulting rise and decay of $[Ca^{2+}]_i$ in differentiated pheochromocytoma (PC12) cells. This combination of techniques allows fine control and monitoring of the amplitude and temporal characteristics of Ca^{2+} influx. Differentiated PC12 cells are a neuronal cell line previously used to study the specificity of Ca^{2+} signaling. Examples include the differential induction of gene transcription, regulated by the route of Ca^{2+} entry into the cell (West et al., 2001), and the presence of fast and slow Ca^{2+}-dependent exocytosis, triggered by synaptotagmins with differing Ca^{2+} affinities (Sugita et al., 2002). Moreover, recent studies have explored the characteristics and distribution of ryanodine and IP_3 –mediated calcium stores in this cell line (Johenning et al., 2002). The PC12 cell line contains several VGCC's, the expression of which can be manipulated by nerve growth factor induced differentiation, and that can be isolated pharmacologically and with different voltage protocols, allowing experimental manipulation of the route of entry of Ca^{2+} during a depolarizing pulse. Precedents for channel-specific linkage to CICR in neurons exist (Usachev and Thayer, 1997;Sandler and Barbara, 1999;Akita and Kuba, 2000), although there was a predominance of N-type current over L-type in each case, leaving the possibility that it was the amount of calcium entering each channel type, not the route of entry that was critical. We show that Ca^{2+} influx through N-type channels is amplified by CICR from intracellular stores while Ca^{2+} entering through L-type channels does not lead to coupled CICR. Thus, equal amounts of

Ca^{2+} entering through these two channel types resulted in significantly different $[Ca^{2+}]_i$ temporal profiles.

MATERIALS AND METHODS

Patch clamp studies were performed using the nystatin perforated patch technique with a Dagan 8900 patch clamp amplifier. Current signals were filtered at 3 kHz. Experimental protocols were controlled using Pclamp software (Axon Instruments). Electrodes were coated with Sylgard to reduce pipette capacitance and fire polished just before recording to a resistance of 4 to 6 MΩ. The patch pipette solution consisted of (in mM) 135 CsCl; 10 $CaCl_2$; 1.2 $MgCl_2$; 25 HEPES; 10 glucose in the tip. The electrode was backfilled with the same solution, to which 200 μg/ml nystatin was added. After formation of a gigaseal, the series resistance was monitored to evaluate when perforation was complete and stable

Microscope and Perfusion System.

An inverted Olympus IX70 microscope equipped with an oil immersion 40x objective lens was used to observe cells loaded on glass coverslips (22x22mm No.1) coated with poly-ornithine and laminin attached to a chamber with a bath volume of approximately 50 μl (Warner Instrument Corp., Hamden, CT). Solutions were gravity fed from syringes through an automated snap valve system (Automate Scientific, Oakland, CA) into a micro-manifold with a single output into the chamber. The bath was constantly perfused at a rate of 1 ml/min, providing rapid exchange of the bath solution.

$[Ca^{2+}]_i$ measurement.

Fluorescence images with excitation at 340 and 380 nm were recorded with an intensified CCD camera. The imaging system (Ionoptix Corp.) utilizes a high speed chopper mirror to alternate between wavelengths so that fast calcium events can be measured. Four images were averaged at each wavelength for each time point to improve the signal to noise ratio. The concentration of $[Ca^{2+}]_i$ was calculated from the ratio of the fluorescence at two different wavelengths using the equation $[Ca^{2+}]_i = Kd \times (R-R_{min})/(R_{max}-R) \times \beta$, where Kd is the dissociation constant for fura-2; R_{min} and R_{max} are the 340/380 nm (background subtracted) ratio for fura-2 free acid in zero Ca^{2+} and 1 mM Ca^{2+}, respectively; and β is the ratio (background subtracted) between fura-2 free acid in zero Ca^{2+} and 1 mM Ca^{2+} at 380 nm excitation (Grynkiewicz et al., 1985).

Culturing of PC12 Cells.

PC12 cells were grown in Dulbecco's modified Eagle's medium (Sigma, St. Louis, MO) supplemented with 5% fetal calf serum (Sigma), 10% horse serum (J.H.R Biosciences, Lenexa, KS), 50 units/ml penicillin G (Sigma), and 50 mg/ml streptomycin (Sigma). A solution containing (mM): 130 NaCl; 5 KCl; 2.2 $CaCl_2$; 1 $MgCl_2$; 25 HEPES; 10 glucose was used for dye loading with 5 μM Fura-2-AM for 30 minutes at 37°C, and perfusion of cells at a rate of 1ml/min at room temperature (20°C). For recordings, the cells were switched to a perfusion solution containing (mM): 65 TEA-Cl; 40 NaCl; 5 KCl; 20 $CaCl_2$; 1 $MgCl_2$; 25 HEPES; 10 Glucose.

Statistics.

The decay of $[Ca^{2+}]_i$ was fit with linear growth curves on natural log values using an ANOVA for a mixed model using restricted estimation by maximal likelihood. The natural log transformation resulted in approximately linear functions with errors that approximate a normal distribution. A model of the natural log transformation with a single slope was compared to a model with different slopes for each condition. The assumption of normality was evaluated both by investigating the plots of variation and using the Kolmogorov-Smirnoff test. The ratios of $[Ca^{2+}]_i$ divided by current (Fig 5) were compared using a one-way ANOVA with post hoc comparisons using a Sheffe test.

RESULTS

Channel isolation by pharmacological blockade

The reproducibility of the current and $[Ca^{2+}]_i$ profile in response to a voltage step (Fig. 1*A*) within each cell allowed for the reliable comparison of signals between control and treatment conditions. In order to achieve reproducible elevations of $[Ca^{2+}]_i$ within a cell it was necessary to wait over 180 seconds between stimulations, presumably reflecting the time for all Ca^{2+} sequestration processes to return to pre-stimulus states. Comparisons between $[Ca^{2+}]_i$ following influx through different types of VGCC's requires the ability to manipulate and measure both electrical signal and digital imaging signal over a critical range of stimulation. We compare the time-integrated (area under the curve for the 20 sec following depolarization) elevation of $[Ca^{2+}]_i$ with the time-integrated Ca^{2+} charge flux. In all cases, the duration of measured $[Ca^{2+}]_i$ elevation was at least two orders of magnitude longer than the duration of current flow. Ca^{2+} influx through voltage-gated channels was modulated in three ways: 1) varying the duration of the depolarizing pulse (Fig. 1*B*), 2) varying the amplitude of the depolarizing pulse (Fig. 1*C*), and 3) varying the extracellular Ca^{2+} concentration while using a constant pulse protocol (Fig. 1*D*). Each of these protocols produced a level of $[Ca^{2+}]_i$ that varied linearly with the level of aggregate Ca^{2+} current. Work done in other neuronal systems (Hua et al., 1993;Stuenkel, 1994), has shown that a non-linear relationship between Ca^{2+} entry and $[Ca^{2+}]_i$ can occur under heavy stimulation protocols, attributable to activation of a high capacity, low affinity buffer (presumably mitochondria), or under light Ca^{2+} loading, where a low capacity

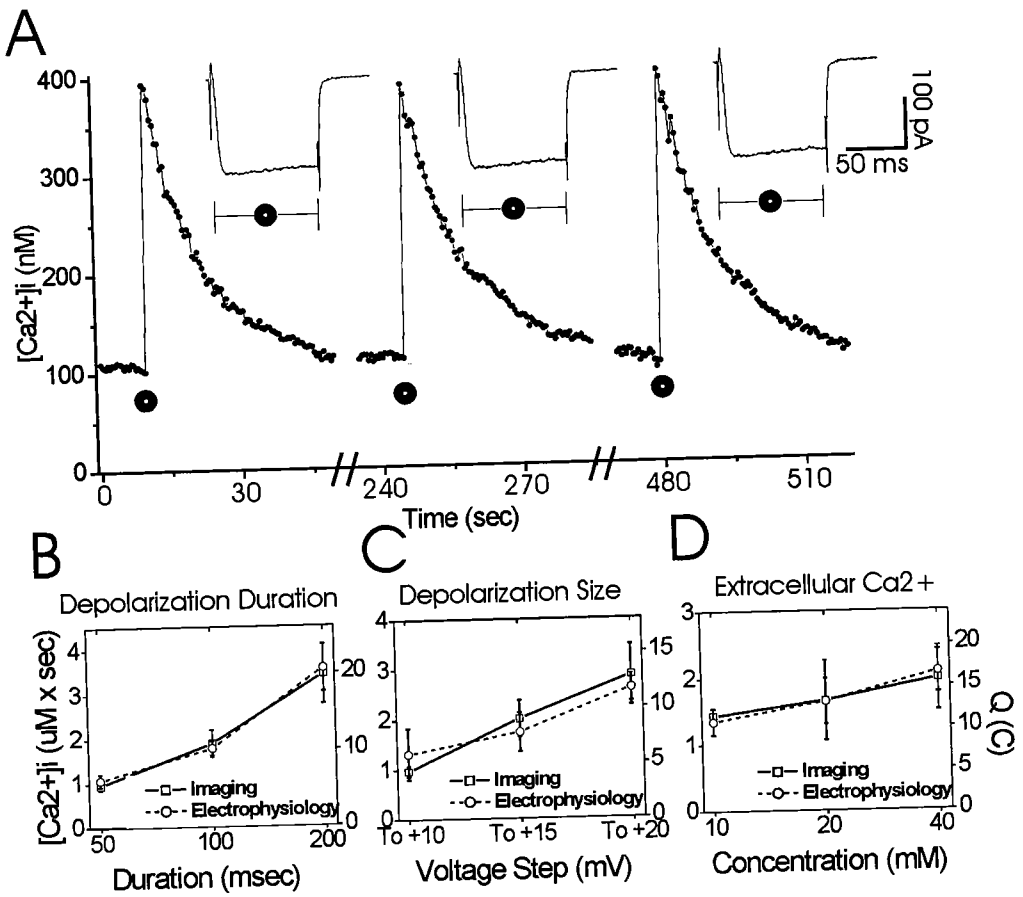

FIG. 1. Relationship between calcium influx (Q) and $[Ca^{2+}]_i$. *A*. Representative traces showing reproducibility of signal acquired by ratiometric calcium imaging within a single cell. Three depolarizing pulses, each from a V_h of -70 mV to +20 mV for 100 msec, given sequentially, with 180 sec pauses between. Inserts show corresponding electrophysiology traces recorded simultaneously at the start of the $[Ca^{2+}]_i$ trace. *B*. Relationship between the integrated (AUC) signals for $[Ca^{2+}]_i$ for 20 sec following stimulus (square with solid line) and current (circle with dashed line) when the duration of a depolarizing step from –70 mV to +20 mV is varied. *C*. Integrated (AUC) signals for $[Ca^{2+}]_i$ for 20 sec following stimulus (square with solid line) and current (circle with dashed line) when the amplitude

of a 100 msec depolarizing step from –70mV is varied. *D*. Integrated (AUC) signals for the elevation in $[Ca^{2+}]_i$ for 20 sec following stimulus (square with solid line) and current (circle with dashed line) for 100 msec depolarizing steps from –70 mV to +20 mV when the extracellular concentration of calcium is varied. Each point in *B*, *C*, and *D* is the average measurement ± SEM from 3 cells

(quickly saturated), high affinity buffer (presumably cytoplasmic Ca^{2+} binding proteins) limits very small Ca^{2+} loads. The Ca^{2+} fluxes in experiments reported here, which induced proportional $[Ca^{2+}]_i$ elevations (Fig. 1*B,C,D*), did not produce $[Ca^{2+}]_i$ levels at either of these extremes. The resting baseline $[Ca^{2+}]_i$ was slightly elevated in patched cells compared to those not patched in the dish, likely due to mechanical disturbance by the electrode in 20 mM Ca^{2+} bath solution.

PC12 Cells treated with NGF (50 ng/ml) for 3-5 days were used since differentiation for this amount of time led to an upregulation of N-type channels, resulting in equivalent Ca^{2+} flux through N- and L-type Ca^{2+} channels during a voltage step (Usowicz et al., 1990;Liu et al., 1996). We chose to focus on the 20 seconds following the voltage step, where $[Ca^{2+}]_i$ decay was most pronounced. Over this time period, the decay could be well fit by a first order exponential (Fig. 2 *A,B*). We choose to present the normalized data to make visual comparison of the kinetics for decaying calcium signals of differing sizes (control vs. pharmacological blockade) easier. Differing amounts of calcium entering each channel type could not have accounted for the differences in decay since the amount of calcium was controlled (see figure legends for average peak $[Ca^{2+}]_i$ amplitudes). An advantage of the combined techniques of electrophysiology and Ca^{2+} imaging is that the amount of calcium entering the cell (Fig. 2*C,D*) can be quantitated and compared to the $[Ca^{2+}]_i$ profile (Fig. 2*A,B*). Our data indicate that the relationship between Ca^{2+} influx and intracellular Ca^{2+} dynamics differed, dependent upon route of entry. When the contribution of N-type channels is reduced by ω-conotoxin MVIIA treatment, the change in the integrated $[Ca^{2+}]_i$ profile is greater than the change in integrated current (-38 ±2%

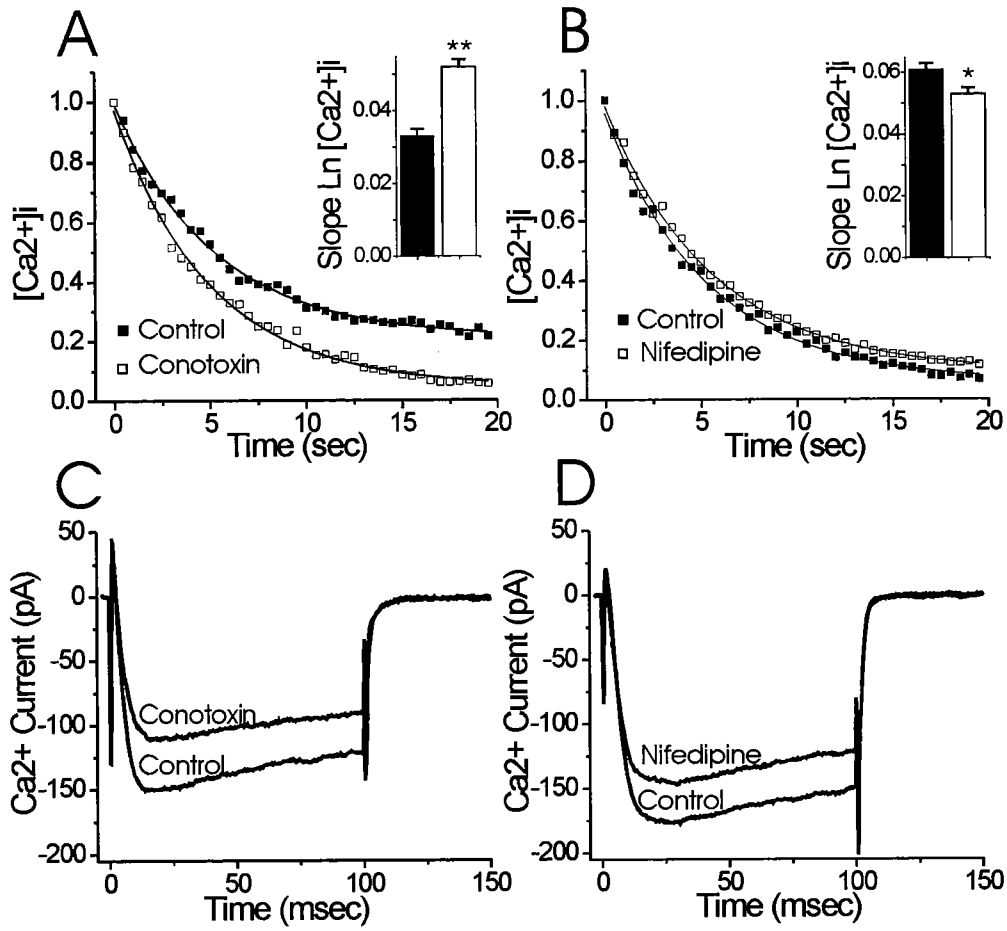

FIG. 2. Route of entry and $[Ca^{2+}]_i$ profile. Data are scaled to produce equivalent initial peak values. $[Ca^{2+}]_i$ levels reflect elevation after subtracting baseline. *A*. Decay of $[Ca^{2+}]_i$ during the 20 seconds following a 100 msec depolarizing step from –70 mV to +20 mV in the absence (■) and presence (□) of 800 nM ω-conotoxin MVIIA (N=8). The slope of the natural log transformed data after ω-conotoxin MVIIA treatment (-0.052 ±0.002)(▯) was significantly greater ($p<0.001$) than control (-0.033 ±0.002)(▮), with average peak $[Ca^{2+}]_i$ amplitudes of 448 ± 19 nM (control) and 390 ± 23 nM (ω-conotoxin MVIIA) . *B*. Decay of $[Ca^{2+}]_i$ during the 20 seconds following a 100 msec

depolarizing step from –70 mV to +20 mV in the absence (■) and presence (□) of 5 μM nifedipine (N=10). The slope of the natural log transformed data after nifedipine treatment (-0.053 ±0.002)(▯) was significantly less (p=0.036) than control (-0.061 ±0.002)(▮), with average peak $[Ca^{2+}]_i$ amplitudes of 504 ± 12 nM (control) and 420 ± 19 nM (nifedipine). *C*, *D*, Currents measured during the first 100 msec of the $[Ca^{2+}]_i$ traces in *A* and *B*, respectively.

vs. –26 ±4% respectively) while the change of integrated $[Ca^{2+}]_i$ profile matches the change in integrated current when the contribution of L-type channels is reduced by nifedipine (-17 ±1%vs -18 ±3%, respectively). This difference in integrated $[Ca^{2+}]_i$ signal resulted from a change in the decay rate, as opposed to a change in the amplitude of the initial $[Ca^{2+}]_i$ rise. The $[Ca^{2+}]_i$ decay in the presence of ω-conotoxin MVIIA (-0.052 ±0.002), described statistically by the slope of the natural log of $[Ca^{2+}]_i$ during the 20 sec following a depolarizing pulse, was more rapid ($p<0.001$) than control (-0.033 ±0.002)(Fig. 2*A*). The decay following a depolarizing pulse in the presence of nifedipine (-0.053 ±0.002) was slower ($p=0.036$) than control (-0.061 ±0.002)(Fig. 2*B*). Thus, decay is slower when there is a greater contribution of N-type channels vs. L-type channels. Although we observed large between cell variability, the change produced by treatment was independent of the starting rate of decay, with 7 out of 8 cells increasing their rate of decay following treatment with ω-conotoxin MVIIA and 10 out of 10 cells decreasing their rate of decay following nifedipine treatment. Both the reduction of current and Ca^{2+} current kinetics are similar for N- and L-type influx (Fig. 2*C,D*), and therefore neither account for differences in the $[Ca^{2+}]_i$ profile. The use of either ω-conotoxin MVIIA or nifedipine to alter the contribution of N- or L-type channels to the whole cell Ca^{2+} current results in a decrease in Ca^{2+} influx, compared to control conditions. We also performed experiments in which either the duration or the amplitude of the voltage pulse was increased, such that the influx in the presence of the blocking agents matched that seen in the absence of the agents. The difference in decay kinetics was unaltered (data not shown), indicating that the reduced influx did not play a role in the effects observed.

PC12 cells contain VGCCs in addition to N- and L-type. The mRNA encoding 3 pore forming α_1 subunits (C,B,A for L-, N-, P/Q-type, respectively and 3 auxiliary β subunits (1,2,3) have been detected in PC12 cells (Liu et al., 1996). There was a minimal contribution of P/Q type voltage gated Ca^{2+} channels, with 5 % of the current blocked by 300 nM AgaIVA. Combining 300 nM AgaIVA with either ω-conotoxin MVIIA or nifedipine did not alter the results obtained in its absence, indicating that P/Q channels were not playing a role (data not shown). There was also a contribution from R-type channels, with 15% of the total current resistant to block by 10μM cadmium. This resistant current could be eliminated by the addition of 25μM nickel.

Channel isolation by pharmacological augmentation

If decay is slower when N-type current makes up more of the total current, we might expect that augmenting the L-type current would lead to faster decay of $[Ca^{2+}]_i$. To test this, Bay K8644 was used to potentiate L-type voltage gated calcium currents, leading to a change in $[Ca^{2+}]_i$ profile (14 ±2%)(Fig. 3*A*) that was less than the change in the integrated current (18 ±2%)(Fig. 3*C*). This indeed, resulted from a more rapid decay ($p=0.016$) of $[Ca^{2+}]_i$ in the presence of 5μM Bay K8644 (-0.067 ±0.003)(5 min. exposure), than in its absence (-0.055 ±0.003)(Fig. 3*A*).

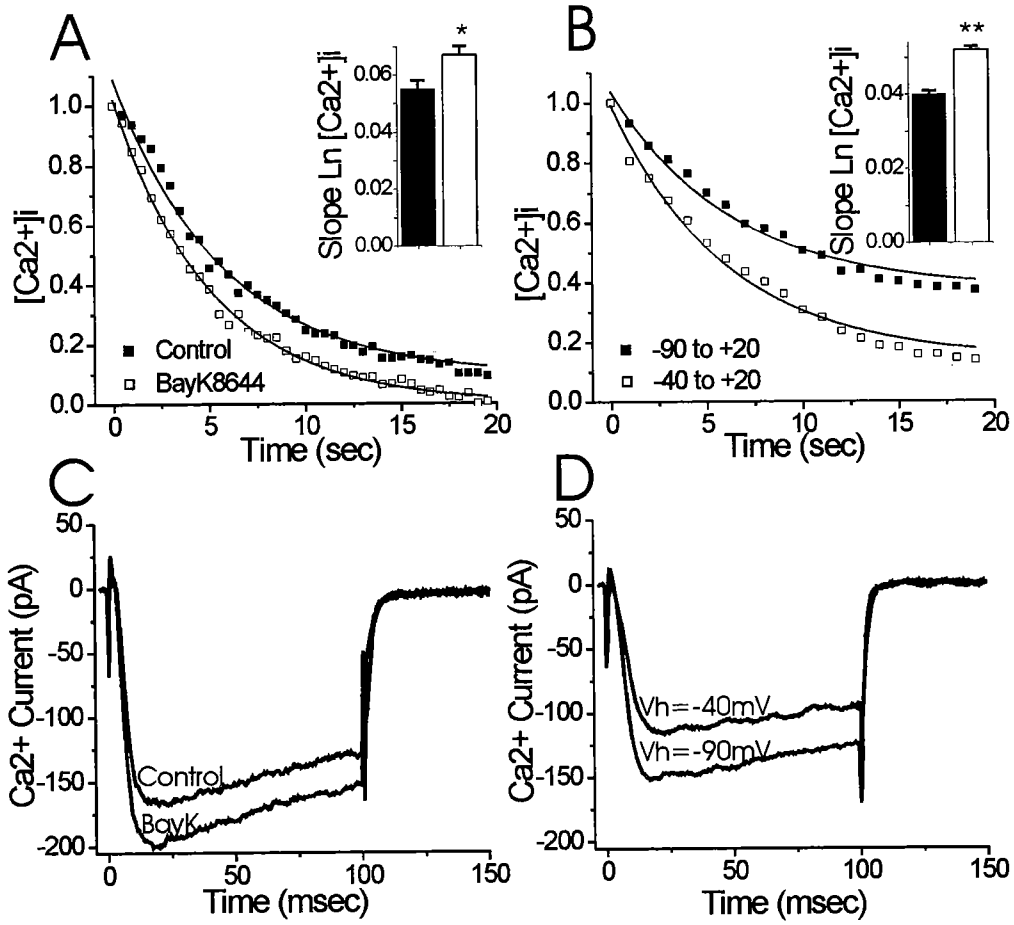

FIG. 3. Channel selection by BayK and voltage. Data are scaled to produce equivalent initial peak values. $[Ca^{2+}]_i$ levels reflect elevation after subtracting baseline. *A*. Decay of $[Ca^{2+}]_i$ during the 20 seconds following a 100 msec depolarizing step from –70 mV to +20 mV in the absence (■) and presence (□) of 5 μM Bay K8644 (N=4). The slope of the natural log transformed data after Bay K8644 treatment (-0.067 ±0.003)(▯) was significantly greater (p=0.016) than control (-0.055 ±0.003)(▮), with average peak $[Ca^{2+}]_i$ amplitudes of 417 ± 10 nM (control) and 508 ± 21 nM (Bay K8644). *B*. Decay of $[Ca^{2+}]_i$ during the 20 seconds following a 100 msec depolarizing steps from either –90

mV V_h to +20 mV (■) or –40 mV V_h to +20 mV (□) (N=6). The slope of the natural log transformed data when V_h =-40 mV (-0.052 ±0.001) (▯) was significantly greater ($p<0.001$) than with a V_h of -90 mV (-0.040 ±0.001)(▮), with average peak $[Ca^{2+}]_i$ amplitudes of 437 ± 8 nM (V_h =-40 mV) and 522 ± 16 nM (V_h =-90 mV). *C*, *D*. Currents measured during the first 100 msec of the $[Ca^{2+}]_i$ traces in *A* and *B*, respectively.

Channel isolation by voltage protocol

To confirm the channel-specificity of the difference in $[Ca^{2+}]_i$ decay independently of pharmacological manipulation, $[Ca^{2+}]_i$ decay was measured after voltage steps from holding potentials (V_h) of either -40 mV or -90 mV (Fig. 3*B*). Since N-type calcium channels are largely inactivated at -40 mV, we would predict that decay would be faster from a V_h of -40 mV, where the contribution of N-type current is minimal. The difference in the integrated intracellular profile (-32 ±3%)(Fig. 3*B*) between the holding potentials was greater than the change in integrated current (-24 ±1%)(Fig. 3*D*). This resulted from a $[Ca^{2+}]_i$ decay from a V_h of –40 mV (-0.052 ±0.001) that was faster ($p<0.001$) than observed from a V_h of –90 mV (-0.040 ±0.001)(Fig. 3*B*), confirming the results obtained with pharmacological current isolation.

CICR is critical for differential effects

Caffeine induces Ca^{2+} release from ryanodine-gated stores in the endoplasmic reticulum in NGF differentiated PC12 cells (Fasolato et al., 1991;Zacchetti et al., 1991;Koizumi et al., 1999). To explore the contribution of CICR to the slower decay of $[Ca^{2+}]_i$ when influx occurs through N-type channels, we examined whether the differences seen in the presence of ω-conotoxin MVIIA and nifedipine were maintained when CICR was blocked. Channel-specific differences in $[Ca^{2+}]_i$ decay rates were abolished by depleting intracellular Ca^{2+} stores by pretreating cells for 60 seconds with 10 μM thapsigargin (Fig. 4 *A*,*B*), or by blocking ryanodine receptors with 100 μM

ryanodine (Fig. 4 *C,D*). When the cells were pre-treated with thapsigargin the $[Ca^{2+}]_i$ decay was the same in both the presence (-0.035 ±0.007) and absence (-0.030 ±0.003) of ω-conotoxin MVIIA (Fig *A*), and the same in both the presence (-0.028 ±0.001) and absence of nifedipine (-0.027 ±0.001)(Fig. *B*). When the cells were treated with ryanodine the $[Ca^{2+}]_i$ decay was the same in both the presence (-0.069 ±0.003) and absence (-0.071 ±0.002) of ω-conotoxin MVIIA (Fig 4*C*), and the same in both the presence (-0.072 ±0.00) and absence (-0.076 ±0.002) of nifedipine (Fig 4D). We conclude that the Ca^{2+} entering through N-type channels is amplified by ryanodine receptor mediated CICR. To confirm the role of CICR in the decay of $[Ca^{2+}]_i$ following a depolarizing pulse we used 5mM caffeine to potentiate CICR (Fig 4*E*) and 100μM ryanodine to inhibit CICR (Fig 4*F*). The $[Ca^{2+}]_i$ decay rate was slowed (p=0.032) in the presence of caffeine (-0.052 ±0.02), when compared to control (-0.059 ±0.01), and increased (p=0.018) in the presence of ryanodine (-0.094 ±0.03), when compared to control (-0.083 ±0.02). Neither caffeine nor ryanodine significantly altered the baseline or peak $[Ca^{2+}]_i$ values.

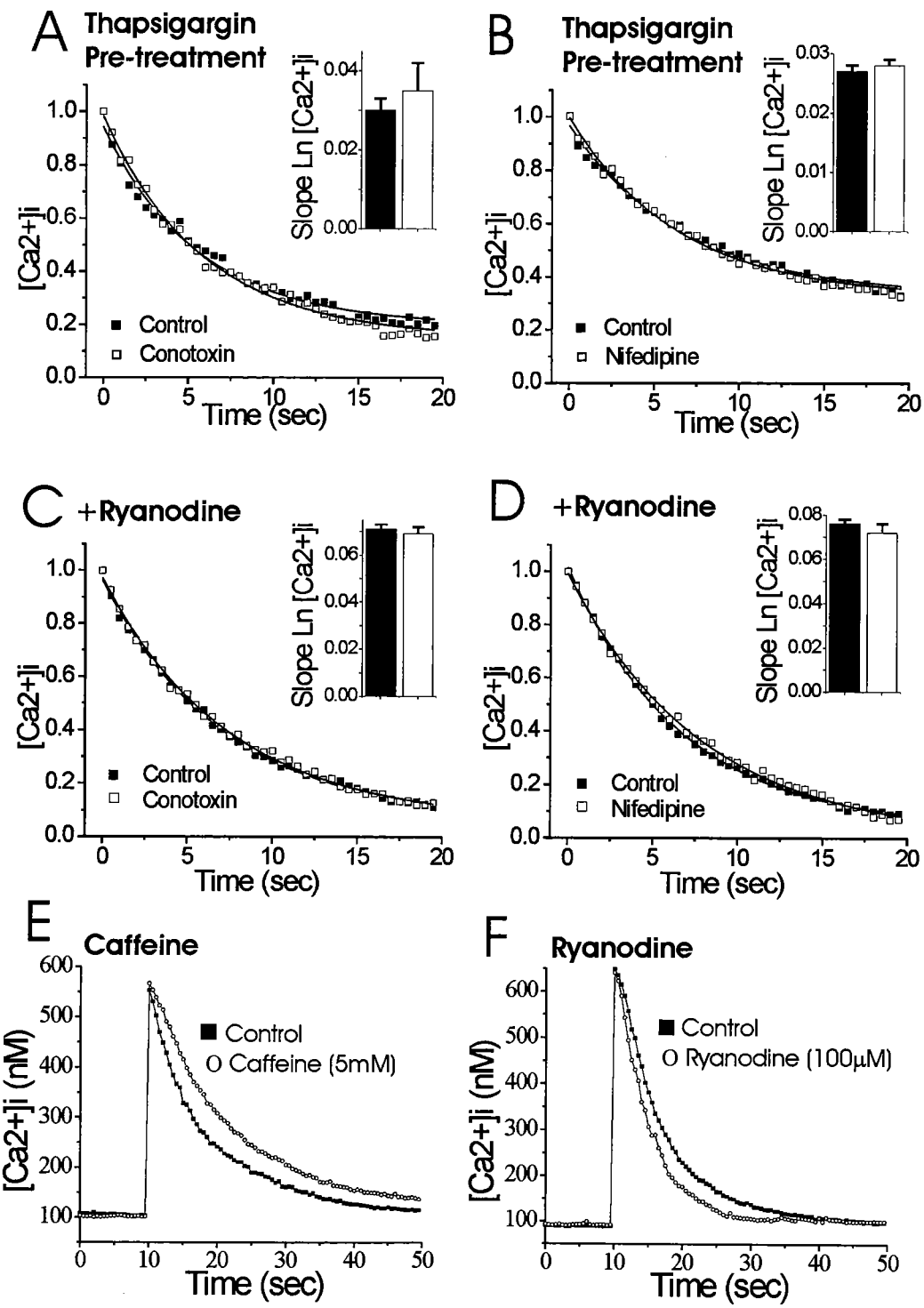

FIG. 4. CICR underlies the differences in $[Ca^{2+}]_i$ profile associated with N- vs L-type channels. Decay functions are scaled to match initial peak values. $[Ca^{2+}]_i$ levels reflect

elevation after subtracting baseline. *A* Cells were pretreated with 10 μM thapsigargin for 60 sec followed by 15 minute wash period before experiment was conducted. Decay of $[Ca^{2+}]_i$ during the 20 seconds following a 100 msec depolarizing step from –70 mV to +20 mV in the absence (■) and presence (□) of 800 nM ω-conotoxin MVIIA (N=3). The slope of the natural log transformed data for $[Ca^{2+}]_i$ decay after ω-conotoxin MVIIA treatment (-0.035 ±0.007)(▯) was not significantly different than control (-0.030 ±0.003)(▮), with average peak $[Ca^{2+}]_i$ amplitudes of 450 ± 7 nM (control) and 377 ± 9 nM (ω-conotoxin MVIIA). *B* Cells were pretreated with 10 μM thapsigargin for 60 sec followed by 15 minute wash period before experiment was conducted. Decay of $[Ca^{2+}]_i$ during the 20 seconds following a 100 msec depolarizing step from –70 mV to +20 mV in the absence (■) and presence (□) of 5 μM nifedipine (N=3). The slope of the natural log transformed data for $[Ca^{2+}]_i$ decay after nifedipine treatment (-0.028 ±0.001)(▯) was not significantly different than control (-0.027 ±0.001)(▮), with average peak $[Ca^{2+}]_i$ amplitudes of 487 ± 14 nM (control) and 404 ± 17 nM (nifedipine). *C*. Ryanodine (100 μM) was present throughout experiment. Decay of $[Ca^{2+}]_i$ during the 20 seconds following a 100 msec depolarizing step from –70 mV to +20 mV in the absence (■) and presence (□) of 800 nM ω-conotoxin MVIIA (N=4). The slope of the natural log transformed data for $[Ca^{2+}]_i$ decay after ω-conotoxin MVIIA treatment (-0.069 ±0.003)(▯) was not significantly different than control (-0.071 ±0.002)(▮), with average peak $[Ca^{2+}]_i$ amplitudes of 519 ± 14 nM (control) and 406 ± 21 nM (ω-conotoxin MVIIA). *D*.

Ryanodine (100 μM) was present throughout experiment. Decay of $[Ca^{2+}]_i$ during the 20 seconds following a 100 msec depolarizing steps from –70 mV to +20 mV in the absence (■) and presence (□) of 5 μM nifedipine (N=4). The slope of the natural log transformed data for $[Ca^{2+}]_i$ decay after nifedipine treatment (-0.072 ±0.00)(▯) was not significantly different than control (-0.076 ±0.002)(▮), with average peak $[Ca^{2+}]_i$ amplitudes of 560 ± 11 nM (control) and 438 ± 17 nM (nifedipine). *E* Average superimposed ratiometric traces for cells before (■)(n=5) and following treatment with 5mM caffeine (○)(n=5). The slope of the natural log transformed data for $[Ca^{2+}]_i$ decay after caffeine treatment (-0.052 ±0.02) was significantly less (p=0.032) than control (-0.059 ±0.01), with average peak $[Ca^{2+}]_i$ amplitudes of 553 ± 10 nM (control) and 566 ± 16 nM (caffeine). *F*. Average superimposed ratiometric traces for cells before (■)(n=5) and following treatment with 100μM ryanodine (○)(n=5). The slope of the natural log transformed data for $[Ca^{2+}]_i$ decay after ryanodine treatment (-0.094 ±0.03) was significantly greater (p=0.018) than control (-0.083 ±0.02), with average peak $[Ca^{2+}]_i$ amplitudes of 649 ± 8 nM (control) and 640 ± 11 nM (ryanodine).

Stimulation size needed to induce CICR is altered by biasing the channel type through which Ca^{2+} enters

Graded amplification of $[Ca^{2+}]_i$ by CICR is commonly observed in neurons (Hua et al., 1993;Kostyuk and Verkhratsky, 1994), although under some circumstances (Usachev and Thayer, 1997) a threshold for inducing CICR can be shown, revealing the potential for regenerative release from intracellular stores. We therefore investigated whether the Ca^{2+} channel class influenced the relationship between Ca^{2+} entry and $[Ca^{2+}]_i$ across a wide range of stimulation voltages. In control cells, the amplification of $[Ca^{2+}]_i$ appears graded, as seen in Figure 5C, by a gradual increase in the ratio of the integrated signals for $[Ca^{2+}]_i$ for 20 sec following stimulus divided by Ca^{2+} charge (Q). Analysis of variance indicated that the $[Ca^{2+}]_i$ / Q ratio differed significantly ($p=0.008$) as a function of voltage step amplitude. Sheffe tests were used for between-group comparisons of the effect of voltage step amplitude, with the $[Ca^{2+}]_i$ / Q ratio becoming significantly different from the step to −10mV at voltage steps to +10mV ($p=0.023$) and +15mV ($p=0.017$). A comparison of the pattern of $[Ca^{2+}]_i$ generated by test pulses of increasing magnitude in the presence of either ω-conotoxin MVIIA (Fig 5*A*) or nifedipine (Fig 5*B*) reveals amplified $[Ca^{2+}]_i$ signals once a certain stimulation size is achieved when the influx is biased through N-type channels. This can be seen in Figure 5*D* by a sudden jump in the ratio of $[Ca^{2+}]_i$ / Q between stimulations to –5 and 0 mV when influx occurs predominately through N-type channels (nifedipine). Analysis of variance indicated that the $[Ca^{2+}]_i$ / Q ratio differed significantly ($p=0.0006$) as a function of voltage step amplitude. Sheffe tests were used

for between-group comparisons of the effect of voltage step amplitude, with the $[Ca^{2+}]_i$ / Q ratio becoming significantly different from the step to –10mV at voltage steps to 0mV (p=0.001), +5mV (p=0.002), +10mV (p=0.027), and +15mV (p=0.027). This amplification is eliminated when influx occurs predominately through L-type channels (ω-conotoxin MVIIA)(Fig 5*E*), with the mean $[Ca^{2+}]_i$ / Q ratio not different (p=0.7) across voltages.

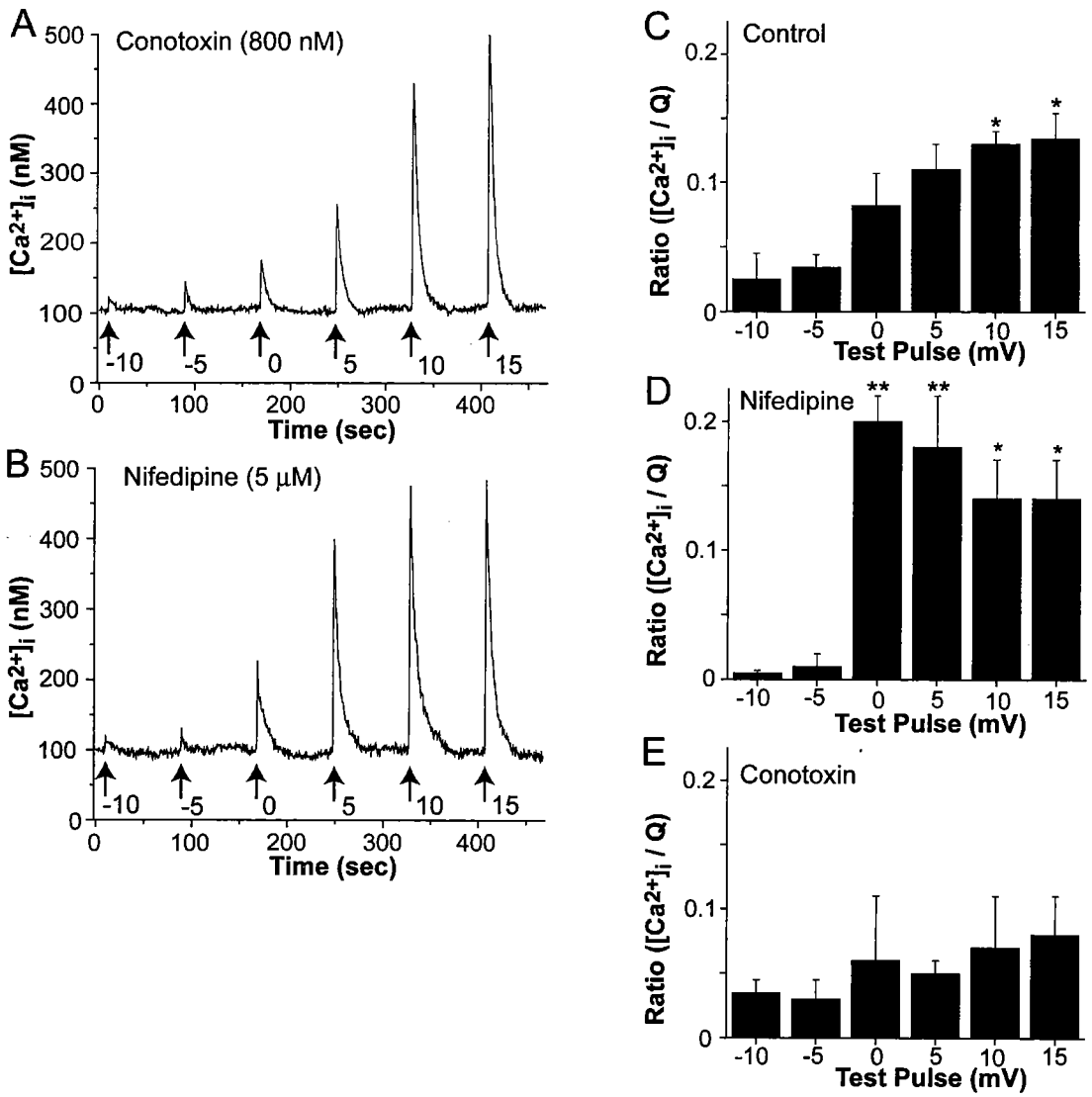

FIG. 5. Discontinuity in the relationship between Ca^{2+} entry and $[Ca^{2+}]_i$ indicates channel specific CICR threshold. Representative ratiometric traces within a single cell in the presence of (*A*) 800 nM ω-conotoxin MVIIA or (*B*) 5 mM nifedipine. Each cell was given five 100 msec depolarizations (arrows indicating test voltage (mV)) from a V_h of -70 mV. Relationships between the $[Ca^{2+}]_i$ / Q ratio and the voltage step amplitude for control cells (*C*) (n=5), cells in the presence of 5μM nifedipine (*D*) (n=5), or cells in the presence of 800 nM ω-conotoxin MVIIA (*E*) (n=5).

DISCUSSION

The use of coupled patch clamp and Ca^{2+} imaging techniques allowed the examination of intracellular Ca^{2+} dynamics after well-controlled and monitored Ca^{2+} entry through different VGCC types. We show that Ca^{2+} influx through different classes of VGCC in PC12 cells produces Ca^{2+} elevations with differing decay kinetics, resulting from the selective activation of CICR by N-type current. Current flux through L-type vs. N-type channels was accomplished by both pharmacological (use of channel blockers and facilitators) and voltage protocols. We further demonstrated that thapsigargin and ryanodine eliminate differences in the intracellular profile between Ca^{2+} channel classes, suggesting CICR mediated by ryanodine receptors as the mechanism. Modulation of the rate of $[Ca^{2+}]_i$ decay by caffeine and ryanodine directly demonstrate that CICR shapes the $[Ca^{2+}]_i$ signal. A role for Ca^{2+} released from ryanodine receptors in the ER of neurons has been established for shaping of neuronal $[Ca^{2+}]_i$ transients (Hua et al., 1993;Shmigol et al., 1995;Llano et al., 1994;Kano et al., 1995;Friel and Tsien, 1992;Garaschuk et al., 1997;Solovyova et al., 2002;Lipscombe et al., 1988a) and we have demonstrated that this shaping of the $[Ca^{2+}]_i$ transient can be determined by the class of VGCC utilized. Channel-specific activation of CICR provides a mechanism whereby the kinetics of intracellular Ca^{2+} leaves a fingerprint of the route of entry, potentially encoding the selective activation of a subset of Ca^{2+}-sensitive targets and processes within the neuron. As an example, activation of D_1 dopamine receptors on rat neostriatal neurons decreases N-type and increases L-type Ca^{2+} currents (Surmeier et al., 1995), which might regulate Ca^{2+} sensitive processes through an effect on the kinetics of the $[Ca^{2+}]_i$ transient.

It is interesting that the memory of route of entry persists for so many seconds beyond the relatively short duration of channel opening, since we might expect that diffusion of Ca^{2+} would blur the initial segregation of the ion. However, this may be explained by the concentration dependency of the initial CICR activation, that then continues to regeneratively release Ca^{2+} from ryanodine receptors well beyond the depolarization. The initiation of CICR may occur within a microdomain surrounding the pore of an N-type VGCC where the $[Ca^{2+}]_i$ would become sufficiently high to activate a co-localized ryanodine receptor. Localized elevations of Ca^{2+} in the μM range are required to activate ryanodine receptors (Fill and Copello, 2002), which indeed, occurs in the vicinity of VGCC's (Narita et al., 2000). The persistent Ca^{2+} signal, which is in the nM concentration range would not impact CICR. Selective activation of CICR is possible since only channels co-localized with ryanodine receptors, and not Ca^{2+} entering more distant channels nor residual Ca^{2+} would create the requisite concentration for ryanodine channel activation. A precedence for functional coupling by co-localization lies in the finding that ryanodine receptors form a functional triad with N-type Ca^{2+} channels and BK channels in bullfrog sympathetic neurons (Akita and Kuba, 2000). An example of the persistence of CICR in neurons over the time course of seconds can be found in the rat visual cortex where a late phase $[Ca^{2+}]_i$ increase reflecting CICR lasts many seconds (Kato et al., 1999).

The coupling of a specific class of VGCC with ryanodine receptors could occur either by non-homogeneous distribution of each in specific regions of a cell, or by colocalization within microdomains throughout a cell. A slower decay in the neurites

would be predicted if both N-type channels and ryanodine receptors were more highly expressed in this region. In neurites of differentiated PC12 cells both a predominance of N-type current (Reber and Reuter, 1991) and preferential occurrence of elementary Ca^{2+} release from ryanodine receptors in response to caffeine have been shown (Koizumi et al., 1999). We favor colocalization within microdomains throughout a cell, as we were unable to detect a slower decay of $[Ca^{2+}]_i$ in the neurites than in the cell bodies (data not shown), consistent with the finding of ryanodine receptors types 2 and 3 distributed throughout the cytoplasm of differentiated PC12 cells (Johenning et al., 2002). L-type and N-type Ca^{2+} channels appear concentrated in local hot spots in frog sympathetic neurons, sometimes dominated by one channel type (Lipscombe et al., 1988b). Subsurface cisterns, extensions of the endoplasmic reticulum containing ryanodine receptors, exist in close apposition to the cell membrane (Berridge, 1998), allowing the colocalization necessary for functional coupling.

Our ω-conotoxin MVIIA and nifedipine treatments did not fully isolate each channel type, but rather shifted the contribution of N- vs. L-type channels during influx. In all cases the influx occurs through a mixed population of VGCC's, but with a predominance of current flowing through L-type channels in the presence of ω-conotoxin MVIIA and through N-type channels in the presence of nifedipine. A small contribution from R-type or P/Q type current cannot be ruled out. Our interpretations are strengthened by the correlative data from BayK and voltage protocols, that do not depend upon channel blockade. Although a functional coupling of N-type channels to CICR can explain the

differential shaping of the $[Ca^{2+}]_i$ profile, the possibility of coupling to other processes, such as extrusion by Ca^{2+}-ATPase or store operated capacitative Ca^{2+} entry also exists.

Although an all or none release of calcium can be demonstrated in some neurons when ryanodine receptors are sensitized by caffeine (Usachev and Thayer, 1997), it is more common for CICR to be graded with increasing stimulus strength (Hua et al., 1993;Kostyuk and Verkhratsky, 1994). Our data indicates that under normal conditions the amplification of Ca^{2+} influx by CICR varies in a graded fashion with stimulation size. The presence of an apparent threshold when calcium enters through a channel type that is privileged in its ability to trigger CICR (Fig 5*D*) indicates that CICR has regenerative capacity in neurons. Additionally, smaller depolarizations may more successfully activate Ca^{2+} sensitive cascades depending on the route of entry due to the channel specific amplification by CICR.

CICR is directly involved in many neuronal functions, such as modulating firing patterns by altering the after-hyperpolarization (Akita and Kuba, 2000), promoting synaptic plasticity by integrating coincident inputs with residual Ca^{2+} following stimulation (Svoboda and Mainen, 1999), by mediating neurotransmitter release (Smith and Cunnane, 1996;Narita et al., 2000;Emptage et al., 2001), and by altering gene expression through mechanisms such as the induction of specific forms of phospho-CREB (Deisseroth and Tsien, 2002). Genes whose transcription is mediated by CREB phosphorylation can show expression patterns that reflect the temporal features of Ca^{2+} transients (Bito et al., 1996;Curtis and Finkbeiner, 1999). The same amount of Ca^{2+} entering through different VGCC's have been reported to selectively modulate release of

vasopressin and oxytocin in preparations from the rat neurohypophysis (von Spreckelsen et al., 1990;Wang et al., 1999;Wang et al., 1997) and acetylcholine release in rat superior cervical ganglion (Gonzalez Burgos et al., 1995). CICR can contribute to Ca^{2+} signals triggered by a single action potential in some neurons (Sandler and Barbara, 1999). The regenerative release of Ca^{2+} from ryanodine receptors can stimulate processes locally in the vicinity of ryanodine channels and also alter the duration of the global cytosolic Ca^{2+} rise. The linkage between CICR and a specific class of VGCC within a neuron couples discrete Ca^{2+} activated processes with the route of Ca^{2+} entry.

ACKNOWLEDGEMENTS

This work was supported by National Institutes of Health Grants AA08003 to S.N.T. and pre-doctoral fellowship AA05552 to K.T.

REFERENCES

Akita T and Kuba K. Functional triads consisting of ryanodine receptors, Ca(2+) channels, and Ca(2+)-activated K(+) channels in bullfrog sympathetic neurons. Plastic modulation of action potential. *J Gen Physiol* 116: 697-720, 2000.

Berridge MJ. Neuronal calcium signaling. *Neuron* 21: 13-26, 1998.

Bito H, Deisseroth K and Tsien RW. CREB phosphorylation and dephosphorylation: a Ca(2+)- and stimulus duration-dependent switch for hippocampal gene expression. *Cell* 87: 1203-1214, 1996.

Chawla S and Bading H. CREB/CBP and SRE-interacting transcriptional regulators are fast on-off switches: duration of calcium transients specifies the magnitude of transcriptional responses. *J Neurochem* 79: 849-858, 2001.

Curtis J and Finkbeiner S. Sending signals from the synapse to the nucleus: possible roles for CaMK, Ras/ERK, and SAPK pathways in the regulation of synaptic plasticity and neuronal growth. *J Neurosci Res* 58: 88-95, 1999.

Deisseroth K and Tsien RW. Dynamic multiphosphorylation passwords for activity-dependent gene expression. *Neuron* 34: 179-182, 2002.

Dolmetsch RE, Lewis RS, Goodnow CC and Healy JI. Differential activation of transcription factors induced by Ca2+ response amplitude and duration. *Nature* 386: 855-858, 1997.

Emptage NJ, Reid CA and Fine A. Calcium stores in hippocampal synaptic boutons mediate short-term plasticity, store-operated Ca2+ entry, and spontaneous transmitter release. *Neuron* 29: 197-208, 2001.

Fasolato C, Zottini M, Clementi E, Zacchetti D, Meldolesi J and Pozzan T. Intracellular Ca2+ pools in PC12 cells. Three intracellular pools are distinguished by their turnover and mechanisms of Ca2+ accumulation, storage, and release. *J Biol Chem* 266: 20159-20167, 1991.

Fill M and Copello JA. Ryanodine receptor calcium release channels. *Physiol Rev* 82: 893-922, 2002.

Friel DD and Tsien RW. A caffeine- and ryanodine-sensitive Ca2+ store in bullfrog sympathetic neurones modulates effects of Ca2+ entry on [Ca2+]i. *J Physiol* 450: 217-246, 1992.

Garaschuk O, Yaari Y and Konnerth A. Release and sequestration of calcium by ryanodine-sensitive stores in rat hippocampal neurones. *J Physiol* 502 (Pt 1): 13-30, 1997.

Gonzalez Burgos GR, Biali FI, Cherksey BD, Sugimori M, Llinas RR and Uchitel OD. Different calcium channels mediate transmitter release evoked by transient or sustained depolarization at mammalian sympathetic ganglia. *Neuroscience* 64: 117-123, 1995.

Grynkiewicz G, Poenie M and Tsien RY. A new generation of Ca2+ indicators with greatly improved fluorescence properties. *J Biol Chem* 260: 3440-3450, 1985.

Hua SY, Nohmi M and Kuba K. Characteristics of Ca2+ release induced by Ca2+ influx in cultured bullfrog sympathetic neurones. *J Physiol* 464: 245-272, 1993.

Johenning FW, Zochowski M, Conway SJ, Holmes AB, Koulen P and Ehrlich BE. Distinct intracellular calcium transients in neurites and somata integrate neuronal signals. *J Neurosci* 22: 5344-5353, 2002.

Kano M, Garaschuk O, Verkhratsky A and Konnerth A. Ryanodine receptor-mediated intracellular calcium release in rat cerebellar Purkinje neurones. *J Physiol* 487 (Pt 1): 1-16, 1995.

Kato N, Tanaka T, Yamamoto K and Isomura Y. Distinct temporal profiles of activity-dependent calcium increase in pyramidal neurons of the rat visual cortex. *J Physiol* 519 Pt 2: 467-479, 1999.

Koizumi S, Bootman MD, Bobanovic LK, Schell MJ, Berridge MJ and Lipp P. Characterization of elementary Ca2+ release signals in NGF-differentiated PC12 cells and hippocampal neurons. *Neuron* 22: 125-137, 1999.

Kostyuk P and Verkhratsky A. Calcium stores in neurons and glia. *Neuroscience* 63: 381-404, 1994.

Lipscombe D, Madison DV, Poenie M, Reuter H, Tsien RW and Tsien RY. Imaging of cytosolic Ca2+ transients arising from Ca2+ stores and Ca2+ channels in sympathetic neurons. *Neuron* 1: 355-365, 1988.

Lipscombe D, Madison DV, Poenie M, Reuter H, Tsien RY and Tsien RW. Spatial distribution of calcium channels and cytosolic calcium transients in growth cones and cell bodies of sympathetic neurons. *Proc Natl Acad Sci U S A* 85: 2398-2402, 1988.

Liu H, Felix R, Gurnett CA, De Waard M, Witcher DR and Campbell KP. Expression and subunit interaction of voltage-dependent Ca2+ channels in PC12 cells. *J Neurosci* 16: 7557-7565, 1996.

Llano I, DiPolo R and Marty A. Calcium-induced calcium release in cerebellar Purkinje cells. *Neuron* 12: 663-673, 1994.

Marrion NV and Tavalin SJ. Selective activation of Ca2+-activated K+ channels by co-localized Ca2+ channels in hippocampal neurons. *Nature* 395: 900-905, 1998.

Miller SG and Kennedy MB. Regulation of brain type II Ca2+/calmodulin-dependent protein kinase by autophosphorylation: a Ca2+-triggered molecular switch. *Cell* 44: 861-870, 1986.

Narita K, Akita T, Hachisuka J, Huang S, Ochi K and Kuba K. Functional coupling of Ca(2+) channels to ryanodine receptors at presynaptic terminals. Amplification of exocytosis and plasticity. *J Gen Physiol* 115: 519-532, 2000.

Reber BF and Reuter H. Dependence of cytosolic calcium in differentiating rat pheochromocytoma cells on calcium channels and intracellular stores. *J Physiol* 435: 145-162, 1991.

Sandler VM and Barbara JG. Calcium-induced calcium release contributes to action potential-evoked calcium transients in hippocampal CA1 pyramidal neurons. *J Neurosci* 19: 4325-4336, 1999.

Sheng M and Sala C. PDZ domains and the organization of supramolecular complexes. *Annu Rev Neurosci* 24: 1-29, 2001.

Shmigol A, Verkhratsky A and Isenberg G. Calcium-induced calcium release in rat sensory neurons. *J Physiol* 489 (Pt 3): 627-636, 1995.

Smith AB and Cunnane TC. Ryanodine-sensitive calcium stores involved in neurotransmitter release from sympathetic nerve terminals of the guinea-pig. *J Physiol* 497 (Pt 3): 657-664, 1996.

Solovyova N, Veselovsky N, Toescu EC and Verkhratsky A. Ca(2+) dynamics in the lumen of the endoplasmic reticulum in sensory neurons: direct visualization of Ca(2+)-induced Ca(2+) release triggered by physiological Ca(2+) entry. *EMBO J* 21: 622-630, 2002.

Stuenkel EL. Regulation of intracellular calcium and calcium buffering properties of rat isolated neurohypophysial nerve endings. *J Physiol* 481 (Pt 2): 251-271, 1994.

Sugita S, Shin OH, Han W, Lao Y and Sudhof TC. Synaptotagmins form a hierarchy of exocytotic Ca(2+) sensors with distinct Ca(2+) affinities. *EMBO J* 21: 270-280, 2002.

Surmeier DJ, Bargas J, Hemmings HC, Jr., Nairn AC and Greengard P. Modulation of calcium currents by a D1 dopaminergic protein kinase/phosphatase cascade in rat neostriatal neurons. *Neuron* 14: 385-397, 1995.

Svoboda K and Mainen ZF. Synaptic [Ca2+]: intracellular stores spill their guts. *Neuron* 22: 427-430, 1999.

Usachev YM and Thayer SA. All-or-none Ca2+ release from intracellular stores triggered by Ca2+ influx through voltage-gated Ca2+ channels in rat sensory neurons. *J Neurosci* 17: 7404-7414, 1997.

Usowicz MM, Porzig H, Becker C and Reuter H. Differential expression by nerve growth factor of two types of Ca2+ channels in rat phaeochromocytoma cell lines. *J Physiol* 426: 95-116, 1990.

von Spreckelsen S, Lollike K and Treiman M. Ca2+ and vasopressin release in isolated rat neurohypophysis: differential effects of four classes of Ca2+ channel ligands. *Brain Res* 514: 68-76, 1990.

Wang G, Dayanithi G, Kim S, Hom D, Nadasdi L, Kristipati R, Ramachandran J, Stuenkel EL, Nordmann JJ, Newcomb R and Lemos JR. Role of Q-type Ca2+ channels in vasopressin secretion from neurohypophysial terminals of the rat. *J Physiol* 502 (Pt 2): 351-363, 1997.

Wang G, Dayanithi G, Newcomb R and Lemos JR. An R-type Ca(2+) current in neurohypophysial terminals preferentially regulates oxytocin secretion. *J Neurosci* 19: 9235-9241, 1999.

West AE, Chen WG, Dalva MB, Dolmetsch RE, Kornhauser JM, Shaywitz AJ, Takasu MA, Tao X and Greenberg ME. Calcium regulation of neuronal gene expression. *Proc Natl Acad Sci U S A* 98: 11024-11031, 2001.

Zacchetti D, Clementi E, Fasolato C, Lorenzon P, Zottini M, Grohovaz F, Fumagalli G, Pozzan T and Meldolesi J. Intracellular Ca2+ pools in PC12 cells. A unique, rapidly exchanging pool is sensitive to both inositol 1,4,5-trisphosphate and caffeine-ryanodine. *J Biol Chem* 266: 20152-20158, 1991.

GENERAL DISCUSSION

My graduate work has focused on the importance of calcium in neuronal function. This thesis is comprised of studies that look at 1) an environmental toxin that could impact human health through the perturbation of $[Ca^{2+}]_i$ in nervous tissue, 2) how the drug ethanol may be addictive through its actions and regulation of specific voltage gated calcium channels, and 3) a basic science approach to understanding how calcium can encode specific neuronal functions depending on which VGCC influx occurs through.

The Health Risk That DEHP May Present to Humans

DEHP is a plasticiser commonly used to soften PVC based plastics. Human exposure to DEHP is quite common due to its wide use and its propensity to leach out of plastic materials into the environment. A particularly dangerous circumstance arises when this compound is used in medical devises that create direct exposure of human blood to this compound. A substantial literature exists showing that this compound can be carcinogenic, although the mechanism underlying such findings has not been determined. It is also unclear if humans are exposed at levels used to induce carcinogenisis in animal studies. My work presents an important link, as indicated by its citation in the Toxicological Profile for DEHP published by the U.S. Department of Health and Human Service (PB2003-100138), demonstrating an acute action of DEHP at levels that do occur in humans. The elevation of $[Ca^{2+}]_i$ in mammalian neurosecretory terminals in response to DEHP that had leached out of IV drip chambers provides an important clue as to how

DEHP might initiate calcium induced changes in excitable tissue that could lead to long term deleterious health consequences.

A Novel Mechanism Underlying Tolerance to Ethanol

Alcoholism is a substantial health problem that strongly affects society through alcohol related crime, violence, illness, lost productivity and death. It is hoped that understanding the biological mechanisms involved in alcohol intoxication and tolerance will allow interventions for dependant individuals. Molecular targets identified in neurons that may underlie the behavioral response to ethanol are the L-type and N-type VGCC's. The inhibition of specific VGCC's would both decrease excitability and shift the route of entry of Ca^{2+} ions into a neuron. The experiment below demonstrates the acute action of ethanol (Figures that did not appear in published manuscripts, but that supplement the discussion of these works appear throughout final discussion). Combined electrophysiology and ratiometric calcium imaging were used to study individual PC12 cells. The cells were voltage clamped using the nystatin perforated patch technique, and given 100 msec test pulses to induce a rise in $[Ca^{2+}]_i$. In the presence of 50 mM ethanol (denoted by bar), the amplitude of the $[Ca^{2+}]_i$ signal was reduced, presumably reflecting an inhibition of voltage gated calcium channels.

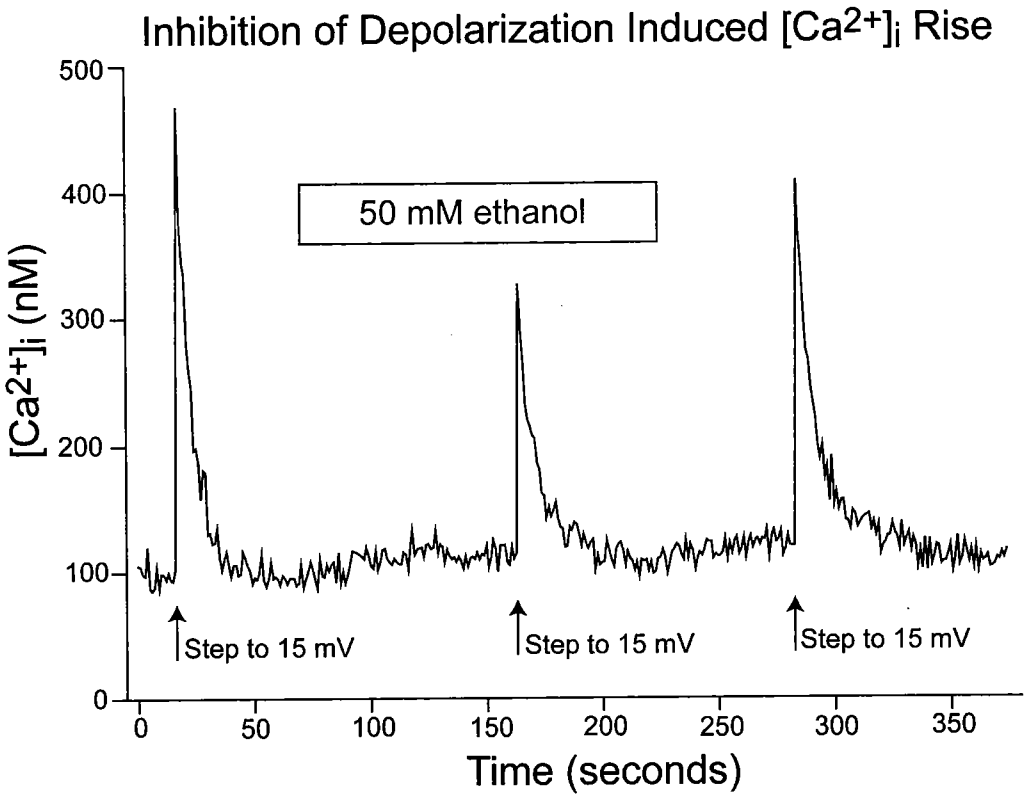

Ethanol has been documented to inhibit the function of L-type channels (Wang et al., 1994; Walter et al., 1999). This is coupled with an increased expression of L-type channels with chronic exposure (Messing et al., 1986; Grant et al., 1993), an adaptive mechanism that likely underlies tolerance. A change in the expression of a specific channel could both counter the inhibition by increasing the excitability of a cell and maintaining the proportion of influx that occurs through that channel type. Previous work in our lab has shown that tolerance in rats maintained on an ethanol diet to the reduction

of peptide hormone release in the neurohypophysis in response to acute ethanol can be, in part, attributed to a decreased sensitivity of VGCCs to ethanol together with an increase in the current density (Knott et al., 2002).

N-type channels may also be an important target as they regulate neurotransmitter release and dendritic calcium signals at many synapses in the mammalian brain, and have been shown to be sensitive to ethanol (Woodward et al., 1990; Wang et al., 1991; Solem et al., 1997). The laboratory of Dr. Robert Messing at UCSF has been studying the upregulation of N-type channels in response to chronic ethanol exposure. While exploring the expression of mRNA levels that encode the α subunit of the N-type channel, they made the critical finding that chronic ethanol selectively shifts the expression of a splice variant lacking the dipeptide sequence Glu Thr. This splice variant was known to alter the channel kinetics (Lin et al., 1997) and presented a novel mechanism by which ethanol's regulation of ion channel function could lead to tolerance. Our laboratory collaborated to confirm that the functional consequences of ethanol exposure was due to a shift in this splice variant. I performed the electrophysiology showing that chronic ethanol exposure did, indeed, cause a faster rate of channel activation and a shift in the voltage dependence of activation to more negative potentials. These combined results demonstrate that chronic ethanol can increase the abundance of an N-type channel's splice variant that can support a larger and faster rising intracellular calcium signal, therefore inducing tolerance to the acute actions of the drug. Alternative splicing allows a set of different proteins to be produced from the same gene, a mechanism that allows a cell to change expression of

their genes. Splicing takes place in a splicesome which brings together a pre-mRNA, small nuclear ribonucleoproteins, and pre-mRNA binding proteins to join 5' and 3' splice sites. Ethanol seems to influence the selection of alternative splice sites as a targeted compensatory change for the inhibition of N-type channels.

Mechanism of Specific Calcium Ion Function

The final and primary component of my graduate work focused on how calcium can encode numerous neuronal functions with high fidelity. Calcium entering a neuron through various types of ion channels can have discrete functional outcomes. For example, it is known that neuronal membrane depolarization and the subsequent calcium influx into the cytoplasm can drive gene expression, and that the ability of calcium influx to induce transcription is regulated by the route of calcium entry into the cell (West et al., 2001). In addition to calcium's role in long term synaptic modifications, calcium plays a role in short term changes in membrane excitability, synaptic structural plasticity, and regulation of enzymes that trigger rapid modifications of synaptic strength (Sabatini et al., 2001). How can this single second messenger encode all of these functions? The answer is that the localization, amplitude, and duration allow different calcium signals to carry different biochemical meanings for a neuron. I was able to show, using both pharmacology and voltage protocols, that equal amounts of Ca^{2+} entering through N-type and L-type voltage gated Ca^{2+} channels result in significantly different $[Ca^{2+}]_i$ temporal profiles. Calcium entering through N-type channels appeared to be amplified, leading to a

slower $[Ca^{2+}]_i$ decay. Channel specific decay rates provide a mechanism for the selective activation of calcium sensitive processes within a neuron.

In addition to entry of external calcium through ion channels residing in the extracellular membrane, calcium released from the endoplasmic reticulum serves as another major source of calcium. The neuronal endoplasmic reticulum contributes to the dynamic signaling by acting either as a source or a sink for calcium, and can shape neuronal calcium signals. The endoplasmic reticulum contains both Inositol 1,4,5-tris-phosphate receptors and ryanodine receptors, which are capable of regenerative calcium release. My work shows that channel-specific differences in $[Ca^{2+}]_i$ decay rates were abolished by depleting intracellular Ca^{2+} stores with thapsigargin or by blocking ryanodine receptors with ryanodine, suggesting the involvement of Ca^{2+}-induced Ca^{2+} release (CICR). Further support for involvement of CICR is provided by the demonstration that caffeine slowed $[Ca^{2+}]_i$ decay while ryanodine at high concentrations increased the rate of $[Ca^{2+}]_i$ decay. We concluded that Ca^{2+} entering through N-type channels is amplified by ryanodine receptor mediated CICR. This would require the coupling of N-type channels with ryanodine receptors.

Colocalization of N-type Channels and Ryanodine Receptors

To explore the nature of coupling between N-type channels and ryanodine receptors, we considered that in polarized neurons, that the two channels could be segregated together in separate regions of a cell. If both N-type channels and ryanodine receptors were more

highly expressed in neurites in the differentiated PC12 cells that we were examining, one would predict a slower decay of calcium in this region than in the cell body. We examined whether decay kinetics in neuritic processes differed from decay in the cell body, as shown below (this figure is mentioned as "data not shown" in chapter three).

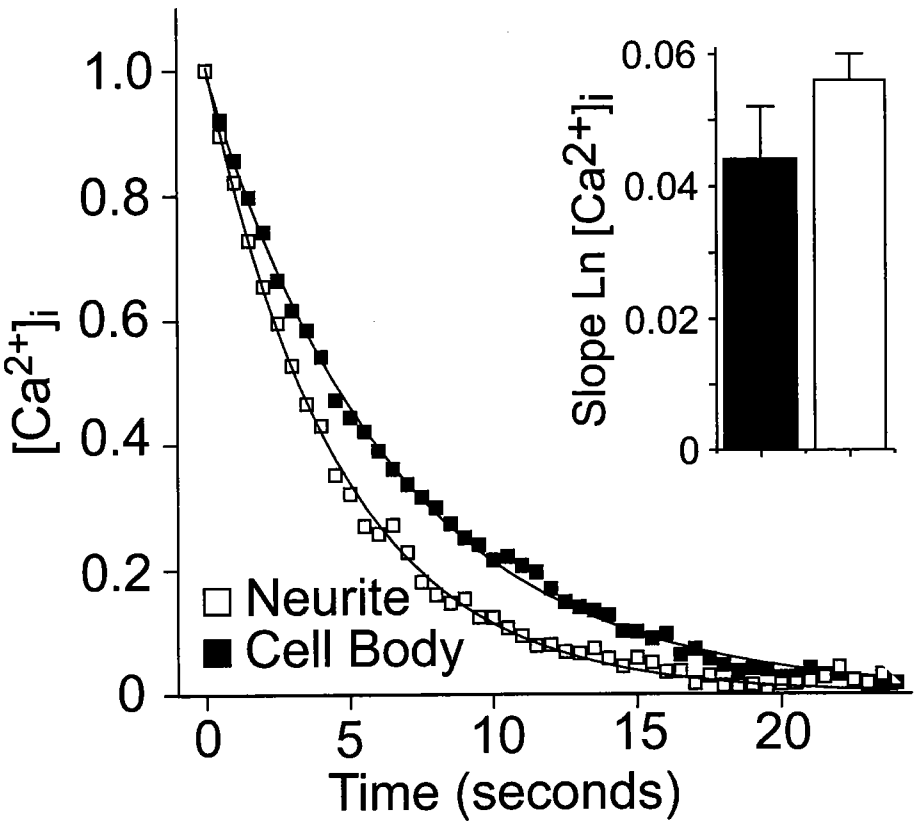

When cells with longer processes than I typically used were examined, the decay of $[Ca^{2+}]_i$ after a voltage step was not slower in a process approximately 35 μm from the cell body, than in the cell body. The slope of the natural log transformed data for $[Ca^{2+}]_i$ decay in the neurites (-0.056 ±0.004) was not significantly different (P=0.13) than in the cell body (-0.044 ±0.008). The interpretation of this data is complicated since our cells

may not have been differentiated sufficiently (5 days NGF) to produce regional segregation of channel types, or other conditions, such as more effective Ca^{2+}-extrusion in the neurite, a region with a greater surface to volume ratio, may have confounded the effects of selective channel association with CICR. Despite these complications, this data does not support a regional activation of CICR, and I therefore favor the colocalization of N-type channels and ryanodine receptors throughout a neuron as a mechanistic explanation for the coupling of N-type channels to ryanodine receptors. This conclusion could be strengthened by future studies that consider a co-localization of N-type channels with ryanodine receptors using such techniques as high resolution immunocytochemisty or biochemical studies probing for binding interactions between these two proteins.

Alternative Mechanisms

Ryanodine receptor mediated CICR is offered as a mechanism for the differing $[Ca^{2+}]_i$ profiles, although numerous alternatives exist, including roles for Ca^{2+}-ATPase pumps, capacitative calcium entry (CCE), Inositol 1,4,5-trisphosphate (IP3) receptors, and mitochondrial buffering in the channel-specific shaping of the $[Ca^{2+}]_i$ profiles. For example, the rate of $[Ca^{2+}]_i$ decline was enhanced in voltage clamped smooth muscle cells after higher, more prolonged increase in $[Ca^{2+}]_i$ (Becker et al., 1989). This enhancement of net Ca^{2+} removal resulted from a feedback stimulation by $[Ca^{2+}]_i$ on Ca^{2+} extrusion mechanisms. It is therefore possible that a unique relationship between one type of VGCC and Ca^{2+}-ATPase pumps could result in the observed channel specific decay rates. Capacitative calcium entry presents an additional mechanism that could shape the

calcium decay. CCE in some neurons occurs as depletion of Ca^{2+} from intracellular stores activates plasma membrane Ca^{2+} channels, providing for rapid replenishment of stores so that the cell is quickly readied for another stimulus (Putney, 2003). Although the identity of the capacitative calcium entry channels and the mechanism by which store depletion activates them is still being determined, it is clear that channels remain open until the stores are replenished, potentially providing a mechanism which could shape the $[Ca^{2+}]_i$ decay over many seconds.

The principal Ca^{2+} release channels on the ER belong to the ryanodine receptor and the Inositol 1,4,5-trisphosphate receptors (IP3R) families. The role I have shown for ryanodine receptors in shaping $[Ca^{2+}]_i$ decay does not preclude involvement of IP3Rs. Although a direct activation of IP3Rs by a brief depolarization would be unexpected, findings regarding the regulation of IP3R present the possibility that it could be activated indirectly by calcium or perhaps by voltage itself. Ca^{2+} biphasically regulates IP3Rs, serving as a co-agonist with IP3, and phospholipase C can be activated by an increase in $[Ca^{2+}]_i$. Ca^{2+} may function through Ca^{2+}-sensing proteins that either bind directly to or modify IP3R channel activity by changing the phosphorylation state (Kasri et al., 2004). Calmodulin, and a family of neuronal Ca^{2+}-binding proteins (CaBPs) have been shown to modulate the activity of IP3Rs in both Ca^{2+}-dependent and –independent manners. CaBP activation of IP3Rs could potentially allow for a novel form of Ca^{2+} induced Ca^{2+} release. IP3 receptors have also been found in complexes that allow a physical and functional association with plasma membrane TRP channels (Yuan et al., 2003), the

likely channels underlying CCE. Due to its complex interactions with Ca^{2+}, IP3Rs should not be ruled out when evaluating potential mechanisms for changes in $[Ca^{2+}]_i$ decay. Another consideration is that the voltage step itself may activate relevant processes other than the opening of VGCCs. For example De Crescenzo et al. (2004) reported mobilization of Ca^{2+} from intracellular stores in isolated nerve terminals by depolarization without Ca^{2+} influx. In skeletal muscle, voltage sensing Ca^{2+} channels are structurally coupled to ryanodine receptors. There is also emerging evidence that G protein-coupled receptors can be voltage dependent (Bolton and Zholos, 2003). IP3 dependent Ca^{2+} release is subject to membrane potential-dependent modulation in a way that may not be restricted to an effect of $[Ca^{2+}]_i$. For example, Mason and Mahaut-Smith (2001) reported voltage-dependent Ca^{2+} release during application of IP3 generating agonists in rat megakaryocytes.

Mitochondria are viewed as active participants in cellular Ca^{2+} signaling, limiting the rise and prolonging recovery of $[Ca^{2+}]_i$ (Babcock et al., 1997) by their ability to rapidly accumulate and then release large quantities of Ca^{2+}. A novel role of mitochondria in shaping the size and duration of $[Ca^{2+}]_i$ has been proposed (Rizzuto et al., 2004) by mitochondria preferentially accumulating Ca^{2+} at microdomains of elevated Ca^{2+} concentration that exist near ER release channels.

Regenerative Capacity of CICR

The hypothesis that calcium influx through N-type channels can be selectively amplified is strengthened by the regenerative capacity of CICR. The effects described here on $[Ca^{2+}]_i$ decay occur over many seconds, requiring a regenerative release of calcium lasting beyond the initial depolarization. Although rare, free running $[Ca^{2+}]_i$ oscillations were observed in the PC12 cells being studied. While these cells were excluded from analysis for the purposes of the manuscript since the elevation of $[Ca^{2+}]_i$ could not be attributed to the depolarizing stimulation, they provide a clear example of the regenerative capacity of $[Ca^{2+}]_i$ in these cells. The figure below shows an instance where 100 msec depolarizations of increasing step amplitude (denoted by arrows) triggered such oscillations in PC12 cells.

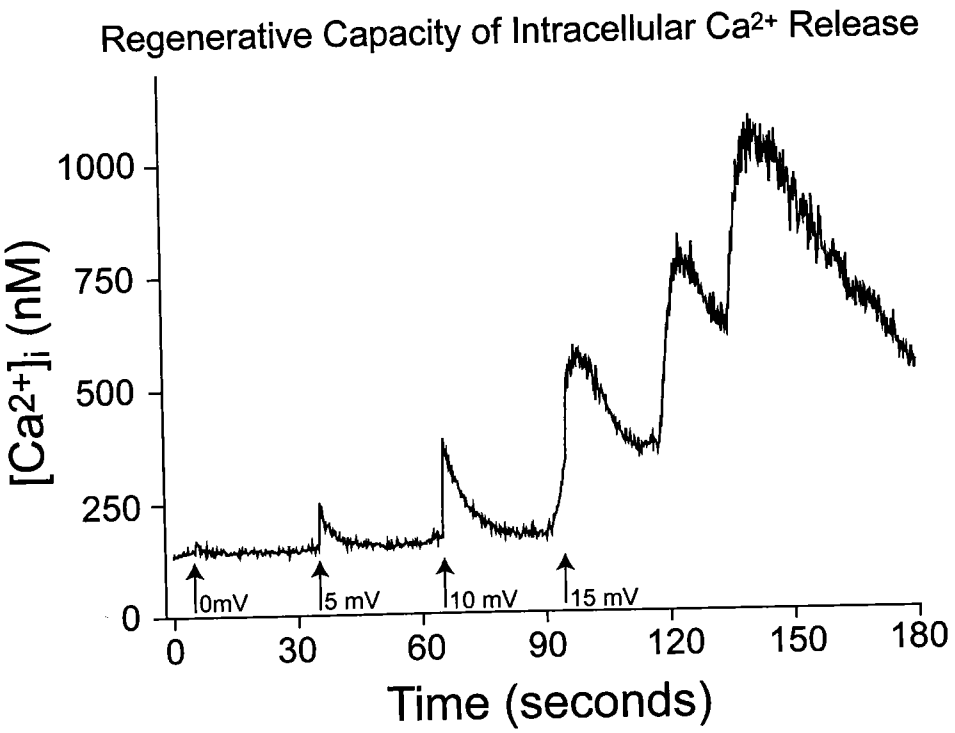

Recent work by Solovyova et al. (2002) have directly demonstrated the processes of CICR in neurons by using electrophysiological depolarization and simultaneously measuring transmembrane calcium current and changes in intraluminal free calcium, indicating the release of calcium from the ER. There is disagreement in the literature as to whether CICR in neurons serves only to amplify calcium influx in a graded manner, or whether calcium released from the ER can lead to further regenerative CICR. Oscillations indicate the potential for feed-forward amplification in which Ca^{2+} triggers additional Ca^{2+} release by interacting with neighboring ryanodine receptors. This gives a further context for the presence of an apparent threshold for amplification that I observed when calcium enters through a channel that is privileged in its ability to trigger CICR. While graded amplification of $[Ca^{2+}]_i$ by CICR is commonly observed in neurons (Hua et al., 1993;Kostyuk and Verkhratsky, 1994), as it was in our control cells, the sudden jump in the ratio of $[Ca^{2+}]_i$ / Q when we investigated the relationship between Ca^{2+} entry and $[Ca^{2+}]_i$ across a wide range of stimulation voltages when the influx is biased through N-type channels is instructive as to the underlying positive feedback capacity of CICR. The presence of a threshold for inducing CICR is consistent with the all or none intracellular release seen in the presence of caffeine when $[Ca^{2+}]_i$ exceeds a certain threshold (Usachev and Thayer, 1997).

Residual Ca^{2+}

While the changes in $[Ca^{2+}]_i$ decay rates may appear subtle in the work described in chapter three, the impact that such changes can have on function become apparent when

one considers the buildup of residual calcium that occurs during repetitive stimulation. Muschol and Salzberg (2000), studying calcium dynamics in the neurohypophysis, showed that vasopressin release is sensitive to both the rapid Ca^{2+} rise from each action potential and the gradual increases in residual Ca^{2+} from multiple action potentials. The figure below shows how multiple stimulations (50 msec step pulses to 15mV spaced 2.5 sec apart, denoted by arrows) lead to a buildup of residual calcium. Slight changes in the decay rate can strongly influence the accumulation of residual $[Ca^{2+}]_i$ under these conditions. One would predict that biasing influx through N-type channels would lead to a greater buildup of residual calcium with repetitive stimulations due to the slower decay kinetics. Such an increase in residual calcium could enhance the ability of influx through N-type channels to trigger functions such as neurotransmitter release.

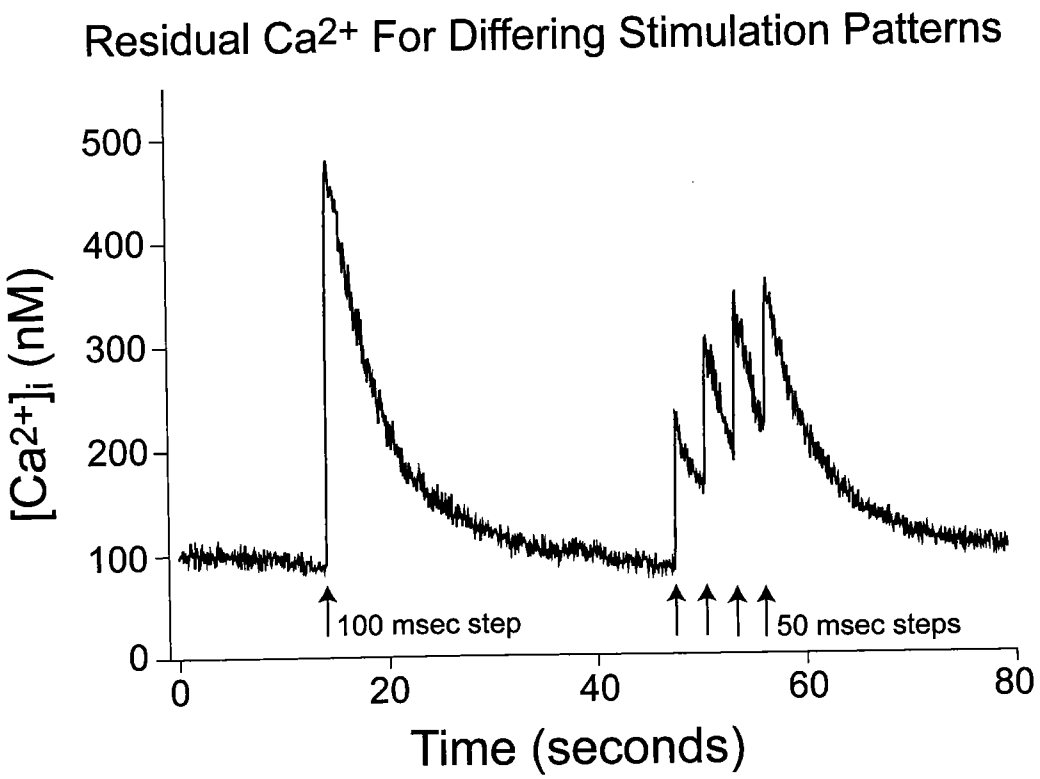

In addition to the consequences of a change in the duration of elevated $[Ca^{2+}]_i$ levels, discrete processes may be tied to calcium released from ryanodine receptors. If a calcium sensitive signaling protein with low Ca^{2+} binding affinity were complexed with a ryanodine receptor such that it was only activated by high local concentrations attained near the pore of an open ryanodine receptor , it might only be activated during influx that leads to CICR. The diffusion of Ca^{2+} within cells is greatly retarded by buffers. A type of VGCC linked to CICR provides a means for amplification of microscopic initiation events into propagating calcium signals, allowing for control of cellular activities involving targets that may be at a distance from initiation sites. Influx through a type of VGCC that is not linked to CICR would be limited by the slow dissipative diffusion of Ca^{2+}.

How Ryanodine Receptors Mediate CICR

Ryanodine receptors are large tetrameric channels that coordinate calcium release from the ER. The massive cytoplasmic domain of the ryanodine receptor is believed to be responsible for regulating channel function (George et al., 2004). The transmembrane carboxyl-terminal constitutes the Ca^{2+} pore (Bhat et al., 1997), contains the binding site for ryanodine (Callaway et al., 1994), and is critical for tetrameric oligomerization of the intact channel (Stewart et al., 2003). Activation of the ryanodine receptor is associated with conformational reorganization of the cytoplasmic amino terminus and rotation of the carboxyl terminal (Sharma et al., 2000).

Elementary release events from ryanodine receptors can either generate a confined Ca^{2+} rise, display local coordinated release generating a Ca^{2+} signal with limited propogation spanning several micrometers, or lead to a regenerative signal throughout a cell. The nature of Ca^{2+} release events can be determined by several factors including the isoforms of ryanodine receptors expressed, the spatial distribution relative to each other and VGCC's, modulation by second messengers and channel associated proteins, and intra-luminal Ca^{2+} content of the ER. The regulation of a single ryanodine receptor by Ca^{2+} is complex, with Ca^{2+} ions turning on, turning off, and conducting through the channel. Studies of individual ryanodine receptors in artificial planer bilayers has provided information such as the conductance, the open probability, dwell times, responses to ligands, and patterns of modal gating. In vivo ryanodine receptor function, which occurs in a rich modulatory environment, remains an active area of investigation. Ryanodine receptor activity is generally a bell-shaped function of cytosolic Ca^{2+} concentration, but with type 2 and 3 channels requiring substantially higher Ca^{2+} levels for inhibition than type 1 channels (Fill and Copello, 2002). While CICR can be self-regenerating, negative feedback such as Ca^{2+} dependent inactivation often limits CICR.

Conclusion

The remarkable range of human experience, behavior, and accomplishments depends on a nervous system that functions due to the actions of individual neurons. During my graduate studies I became fascinated by the organizing principles of a neuron, and in

particular calcium's central integrating role in functions such as neurotransmitter release, membrane excitability, gene expression, enzyme activity, cell growth, and apoptosis. Because so many intracellular signaling pathways and membrane channels are modulated by calcium, there must be mechanisms that determine the selective activation of subsets of these processes. I explored the possibility that a neuron could handle calcium differently based on it's route of entry, demonstrating that Ca^{2+} entry through N-type and L-type channels leads to different intracellular Ca^{2+} profiles. I conclude that the calcium entering through N-type channels is uniquely amplified by ryanodine receptor mediated Ca^{2+}-induced Ca^{2+} release (CICR). Precedence for channel-specific linkage to CICR in neurons exist (Usachev and Thayer, 1997;Sandler and Barbara, 1999;Akita and Kuba, 2000), although there was a predominance of N-type current over L-type in each case, leaving the possibility that it was the amount of calcium entering each channel type, not the route of entry that was critical. I utilized PC12 cells differentiated with NGF for 3-5 days, and undertook the difficulty of combining electrophysiology and imaging in order to both control and verify the equivalence of the two current types. I am the first to show that the same amount of calcium entering through each channel type can have different effects on CICR, providing a mechanism for selective activation of Ca^{2+}-activated processes.

CUMULATIVE REFERENCES

Akita T and Kuba K. Functional triads consisting of ryanodine receptors, Ca(2+) channels, and Ca(2+)-activated K(+) channels in bullfrog sympathetic neurons. Plastic modulation of action potential. *J Gen Physiol* 116: 697-720, 2000.

Augustine GJ and Neher E. Neuronal Ca2+ signalling takes the local route. *Curr Opin Neurobiol* 2: 302-307, 1992.

Augustine GJ, Santamaria F and Tanaka K. Local calcium signaling in neurons. *Neuron* 40: 331-346, 2003.

Babcock DF, Herrington J, Goodwin PC, Park YB and Hille B. Mitochondrial participation in the intracellular Ca2+ network. *J Cell Biol* 136: 833-844, 1997.

Bae J, Stuenkel EL and Loch-Caruso R. Stimulation of oscillatory uterine contraction by the PCB mixture Aroclor 1242 may involve increased [Ca2+]i through voltage-operated calcium channels. *Toxicol Appl Pharmacol* 155: 261-272, 1999.

Becker PL, Singer JJ, Walsh JV, Jr. and Fay FS. Regulation of calcium concentration in voltage-clamped smooth muscle cells. *Science* 244: 211-214, 1989.

Berridge MJ. Neuronal calcium signaling. *Neuron* 21: 13-26, 1998.

Bhat MB, Zhao J, Takeshima H and Ma J. Functional calcium release channel formed by the carboxyl-terminal portion of ryanodine receptor. *Biophys J* 73: 1329-1336, 1997.

Bito H, Deisseroth K and Tsien RW. CREB phosphorylation and dephosphorylation: a Ca(2+)- and stimulus duration-dependent switch for hippocampal gene expression. *Cell* 87: 1203-1214, 1996.

Blaustein MP and Ector AC. Carrier-mediated sodium-dependent and calcium-dependent calcium efflux from pinched-off presynaptic nerve terminals (synaptosomes) in vitro. *Biochim Biophys Acta* 419: 295-308, 1976.

Blaustein MP, Ratzlaff RW, Kendrick NC and Schweitzer ES . Calcium buffering in presynaptic nerve terminals. I. Evidence for involvement of a nonmitochondrial ATP-dependent sequestration mechanism. *J Gen Physiol* 72: 15-41, 1978.

Bolton TB and Zholos AV. Potential synergy: voltage-driven steps in receptor-G protein coupling and beyond. *Sci STKE* 2003: e52, 2003.

Brennan CH, Crabbe J and Littleton JM. Genetic regulation of dihydropyridine-sensitive calcium channels in brain may determine susceptibility to physical dependence on alcohol. *Neuropharmacology* 29: 429-432, 1990.

Callaway C, Seryshev A, Wang JP, Slavik KJ, Needleman DH, Cantu C, III, Wu Y, Jayaraman T, Marks AR and Hamilton SL. Localization of the high and low

affinity [3H]ryanodine binding sites on the skeletal muscle Ca2+ release channel. *J Biol Chem* 269: 15876-15884, 1994.

Cattley RC, Conway JG and Popp JA. Association of persistent peroxisome proliferation and oxidative injury with hepatocarcinogenicity in female F-344 rats fed di(2-ethylhexyl)phthalate for 2 years. *Cancer Lett* 38: 15-22, 1987.

Charness ME, Hu G, Edwards RH and Querimit LA. Ethanol increases delta-opioid receptor gene expression in neuronal cell lines. *Mol Pharmacol* 44: 1119-1127, 1993.

Chawla S and Bading H. CREB/CBP and SRE-interacting transcriptional regulators are fast on-off switches: duration of calcium transients specifies the magnitude of transcriptional responses. *J Neurochem* 79: 849-858, 2001.

Crabtree GR. Calcium, calcineurin, and the control of transcription. *J Biol Chem* 276: 2313-2316, 2001.

Curtis J and Finkbeiner S. Sending signals from the synapse to the nucleus: possible roles for CaMK, Ras/ERK, and SAPK pathways in the regulation of synaptic plasticity and neuronal growth. *J Neurosci Res* 58: 88-95, 1999.

Deisseroth K and Tsien RW. Dynamic multiphosphorylation passwords for activity-dependent gene expression. *Neuron* 34: 179-182, 2002.

De Waard M and Campbell KP. Subunit regulation of the neuronal alpha 1A Ca2+ channel expressed in Xenopus oocytes. *J Physiol* 485 (Pt 3): 619-634, 1995.

De Crescenzo, V, ZhuGe R, Velazquez-Marrero C, Lifshitz LM, Custer E, Carmichael J, Lai FA, Tuft RA, Fogarty KE, Lemos JR and Walsh JV, Jr. Ca2+ syntillas, miniature Ca2+ release events in terminals of hypothalamic neurons, are increased in frequency by depolarization in the absence of Ca2+ influx. *J Neurosci* 24: 1226-1235, 2004.

Dolmetsch RE, Lewis RS, Goodnow CC and Healy JI. Differential activation of transcription factors induced by Ca2+ response amplitude and duration. *Nature* 386: 855-858, 1997.

Dopico AM, Lemos JR and Treistman SN. Ethanol increases the activity of large conductance, Ca(2+)-activated K+ channels in isolated neurohypophysial terminals. *Mol Pharmacol* 49: 40-48, 1996.

Dunlap K, Luebke JI and Turner TJ. Exocytotic Ca2+ channels in mammalian central neurons. *Trends Neurosci* 18: 89-98, 1995.

Emptage NJ, Reid CA and Fine A. Calcium stores in hippocampal synaptic boutons mediate short-term plasticity, store-operated Ca2+ entry, and spontaneous transmitter release. *Neuron* 29: 197-208, 2001.

Ertel EA, Campbell KP, Harpold MM, Hofmann F, Mori Y, Perez-Reyes E, Schwartz A, Snutch TP, Tanabe T, Birnbaumer L, Tsien RW and Catterall WA. Nomenclature of voltage-gated calcium channels. *Neuron* 25: 533-535, 2000.

Fabiato A. Time and calcium dependence of activation and inactivation of calcium-induced release of calcium from the sarcoplasmic reticulum of a skinned canine cardiac Purkinje cell. *J Gen Physiol* 85: 247-289, 1985.

Fasolato C, Zottini M, Clementi E, Zacchetti D, Meldolesi J and Pozzan T. Intracellular Ca2+ pools in PC12 cells. Three intracellular pools are distinguished by their turnover and mechanisms of Ca2+ accumulation, storage, and release. *J Biol Chem* 266: 20159-20167, 1991.

Fill M and Copello JA. Ryanodine receptor calcium release channels. *Physiol Rev* 82: 893-922, 2002.

Fletcher TL and Shain W. Ethanol-induced changes in astrocyte gene expression during rat central nervous system development. *Alcohol Clin Exp Res* 17: 993-1001, 1993.

Friel DD and Tsien RW. A caffeine- and ryanodine-sensitive Ca2+ store in bullfrog sympathetic neurones modulates effects of Ca2+ entry on [Ca2+]i. *J Physiol* 450: 217-246, 1992.

Ganning AE, Olsson MJ, Brunk U and Dallner G. Effects of prolonged treatment with phthalate ester on rat liver. *Pharmacol Toxicol* 67: 392-401, 1990.

Garaschuk O, Yaari Y and Konnerth A. Release and sequestration of calcium by ryanodine-sensitive stores in rat hippocampal neurones. *J Physiol* 502 (Pt 1): 13-30, 1997.

George CH, Jundi H, Thomas NL, Scoote M, Walters N, Williams AJ and Lai FA. Ryanodine Receptor Regulation by Intramolecular Interaction between Cytoplasmic and Transmembrane Domains. *Mol Biol Cell* 15: 2627-2638, 2004.

Gerstin EH, Jr., McMahon T, Dadgar J and Messing RO. Protein kinase Cdelta mediates ethanol-induced up-regulation of L-type calcium channels. *J Biol Chem* 273: 16409-16414, 1998.

Ghosh A and Greenberg ME. Calcium signaling in neurons: molecular mechanisms and cellular consequences. *Science* 268: 239-247, 1995.

Giovannucci DR and Stuenkel EL. Regulation of secretory granule recruitment and exocytosis at rat neurohypophysial nerve endings. *J Physiol* 498 (Pt 3): 735-751, 1997.

Gonzalez Burgos GR, Biali FI, Cherksey BD, Sugimori M, Llinas RR and Uchitel OD. Different calcium channels mediate transmitter release evoked by transient or sustained depolarization at mammalian sympathetic ganglia. *Neuroscience* 64: 117-123, 1995.

Grant AJ, Koski G and Treistman SN. Effect of chronic ethanol on calcium currents and calcium uptake in undifferentiated PC12 cells. *Brain Res* 600: 280-284, 1993.

Greene LA and Tischler AS. Establishment of a noradrenergic clonal line of rat adrenal pheochromocytoma cells which respond to nerve growth factor. *Proc Natl Acad Sci U S A* 73: 2424-2428, 1976.

Greene LA and Rein G. Synthesis, storage and release of acetylcholine by a noradrenergic pheochromocytoma cell line. *Nature* 268: 349-351, 1977.

Grynkiewicz G, Poenie M and Tsien RY. A new generation of Ca2+ indicators with greatly improved fluorescence properties. *J Biol Chem* 260: 3440-3450, 1985.

Hagiwara S and Byerly L. Calcium channel. *Annu Rev Neurosci* 4: 69-125, 1981.

Hirouchi M, Hashimoto T and Kuriyama K. Alteration of GABAA receptor alpha 1-subunit mRNA in mouse brain following continuous ethanol inhalation. *Eur J Pharmacol* 247: 127-130, 1993.

Hu G, Querimit LA, Downing LA and Charness ME. Ethanol differentially increases alpha 2-adrenergic and muscarinic acetylcholine receptor gene expression in NG108-15 cells. *J Biol Chem* 268: 23441-23447, 1993.

Hua SY, Nohmi M and Kuba K. Characteristics of Ca2+ release induced by Ca2+ influx in cultured bullfrog sympathetic neurones. *J Physiol* 464: 245-272, 1993.

Hua SY, Liu C, Lu FM, Nohmi M and Kuba K. Modes of propagation of Ca(2+)-induced Ca2+ release in bullfrog sympathetic ganglion cells. *Cell Calcium* 27: 195-204, 2000.

Huber WW, Grasl-Kraupp B and Schulte-Hermann R. Hepatocarcinogenic potential of di(2-ethylhexyl)phthalate in rodents and its implications on human risk. *Crit Rev Toxicol* 26: 365-481, 1996.

Hundle B, McMahon T, Dadgar J, Chen CH, Mochly-Rosen D and Messing RO. An inhibitory fragment derived from protein kinase Cepsilon prevents enhancement of nerve growth factor responses by ethanol and phorbol esters. *J Biol Chem* 272: 15028-15035, 1997.

Johenning FW, Zochowski M, Conway SJ, Holmes AB, Koulen P and Ehrlich BE. Distinct intracellular calcium transients in neurites and somata integrate neuronal signals. *J Neurosci* 22: 5344-5353, 2002.

Kano M, Garaschuk O, Verkhratsky A and Konnerth A. Ryanodine receptor-mediated intracellular calcium release in rat cerebellar Purkinje neurones. *J Physiol* 487 (Pt 1): 1-16, 1995.

Kasri NN, Holmes AM, Bultynck G, Parys JB, Bootman MD, Rietdorf K, Missiaen L, McDonald F, Smedt HD, Conway SJ, Holmes AB, Berridge MJ and Roderick HL. Regulation of InsP(3) receptor activity by neuronal Ca(2+)-binding proteins. *EMBO J* 23: 312-321, 2004.

Kato N, Tanaka T, Yamamoto K and Isomura Y. Distinct temporal profiles of activity-dependent calcium increase in pyramidal neurons of the rat visual cortex. *J Physiol* 519 Pt 2: 467-479, 1999.

Kim SJ, Lim W and Kim J. Contribution of L- and N-type calcium currents to exocytosis in rat adrenal medullary chromaffin cells. *Brain Res* 675: 289-296, 1995.

Kluwe WM, Haseman JK, Douglas JF and Huff JE. The carcinogenicity of dietary di(2-ethylhexyl) phthalate (DEHP) in Fischer 344 rats and B6C3F1 mice. *J Toxicol Environ Health* 10: 797-815, 1982.

Knott TK, Dopico AM, Dayanithi G, Lemos J and Treistman SN. Integrated channel plasticity contributes to alcohol tolerance in neurohypophysial terminals. *Mol Pharmacol* 62: 135-142, 2002.

Koizumi S, Bootman MD, Bobanovic LK, Schell MJ, Berridge MJ and Lipp P. Characterization of elementary Ca2+ release signals in NGF-differentiated PC12 cells and hippocampal neurons. *Neuron* 22: 125-137, 1999.

Kostyuk P and Verkhratsky A. Calcium stores in neurons and glia. *Neuroscience* 63: 381-404, 1994.

Kumari M. Differential effects of chronic ethanol treatment on N-methyl-D-aspartate R1 splice variants in fetal cortical neurons. *J Biol Chem* 276: 29764-29771, 2001.

Ledwith BJ, Pauley CJ, Wagner LK, Rokos CL, Alberts DW and Manam S. Induction of cyclooxygenase-2 expression by peroxisome proliferators and non-tetradecanoylphorbol 12,13-myristate-type tumor promoters in immortalized mouse liver cells. *J Biol Chem* 272: 3707-3714, 1997.

Lin Z, Haus S, Edgerton J and Lipscombe D. Identification of functionally distinct isoforms of the N-type Ca2+ channel in rat sympathetic ganglia and brain. *Neuron* 18: 153-166, 1997.

Lin Z, Lin Y, Schorge S, Pan JQ, Beierlein M and Lipscombe D. Alternative splicing of a short cassette exon in alpha1B generates functionally distinct N-type calcium channels in central and peripheral neurons. *J Neurosci* 19: 5322-5331, 1999.

Lipscombe D, Madison DV, Poenie M, Reuter H, Tsien RW and Tsien RY. Imaging of cytosolic Ca2+ transients arising from Ca2+ stores and Ca2+ channels in sympathetic neurons. *Neuron* 1: 355-365, 1988.

Lipscombe D, Madison DV, Poenie M, Reuter H, Tsien RY and Tsien RW. Spatial distribution of calcium channels and cytosolic calcium transients in growth cones and cell bodies of sympathetic neurons. *Proc Natl Acad Sci U S A* 85: 2398-2402, 1988.

Lipscombe D, Pan JQ and Gray AC. Functional diversity in neuronal voltage-gated calcium channels by alternative splicing of Ca(v)alpha1. *Mol Neurobiol* 26: 21-44, 2002.

Little HJ, Dolin SJ and Halsey MJ. Calcium channel antagonists decrease the ethanol withdrawal syndrome. *Life Sci* 39: 2059-2065, 1986.

Little HJ. Mechanisms that may underlie the behavioural effects of ethanol. *Prog Neurobiol* 36: 171-194, 1991.

Liu H, Felix R, Gurnett CA, De Waard M, Witcher DR and Campbell KP. Expression and subunit interaction of voltage-dependent Ca2+ channels in PC12 cells. *J Neurosci* 16: 7557-7565, 1996.

Llano I, DiPolo R and Marty A. Calcium-induced calcium release in cerebellar Purkinje cells. *Neuron* 12: 663-673, 1994.

Lukyanetz EA and Neher E. Different types of calcium channels and secretion from bovine chromaffin cells. *Eur J Neurosci* 11: 2865-2873, 1999.

Meakin SO and Shooter EM. The nerve growth factor family of receptors. *Trends Neurosci* 15: 323-331, 1992.

Maeno-Hikichi Y, Chang S, Matsumura K, Lai M, Lin H, Nakagawa N, Kuroda S and Zhang JF. A PKC epsilon-ENH-channel complex specifically modulates N-type Ca2+ channels. *Nat Neurosci* 6: 468-475, 2003.

Marrion NV and Tavalin SJ. Selective activation of Ca2+-activated K+ channels by co-localized Ca2+ channels in hippocampal neurons. *Nature* 395: 900-905, 1998.

Mason MJ and Mahaut-Smith MP. Voltage-dependent Ca2+ release in rat megakaryocytes requires functional IP3 receptors. *J Physiol* 533: 175-183, 2001.

McMahon T, Andersen R, Metten P, Crabbe JC and Messing RO. Protein kinase C epsilon mediates up-regulation of N-type calcium channels by ethanol. *Mol Pharmacol* 57: 53-58, 2000.

Messing RO, Carpenter CL, Diamond I and Greenberg DA. Ethanol regulates calcium channels in clonal neural cells. *Proc Natl Acad Sci U S A* 83: 6213-6215, 1986.

Miles MF, Diaz JE and DeGuzman VS. Mechanisms of neuronal adaptation to ethanol. Ethanol induces Hsc70 gene transcription in NG108-15 neuroblastoma x glioma cells. *J Biol Chem* 266: 2409-2414, 1991.

Miles MF, Wilke N, Elliot M, Tanner W and Shah S. Ethanol-responsive genes in neural cells include the 78-kilodalton glucose-regulated protein (GRP78) and 94-kilodalton glucose-regulated protein (GRP94) molecular chaperones. *Mol Pharmacol* 46: 873-879, 1994.

Miller SG and Kennedy MB. Regulation of brain type II Ca2+/calmodulin-dependent protein kinase by autophosphorylation: a Ca2+-triggered molecular switch. *Cell* 44: 861-870, 1986.

Mills LR, Niesen CE, So AP, Carlen PL, Spigelman I and Jones OT. N-type Ca2+ channels are located on somata, dendrites, and a subpopulation of dendritic spines on live hippocampal pyramidal neurons. *J Neurosci* 14: 6815-6824, 1994.

Muschol M and Salzberg BM. Dependence of transient and residual calcium dynamics on action-potential patterning during neuropeptide secretion. *J Neurosci* 20: 6773-6780, 2000.

Narita K, Akita T, Hachisuka J, Huang S, Ochi K and Kuba K. Functional coupling of Ca(2+) channels to ryanodine receptors at presynaptic terminals. Amplification of exocytosis and plasticity. *J Gen Physiol* 115: 519-532, 2000.

Neher E. Vesicle pools and Ca2+ microdomains: new tools for understanding their roles in neurotransmitter release. *Neuron* 20: 389-399, 1998.

N'Gouemo P and Morad M. Ethanol withdrawal seizure susceptibility is associated with upregulation of L- and P-type Ca2+ channel currents in rat inferior colliculus neurons. *Neuropharmacology* 45: 429-437, 2003.

Nakahara T, Hirano M, Uchimura H, Shirali S, Martin CR, Bonner AB and Preedy VR. Chronic alcohol feeding and its influence on c-Fos and heat shock protein-70 gene expression in different brain regions of male and female rats. *Metabolism* 51: 1562-1568, 2002.

Pan JQ and Lipscombe D. Alternative splicing in the cytoplasmic II-III loop of the N-type Ca channel alpha 1B subunit: functional differences are beta subunit-specific. *J Neurosci* 20: 4769-4775, 2000.

Plummer MR, Logothetis DE and Hess P. Elementary properties and pharmacological sensitivities of calcium channels in mammalian peripheral neurons. *Neuron* 2: 1453-1463, 1989.

Putney JW, Jr. Capacitative calcium entry in the nervous system. *Cell Calcium* 34: 339-344, 2003.

Rabe CS, Delorme E and Weight FF. Muscarine-stimulated neurotransmitter release from PC12 cells. *J Pharmacol Exp Ther* 243: 534-541, 1987.

Rao MS, Yeldandi AV and Subbarao V. Quantitative analysis of hepatocellular lesions induced by di(2-ethylhexyl)phthalate in F-344 rats. *J Toxicol Environ Health* 30: 85-89, 1990.

Reber BF and Reuter H. Dependence of cytosolic calcium in differentiating rat pheochromocytoma cells on calcium channels and intracellular stores. *J Physiol* 435: 145-162, 1991.

Rizzuto R, Duchen MR and Pozzan T. Flirting in little space: the ER/mitochondria Ca2+ liaison. *Sci STKE* 2004: re1, 2004.

Rose CR and Konnerth A. Stores not just for storage. intracellular calcium release and synaptic plasticity. *Neuron* 31: 519-522, 2001.

Rose ML, Rivera CA, Bradford BU, Graves LM, Cattley RC, Schoonhoven R, Swenberg JA and Thurman RG. Kupffer cell oxidant production is central to the mechanism of peroxisome proliferators. *Carcinogenesis* 20: 27-33, 1999.

Sabatini BL, Maravall M and Svoboda K. Ca(2+) signaling in dendritic spines. *Curr Opin Neurobiol* 11: 349-356, 2001.

Saito N, Itouji A, Totani Y, Osawa I, Koide H, Fujisawa N, Ogita K and Tanaka C. Cellular and intracellular localization of epsilon-subspecies of protein kinase C in the rat brain; presynaptic localization of the epsilon-subspecies. *Brain Res* 607: 241-248, 1993.

Sandler VM and Barbara JG. Calcium-induced calcium release contributes to action potential-evoked calcium transients in hippocampal CA1 pyramidal neurons. *J Neurosci* 19: 4325-4336, 1999.

Schneggenburger R and Neher E. Intracellular calcium dependence of transmitter release rates at a fast central synapse. *Nature* 406: 889-893, 2000.

Scott VE, De Waard M, Liu H, Gurnett CA, Venzke DP, Lennon VA and Campbell KP. Beta subunit heterogeneity in N-type Ca2+ channels. *J Biol Chem* 271: 3207-3212, 1996.

Shafer TJ and Atchison WD. Transmitter, ion channel and receptor properties of pheochromocytoma (PC12) cells: a model for neurotoxicological studies. *Neurotoxicology* 12: 473-492, 1991.

Sharma MR, Jeyakumar LH, Fleischer S and Wagenknecht T. Three-dimensional structure of ryanodine receptor isoform three in two conformational states as visualized by cryo-electron microscopy. *J Biol Chem* 275: 9485-9491, 2000.

Sheng M and Sala C. PDZ domains and the organization of supramolecular complexes. *Annu Rev Neurosci* 24: 1-29, 2001.

Shmigol A, Verkhratsky A and Isenberg G. Calcium-induced calcium release in rat sensory neurons. *J Physiol* 489 (Pt 3): 627-636, 1995.

Shukla RR, Albro PW, Corbett JT and Schroeder JL. In vitro studies of the inhibition of protein kinase C from rat brain by di-(2-ethylhexyl)phthalate. *Chem Biol Interact* 69: 73-85, 1989.

Smith AB and Cunnane TC. Ryanodine-sensitive calcium stores involved in neurotransmitter release from sympathetic nerve terminals of the guinea-pig. *J Physiol* 497 (Pt 3): 657-664, 1996.

Sohma H, Hashimoto E, Shirasaka T, Tsunematsu R, Ozawa H, Boissl KW, Boning J, Riederer P and Saito T. Quantitative reduction of type I adenylyl cyclase in human alcoholics. *Biochim Biophys Acta* 1454: 11-18, 1999.

Solem M, McMahon T and Messing RO. Protein kinase A regulates regulates inhibition of N- and P/Q-type calcium channels by ethanol in PC12 cells. *J Pharmacol Exp Ther* 282: 1487-1495, 1997.

Solovyova N, Veselovsky N, Toescu EC and Verkhratsky A. Ca(2+) dynamics in the lumen of the endoplasmic reticulum in sensory neurons: direct visualization of Ca(2+)-induced Ca(2+) release triggered by physiological Ca(2+) entry. *EMBO J* 21: 622-630, 2002.

Spafford JD and Zamponi GW. Functional interactions between presynaptic calcium channels and the neurotransmitter release machinery. *Curr Opin Neurobiol* 13: 308-314, 2003.

Stewart R, Zissimopoulos S and Lai FA. Oligomerization of the cardiac ryanodine receptor C-terminal tail. *Biochem J* 376: 795-799, 2003.

Stuenkel EL. Regulation of intracellular calcium and calcium buffering properties of rat isolated neurohypophysial nerve endings. *J Physiol* 481 (Pt 2): 251-271, 1994.

Sugita S, Shin OH, Han W, Lao Y and Sudhof TC. Synaptotagmins form a hierarchy of exocytotic Ca(2+) sensors with distinct Ca(2+) affinities. *EMBO J* 21: 270-280, 2002.

Surmeier DJ, Bargas J, Hemmings HC, Jr., Nairn AC and Greengard P. Modulation of calcium currents by a D1 dopaminergic protein kinase/phosphatase cascade in rat neostriatal neurons. *Neuron* 14: 385-397, 1995.

Svoboda K and Mainen ZF. Synaptic [Ca2+]: intracellular stores spill their guts. *Neuron* 22: 427-430, 1999.

Tanabe T, Takeshima H, Mikami A, Flockerzi V, Takahashi H, Kangawa K, Kojima M, Matsuo H, Hirose T and Numa S. Primary structure of the receptor for calcium channel blockers from skeletal muscle. *Nature* 328: 313-318, 1987.

Thibault C, Lai C, Wilke N, Duong B, Olive MF, Rahman S, Dong H, Hodge CW, Lockhart DJ and Miles MF. Expression profiling of neural cells reveals specific patterns of ethanol-responsive gene expression. *Mol Pharmacol* 58: 1593-1600, 2000.

Tinker A and Williams AJ. Probing the structure of the conduction pathway of the sheep cardiac sarcoplasmic reticulum calcium-release channel with permeant and impermeant organic cations. *J Gen Physiol* 102: 1107-1129, 1993.

Tsien RW, Hess P, McCleskey EW and Rosenberg RL. Calcium channels: mechanisms of selectivity, permeation, and block. *Annu Rev Biophys Biophys Chem* 16: 265-290, 1987.

Tsien RW, Lipscombe D, Madison DV, Bley KR and Fox AP. Multiple types of neuronal calcium channels and their selective modulation. *Trends Neurosci* 11: 431-438, 1988.

Usachev Y, Shmigol A, Pronchuk N, Kostyuk P and Verkhratsky A. Caffeine-induced calcium release from internal stores in cultured rat sensory neurons. *Neuroscience* 57: 845-859, 1993.

Usachev YM and Thayer SA. All-or-none Ca2+ release from intracellular stores triggered by Ca2+ influx through voltage-gated Ca2+ channels in rat sensory neurons. *J Neurosci* 17: 7404-7414, 1997.

Usowicz MM, Porzig H, Becker C and Reuter H. Differential expression by nerve growth factor of two types of Ca2+ channels in rat phaeochromocytoma cell lines. *J Physiol* 426: 95-116, 1990.

von Spreckelsen S, Lollike K and Treiman M. Ca2+ and vasopressin release in isolated rat neurohypophysis: differential effects of four classes of Ca2+ channel ligands. *Brain Res* 514: 68-76, 1990.

Walter HJ and Messing RO. Regulation of neuronal voltage-gated calcium channels by ethanol. *Neurochem Int* 35: 95-101, 1999.

Walter HJ, Berry M, Hill DJ, Cwyfan-Hughes S, Holly JM and Logan A. Distinct sites of insulin-like growth factor (IGF)-II expression and localization in lesioned rat brain: possible roles of IGF binding proteins (IGFBPs) in the mediation of IGF-II activity. *Endocrinology* 140: 520-532, 1999.

Walter HJ, McMahon T, Dadgar J, Wang D and Messing RO. Ethanol regulates calcium channel subunits by protein kinase C delta -dependent and -independent mechanisms. *J Biol Chem* 275: 25717-25722, 2000.

Wang G, Dayanithi G, Kim S, Hom D, Nadasdi L, Kristipati R, Ramachandran J, Stuenkel EL, Nordmann JJ, Newcomb R and Lemos JR. Role of Q-type Ca2+ channels in vasopressin secretion from neurohypophysial terminals of the rat. *J Physiol* 502 (Pt 2): 351-363, 1997.

Wang G, Dayanithi G, Newcomb R and Lemos JR. An R-type Ca(2+) current in neurohypophysial terminals preferentially regulates oxytocin secretion. *J Neurosci* 19: 9235-9241, 1999.

Wang X, Wang G, Lemos JR and Treistman SN. Ethanol directly modulates gating of a dihydropyridine-sensitive Ca2+ channel in neurohypophysial terminals. *J Neurosci* 14: 5453-5460, 1994.

Wang XM, Lemos JR, Dayanithi G, Nordmann JJ and Treistman SN. Ethanol reduces vasopressin release by inhibiting calcium currents in nerve terminals. *Brain Res* 551: 338-341, 1991.

West AE, Chen WG, Dalva MB, Dolmetsch RE, Kornhauser JM, Shaywitz AJ, Takasu MA, Tao X and Greenberg ME. Calcium regulation of neuronal gene expression. *Proc Natl Acad Sci U S A* 98: 11024-11031, 2001.

Westenbroek RE, Hell JW, Warner C, Dubel SJ, Snutch TP and Catterall WA. Biochemical properties and subcellular distribution of an N-type calcium channel alpha 1 subunit. *Neuron* 9: 1099-1115, 1992.

Woodward JJ, Machu T and Leslie SW. Chronic ethanol treatment alters omega-conotoxin and Bay K 8644 sensitive calcium channels in rat striatal synaptosomes. *Alcohol* 7: 279-284, 1990.

Yuan JP, Kiselyov K, Shin DM, Chen J, Shcheynikov N, Kang SH, Dehoff MH, Schwarz MK, Seeburg PH, Muallem S and Worley PF. Homer binds TRPC family channels and is required for gating of TRPC1 by IP3 receptors. *Cell* 114: 777-789, 2003.

Yuste R and Katz LC. Control of postsynaptic Ca2+ influx in developing neocortex by excitatory and inhibitory neurotransmitters. *Neuron* 6: 333-344, 1991.

Zacchetti D, Clementi E, Fasolato C, Lorenzon P, Zottini M, Grohovaz F, Fumagalli G, Pozzan T and Meldolesi J. Intracellular Ca2+ pools in PC12 cells. A unique, rapidly exchanging pool is sensitive to both inositol 1,4,5-trisphosphate and caffeine-ryanodine. *J Biol Chem* 266: 20152-20158, 1991.